Université du Québec (UQ)
INRS-Eau, Terre & Environnement (INRS-ETE)

La datation par les séries de l'uranium en archéologie: nouvelles applications à la datation de l'art rupestre et des fossiles humains

Par

Maxime Aubert

Thèse présentée pour l'obtention
du grade de Philosophiae doctor (Ph.D.)
(Sciences de la Terre)

Jury d'évaluation

Examinateur interne	Normand Tassé, Ph.D. Université du Québec (INRS-ETE)
Examinateur externe	Bassam Ghaleb, Ph.D. GEOTOP-UQAM
Examinateur externe	Gilles Tassé, Ph.D. Université du Québec (UQAM)
Directeur de recherche	Marc Richer-LaFlèche, Ph.D. Université du Québec (INRS-ETE)
Codirecteur de recherche	Alan Watchman, Ph.D. Australian National University
Codirecteur de recherche	Daniel Arsenault, Ph.D. Université du Québec (UQAM)

RÉSUMÉ

L'introduction de la datation absolue en archéologie entraîna une véritable révolution pour la discipline, particulièrement avec le développement de la datation au radiocarbone à la fin des années 1940. Depuis, d'autres méthodes de datation absolues ont été appliquées en archéologie, comme la datation par les séries de l'uranium. Néanmoins, certains matériaux archéologiques, notamment l'art rupestre et les fossiles humains, demeurent très difficiles à dater.

Les dessins, les peintures et les gravures sur support rocheux appelés art rupestre sont un des traits caractéristiques de l'Homme moderne (*Homo sapiens sapiens*). La difficulté d'obtenir l'âge de ces œuvres limite considérablement leur intégration aux autres données archéologiques et environnementales. Dans cette recherche, la dernière génération d'équipement analytique moderne a été utilisée afin de dater les oeuvres rupestres qui sont naturellement microstratifiées avec ou recouvertes d'enduits minéraux. Les dépôts de carbonate ainsi que les vernis minéraux ont été étudiés afin de déterminer la possibilité d'utiliser les séries de l'uranium comme méthode de datation. Les résultats obtenus démontrent la possibilité d'utiliser cette technique pour dater les œuvres rupestres préhistoriques. Elle permettra ainsi de placer ces œuvres dans leurs contextes temporaux et environnementaux.

Afin de connaître l'évolution de l'espèce humaine, il est impératif de pouvoir dater les fossiles humains. Toutefois, ceci ne se fait pas sans entraves. En effet, pour les spécimens âgés de plus de cinquante mille ans, on ne peut pas utiliser la méthode au radiocarbone. De plus, comme les échantillons sont très précieux, toute méthode de datation doit éviter ou minimiser au maximum leur destruction. La spectrométrie de masse à multicollecteurs couplée à un système à ablation laser a donc été utilisée afin de modéliser l'incorporation et la diffusion de l'uranium dans les os et les dents fossiles. Et cette technique révolutionnaire permet la datation des fossiles humains tout en minimisant la détérioration de l'échantillon.

REMERCIEMENTS

Je voudrais tout d'abord remercier mon directeur de recherche Marc Richer-LaFlèche. Un grand merci aussi à Alan Watchman qui m'a initié à la problématique associée à la datation des sites rupestres et qui m'a aussi permis d'avoir accès à de nombreux sites et échantillons nécessaires à cette recherche. J'aimerais également exprimer ma gratitude à Malcolm McCulloch, Rainer Grün, Graham Mortimer, Steve Eggins, John Chappell et Les Kinsley de la Research School of Earth Sciences (RSES)/Australian National University qui m'ont ouvert les portes de leurs laboratoires et qui ont accepté de partager leurs connaissances. J'adresse également des remerciements à Sue O'Connor de la Research School of Pacific and Asian Studies (RSPAS)/Australian National University pour son enthousiasme face à la datation des sites rupestres au Timor, de même qu'à Alistair Pike (Bristol University) pour ses judicieux conseils. Les nombreuses discussions que j'ai eues avec ces chercheurs ont suscité moult réflexions.

Je ne peux passer sous silence l'apport monétaire fourni par le Conseil de Recherches en Sciences Naturelles et en Génie du Canada (CRSNG), le Australian Research Council (ARC), l'Institut culturel Avataq et l'Institut National de la Recherche Scientifique (INRS). Le personnel de l'INRS et de la Research School of Earth Sciences (RSES)/Australian National University ayant contribués de près ou de loin à cette recherche ont aussi droit à ma reconnaissance. Enfin, merci à ma famille et amis pour leur soutien.

TABLE DES MATIÈRES

LISTE DES FIGURES

LISTE DES TABLEAUX

1 INTRODUCTION

1.1 Objectifs

Cette recherche doctorale vise à démontrer que les techniques d'analyse de pointe essentiellement développées en Sciences de la Terre peuvent être directement appliquées en archéologie. Et sa principale visée est d'établir le bien-fondé de la spectrométrie de masse à multicollecteurs (MC-ICP-MS) pour dater l'art rupestre et les fossiles humains. Pour ce faire, la démonstration sera faite à partir d'enduits minéraux récoltés sur deux sites rupestres, l'un au Timor Leste (article 1), l'autre en Australie méridionale (article 2), ainsi que sur une dent de Néanderthalien (article 3). Cette technique demande des quantités minimes de matériel pour produire des résultats significatifs repoussant ainsi les limites d'application sur des matériaux précédemment considérés comme impropres pour la datation.

Les principaux objectifs de cette recherche sont :

- De démontrer la possibilité d'établir l'âge d'œuvres rupestres préhistoriques naturellement recouvertes de dépôts de carbonate par la datation de ces enduits minéraux en utilisant la méthode par les séries de l'uranium (séries-U).
- De déterminer le(s) mode(s) de formation et l'âge des vernis minéraux de type 'rock varnish' en utilisant les techniques d'extractions séquentielles et la méthode de datation par les séries de l'uranium (séries-U).
- D'établir une nouvelle méthodologie virtuellement non destructive permettant de dater les os et les dents fossiles par les séries de l'uranium.

1.2 Contribution de l'auteur et des coauteurs

La problématique et les objectifs de recherche de cette thèse de doctorat ont été discutés et élaborés avec Marc Richer-LaFlèche (INRS-Eau, Terre et Environnement), mon directeur de recherche, ainsi qu'avec mes codirecteurs Alan Watchman (Australian National University) et Daniel Arsenault (UQAM). J'ai préparé et analysé les échantillons et discuté des résultats

d'analyse avec les collaborateurs des articles, articles et thèse que j'ai rédigés. Quant aux analyses, elles ont été réalisées à la Research School of Earth Sciences/Austrailan National University et à l'INRS-ETE.

Plus précisément, Graham Mortimer m'a initié à la préparation et à l'analyse des échantillons. Avec l'aide de Malcolm McCulloch, j'ai élaboré un protocole afin de réduire considérablement la taille des échantillons et améliorer la résolution des instruments. Sue O'Connor et Alan Watchman ont fourni les échantillons et ils ont aussi participé à la rédaction des articles. Marc Richer-Laflèche a collaboré à l'interprétation des données portant sur les terres rares. Enfin, Rainer Grün a contribué à l'interprétation des données et à la rédaction de l'article portant sur la dent de Néanderthalien.

1.3 Définition du problème et approche méthodologique

1.3.1 La datation de l'art rupestre

Le terme art rupestre désigne les manifestations artistiques sur support rocheux. C'est la seule manifestation culturelle de l'humanité qui se soit poursuivie sans interruption pendant plus de trente millénaires pour parvenir jusqu'à nous sous différentes formes inchangées depuis les origines (Clottes 2002). À ce jour, plus de quatre-vingt-dix-neuf pour cent (99%) de l'art préhistorique connu est en fait de l'art rupestre (Anati 2001).

Pour dater les œuvres rupestres, on a adopté un modèle évolutif reposant sur l'idée de base que plus un art est ancien (« archaïque »), plus il doit être d'un style fruste et grossier, le corollaire étant la croyance en un développement relativement linéaire de la création artistique, avec des progrès constants au fil des siècles ou des millénaires. Or, partout dans le monde où il a été possible d'établir des datations quantitatives, ce modèle s'est révélé erroné (Clottes 2000). Néanmoins, l'observation de certains critères présents sur les sites rupestres permet parfois de reconnaître l'ancienneté relative de ces derniers. Par exemple, certaines représentations montrent des objets dont la date d'apparition dans la culture considérée est bien établie archéologiquement ou historiquement.

La méthode de datation au carbone-14 peut théoriquement être utilisée pour dater les œuvres rupestres. Toutefois, lorsque des pigments organiques y sont présents, l'incertitude sur la provenance du carbone peut nous induire à des conclusions erronées (Beck *et al.* 1998). De plus, afin de pouvoir dater directement les peintures rupestres par la méthode au carbone-14, il est nécessaire de trouver des quantités suffisantes de carbone organique dans la peinture. Pour la plupart des sites, la peinture utilisée était constituée de pigments minéraux sans liant organique (hématite).

Plusieurs types de dépôt minéral ont été observés en association avec les oeuvres rupestres. Parmi ceux-ci, on retrouve fréquemment les pellicules de silice amorphe ($SiO_2.nH_2O$) de type opale-A, des revêtements carbonatés et du vernis monéral riche en manganèse. Mesurer l'activité du carbone-14 contenue dans la matière organique (algues microscopiques, diatomées, bactéries, champignons) emprisonnée dans ces revêtements minéraux situés en dessous et/ou au-dessus d'une couche de peinture ou sur la surface d'une gravure constitue une possibilité intéressante pour dater l'œuvre rupestre. La méthode établit donc le moment où les dépôts ont commencé à se former. Idéalement, la méthode permet d'obtenir une date maximum et/ou minimum correspondant à l'époque de la réalisation des oeuvres rupestres associées à ce type de revêtement.

Des études préliminaires utilisant la matière organique emprisonnée dans ces dépôts minéraux et l'analyse par datation au carbone-14 par spectrométrie de masse à accélérateur (AMS ^{14}C) ont démontré la faisabilité de dater plusieurs de ces surfaces et donc d'estimer l'époque de réalisation des oeuvres rupestres qui y sont associées. Ainsi, plusieurs substances organiques ont servi à dater les oeuvres rupestres. Par exemple, des fibres de cellulose (Watchman 1992a; Watchman & Cole 1993), des sels d'acide oxalique (Watchman 1993), des diatomées fossilisées et autres micro-organismes (Watchman 1995), des acides gras (Watchman 1992b) et de la matière organique non identifiée (Francis *et al.* 1993) ont été utilisés afin de dater des oeuvres rupestres. Toutefois, notons que d'autres substances carbonées ont été identifiées dans ces revêtements minéraux, compliquant ainsi le processus de datation et menant à des interprétations parfois controversées sur l'âge de certains sites rupestres et plus spécifiquement sur des sites contenant du charbon (Beck *et al.* 1997), du charbon de bois (McDonald *et al.* 1990; Beck *et al.* 1998; Llosas *et al.* 1999) et du graphite (Watchman 1995).

La datation au carbone-14 de matières organiques non identifiées n'est pas une donnée fiable, car la relation entre les composants carbonés d'origine inconnue et l'événement que l'on veut dater sont incertains. Conséquemment, l'identification des composants organiques sélectionnés pour la datation doit être parfaitement documentée. De plus, il est important de souligner que le carbone peut provenir de plusieurs sources et réservoirs ayant des âges différents (Tableau 1).

Tableau 1 : Sommaire des principaux composants carbonés trouvés dansles dépôts minéraux de surface, étendues typiques de leur environnement et âges de formation. Source Watchman (2000).

Carbon component	Formation conditions	Formation age range
cellulose	plants grow on the Earth's surface, leaf, stem and bark can be transported from one sedimentary environment to another. ^{14}C age reflects atmosphere at time of growth.	Quaternary
lichen	grow on stable surfaces or hyphae penetrate the underlying rock. Dead fragments can be transported. ^{14}C age either reflects atmosphere at time of growth or component from rock nutrient.	Quaternary
algae (diatoms)	live in meteoric water on rock surfaces. ^{14}C age either reflects atmosphere at time of growth or contribution from bicarbonate ions from 'hard' water	Quaternary
fungi	live on stable rock surfaces and in cracks. ^{14}C age either reflects atmosphere at time of growth, old 'dead' micro-organism, bicarbonate ions or nutrient components from rock	Quaternary
oxalate salts	produced from fungi, lichen, algae, bacteria on dusty stable surfaces. ^{14}C age reflects atmosphere at time of growth and/or substrate contribution	Quaternary
charcoal	derived from the burning of wood cellulose at the surface	Quaternary
organic matter	unknown substances from unknown processes and origins. Unreliable ^{14}C age	Quaternary or older
coal	metamorphism of plant remains at elevated temperature and pressure at depth beneath the Earth's surface	Meso-zoic/Palaeozoic
graphite	metamorphism of carbon-bearing substances at high pressure and temperature at depth beneath the Earth's surface	Meso-zoic/Palaeozoic

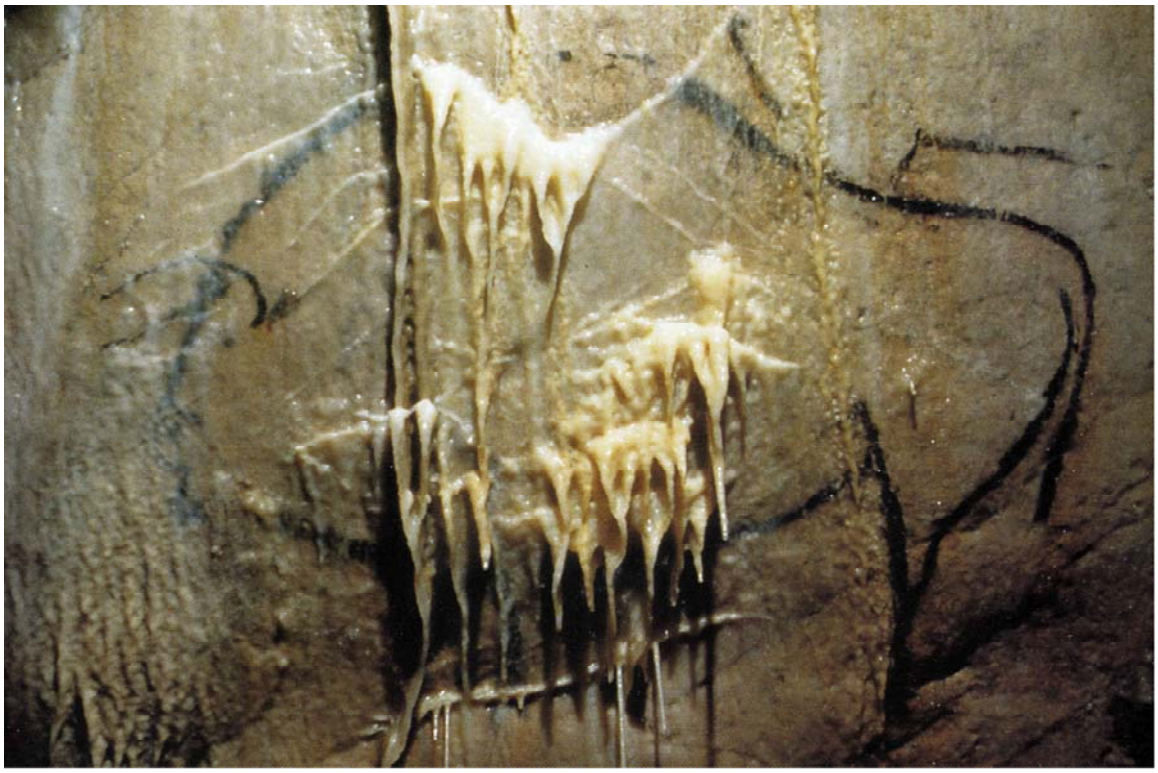

Figure 1. Photographie montrant un dessin au charbon de bois d'âge inconnu, Réseau Clastres, France. Source: Ministère de la Culture et de la Communication, France.

Les enduits minéraux offrent en effet la possibilité d'établir l'âge d'œuvres rupestres lorsque celles-ci en sont recouvertes. Les dépôts de carbonate et les vernis minéraux 'rock varnishes' peuvent théoriquement être datés en utilisant le principe de déséquilibre isotopique urarium-thorium. Dans cette recherche, la datation par les séries de l'uranium sera utilisée pour démontrer la fiabilité de cette technique qui permet de dater les enduits minéraux associés aux œuvres rupestres.

Les travertins et les vernis minéraux ne sont pas purs et le thorium et l'uranium d'origine détritique peuvent être incorporés dans les couches minérales. Afin d'éliminer ces contaminants potentiels, différentes techniques sont proposées. Pour le vernis minéral, un protocole de microextraction chimique séquentielle sera utilisé, cette technique permettant de séparer les phases organiques, carbonatées, les oxydes de fer et de manganèse, les phosphates et les sulfures pouvant contenir des quantités importantes d'uranium et de thorium. À l'aide de la spectrométrie de masse à multicollecteurs (MC-ICP-MS), les échantillons peuvent par la suite être datés en utilisant le principe du déséquilibre isotopique uranium-thorium.

L'art rupestre apporte des renseignements multiples sur les modes de vie et sur tout ce qui constituait le monde matériel et spirituel de civilisations disparues. Les dessins, peintures ou gravures rupestres pourront désormais être datés en déterminant l'ancienneté relative des dépôts minéraux situés soit immédiatement en dessous et au-dessus de la couche de matière pigmentée ayant servie à dessiner ou à peindre des motifs tracés en contexte rupestre, soit à la surface d'une gravure. Étant donné que l'âge des œuvres est d'une importante capitale à toute discussion concernant l'affiliation culturelle du groupe producteur par rapport à l'art rupestre préhistorique, considérant le fait que la méthode de datation proposée n'a jamais été utilisée, la mise au point de cette méthode peut constituer un point tournant pour l'étude de la préhistoire humaine, particulièrement sur l'évolution du développement cognitif et culturel de l'humanité.

1.3.2 La datation des os et des dents fossiles

Pour comprendre l'évolution de l'Homme, il est absolument nécessaire de connaître l'âge des fossiles humains. Cette information est généralement extraite de nombreuses sources incluant la géologie locale, la faune, la flore, ainsi que les artefacts présents en contexte archéologique. Dans la plupart des cas, cette approche de datation indirecte est non satisfaisante car :

(i) les restes humains sont souvent enfouis dans des sédiments et leur relation avec d'autres matériaux est incertaine.

(ii) les restes fauniques et les minéraux présents dans les sédiments proviennent souvent d'anciens dépôts et peuvent être plus vieux que le sédiment lui-même.

(iii) les restes humains ont été découverts à une époque où aucune fouille archéologique minutieuse n'avait été réalisée ayant comme conséquence l'impossibilité de corréler les restes humains avec d'autres matériaux datables. À noter que cette prémisse prévaut pour plus de 90% des fossiles humains découverts.

La datation directe des restes humains règlerait la plupart de ces problèmes. Jusqu'à récemment, ces derniers ne pouvaient être datés directement que par le radiocarbone, cette méthode de datation ayant une limite d'environ cinquante mille ans. Ainsi, les vieux fossiles (âgés de plus de cinquante mille ans) ne peuvent pas être utilisés pour étudier l'évolution de l'Homme. De plus, la plupart des méthodes de datation endommagent les restes humains qui sont rares et précieux. Il

est important de ne pas trop les altérer. Il est donc impératif de développer et d'appliquer des techniques permettant l'analyse de restes humains plus âgés que cinquante mille ans sans les abimer.

La datation par les séries de l'uranium a été appliquée avec succès aux coraux (Edwards *et al.* 1987a,b, Bard *et al.* 1990, 1998) ainsi qu'aux spéléothèmes (Beck *et al.* 2001). Malheureusement, ces matériaux ne sont presque jamais (coraux) ou rarement associés directement aux spécimens paléoanthropologiques. Des incrustations de calcite ou de calcaire ont été observées sur des fossiles humains à Petralona (Liritzis 1980; 1982 Shen et Yokoyama 1984), Guattari (Blanc 1939; Schwarcz et al 1991), Singa (McDermott *et al.* 1996) et Liujiang (Shen *et al.* 2002). Des situations où des sédiments contenant du matériel archéologique sont intercalés entre deux couches de spéléothèmes ont également été observées (à La Chaise-de-Vouthon: Schwarz et Debenath 1979, Blackwell *et al.* 1983, 1992; ou à Tournal Cave: Bischoff *et al.* 1988). Néanmoins, ces situations demeurent extrêmement rares.

La datation par séries-U des os et des dents archéologiques s'avère très problématique, car ils ne se conforment pas aux présuppositions de la méthode selon lesquelles l'uranium doit être présent dès la formation et qu'il ne doit être ni gagné ni perdu sauf par désintégration radioactive. Il est bien établi que les os et les dents constituent des systèmes ouverts pour l'uranium, quoique plusieurs tentatives de datation par les séries de l'uranium y ont été effectuées. Cette situation s'explique en partie par la limite d'âge atteinte par la méthode de datation au radiocarbone (~50 ka) et par le fait qu'il est très rare de retrouver d'autres types de matériel datable en contexte archéologique (voir plus haut). Les os et les dents accumulent l'uranium depuis leurs sites d'enfouissement et l'habileté à les dater repose entièrement sur notre compréhension et sur la modélisation de cette intrusion en uranium.

Dans cette recherche doctorale, les techniques d'ablation laser et d'ICP-MS à multicollecteurs seront utilisées afin de cartographier la distribution isotopique des séries de l'uranium appartenant à une dent de Néanderthalien. Cette méthodologie apportera une nouvelle compréhension de la complexité du processus de diffusion de l'uranium dans les dents

fossilisées. Ces résultats auront sans doute un impact majeur sur l'interprétation la datation des fossiles humains.

2 DATATION PAR LES SÉRIES DE L'URANIUM

Les datations radiométriques s'appuient sur un siècle de développements théoriques et technologiques qui ont permis un raffinement continuel de la justesse et de la précision des dates obtenues. Ce chapitre se veut une introduction aux techniques et instrumentations ; il présente tous les derniers développements technologiques nécessaires à la réalisation de cette thèse.

La datation par les séries de l'uranium (séries-U) est basée sur la mesure du déséquilibre isotopique dans les deux chaînes de désintégration des deux principaux isotopes d'uranium trouvés à l'état naturel, à savoir celles de l'^{238}U (abondance naturelle = 99,28%: Cowan et Alder 1976, $T_{1/2}$ = 4,4683±0,0024 10^9a : Jaffey *et al.* 1971) et l'^{235}U (abondance naturelle = 0,71% : Cowan et Alder 1976, $T_{1/2}$ = 7,0381±0,0048 10^8a : Jaffey *et al.* 1971). Le troisième isotope naturel de l'uranium, l'^{234}U, fait partie de la chaîne de désintégration de l'^{238}U (fig. 2) et ne compte que pour 0,0054% du total des trois isotopes.

L'^{238}U et l'^{235}U se désintègrent par émission d'énergie, principalement sous la forme de rayonnements α (noyau d'hélium [2 protons + 2 neutrons] accompagnant la transformation de l'espèce X en espèce Y) et β (électron [β^-] ou positron [β^-] provenant respectivement de la conversion d'un neutron en proton et d'un proton en neutron). La désintégration produit successivement une série d'éléments fils pour s'interrompre finalement par la formation des isotopes stables ^{206}Pb et ^{207}Pb. Le déséquilibre observé entre l'^{234}U ($T_{1/2}$ = 245259±490a : Cheng *et al.* 2000) et le ^{230}Th ($T_{1/2}$ = 75690±230a : Cheng *et al.* 2000) ainsi que celui observé entre l'^{235}U et le ^{231}Pa ($T_{1/2}$ = 32713±110a : Robert *et al.* 1969) sont d'un intérêt particulier. La seule autre chaîne de désintégration naturelle, celle du ^{232}Th, produit l'isotope stable ^{208}Pb (fig. 2). Cette dernière n'est pas utilisable pour dater les matériaux de la période quaternaire (de l'actuel à 2-3 Ma), car tous les isotopes issus de cette chaîne ont de très courtes demi-vies, de quelques centaines de nanosecondes à quelques années, ce qui les rend inutilisables pour des datations dans le domaine d'âges qui nous intéresse.

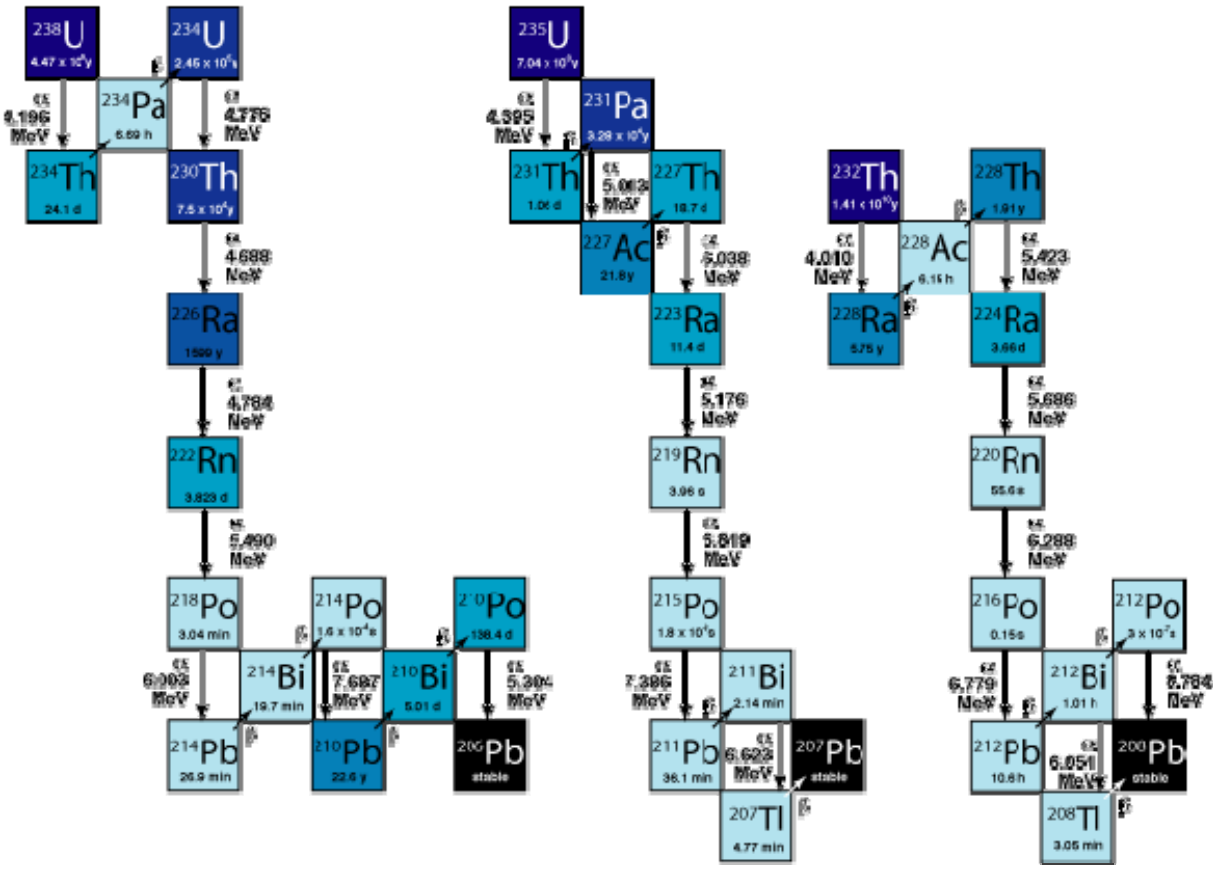

Figure 2. **Les deux chaînes de désintégration de l'uranium et celle du ^{232}Th. Source: Knolls Atomic Power Laboratory.**

2.1 Historique

Le phénomène de la radioactivité fut découvert par Becquerel en 1896 alors qu'il faisait des recherches sur la fluorescence des sels d'uranium (Becquerel 1896a,b). Cette découverte poussa Marie Curie à étudier la radioactivité de plusieurs minéraux et composés minéraux. Elle démontra que la radioactivité provient particulièrement de l'uranium et du thorium (Curie 1898). Après avoir observé que l'uranium pur était moins radioactif que certains composés naturels d'uranium, Curie synthétisa un de ces composés et constata que ce dernier était moins radioactif que le composé naturel. Cette découverte laissait croire à la présence d'impuretés radioactives dans le composé naturel (Curie 1898), mais elles étaient en fait de nouveaux éléments : le polonium et le radium (Curie et Curie 1898; Curie *et al.* 1898).

Rutherford fut le premier à élaborer la théorie de la désintégration en documentant d'abord les rayonnements α et β (Rutherford 1899). Il identifia ensuite de nouvelles substances radioactives et les plaça dans des séries en décrivant le concept de demi-vie (Rutherford 1900, 1903, 1904). Avec l'amélioration des connaissances sur les chaînes de désintégration, il fut ensuite reconnu que certains minéraux pourraient être datés en mesurant les quantités d'uranium et de plomb qu'ils contenaient (Boltwood 1907).

Après avoir constaté que certaines substances ayant des propriétés radioactives et des masses moléculaires différentes ne pouvaient pas être chimiquement séparées, Soddy (1910) proposa en fait l'existence de plusieurs formes du même élément. En 1913, il introduit le terme 'isotope' et établit que chaque isotope possède une masse et une demi-vie distinctes. La même année, Fajans (1913) publia la chaîne de désintégration naturelle de l'^{238}U, celle-ci étant d'ailleurs remarquablement proche de celle utilisée aujourd'hui.

Le travail fondamental nécessaire à l'établissement des chaînes de désintégration de l'uranium et du thorium était presque complété en 1913, dix-sept (17) ans seulement après la découverte de la radioactivité. Quarante (40) années seront nécessaires pour que des techniques de mesure en routine soient développées et systématiquement appliquées en Sciences de la Terre.

Dans les années cinquante, l'analyse systématique du ^{207}Pb /^{206}Pb dans les minéraux terrestres et les météorites a mené à l'âge actuellement admis pour le système solaire d'environ 4,6 milliards d'années (Russell et Farquhar 1960; Allègre *et al.* 1995). Richards *et al.* (1998) furent les premiers à appliquer la datation U-Pb pour dater des spéléothèmes ayant des âges dans la gamme de trois cent mille ans.

Barnes *et al.* (1956) ont mesuré l'^{238}U et le ^{230}Th par spectrométrie alpha dans des carottes de coraux provenant des îles Marshall. Ils ont observé un déséquilibre croissant entre le ^{230}Th et l'^{238}U vers la surface et ont conclu que le rapport thorium-uranium dans un spécimen particulier pourrait indiquer l'âge de celui-ci. Sackett (1958) a suggéré l'utilisation du ^{231}Pa et du ^{230}Th pour dater les carbonates. Ku (1968) a démontré qu'on pouvait utiliser le ^{231}Pa et le ^{230}Th comme contrôle pour s'assurer d'un système fermé. Les premières analyses des séries de l'uranium provenant d'ossements archéologiques ont démontré que ceux-ci se comportent en tant que système ouvert (Rosholt et Antal 1962, Cherdyntsev *et al.* 1963, 1965). L'application de la

spectrométrie de masse à thermo-ionisation (TIMS) pour la mesure de l'^{238}U, de l'^{234}U et du ^{230}Th (Edwards *et al.* 1987a,b) a été une percée majeure pour la datation par les séries de l'uranium, car de petits échantillons peuvent désormais être analysés avec grande précision (semblable à l'AMS pour la datation au ^{14}C). Edwards *et al.* (1997) ont démontré que le ^{231}Pa pouvait également être mesuré par TIMS. Stirling *et al.* (2000) ont utilisé le tout nouveau ICP-MS à multicollecteurs couplé à un système d'ablation laser (LA-MC-ICP-MS) pour mesurer in situ l'^{238}U, l'^{234}U et le ^{230}Th. Eggins *et al.* (2003) ont employé le LA-ICP-MS pour analyser in situ les isotopes d'uranium dans des os et des dents provenant de sites archéologiques.

Les études les plus complètes portant sur l'application des séries de l'uranium en Sciences de la Terre sont écrites dans les livres édités par Ivanovich et Harmon (1992) et plus récemment par Bourdon *et al.* (2003). Des revues sur la datation par les séries de l'uranium ont été publiées aussi par Schwarcz (1993, 1997), Ku (2000), Latham (2001) et Pike et Pettitt (2003).

2.2 Principe de base

L'élément uranium a deux chaînes de désintégration naturelles, les isotopes pères étant l'^{238}U et l'^{235}U (fig. 2). Le principe de datation par les séries de l'uranium est basé sur le comportement géochimique différent de l'uranium (U), du thorium (Th) et du protactinium (Pa). L'uranium dans l'état d'oxydation U^{VI} est hydrosoluble, tandis que le Th et le Pa sont pratiquement insolubles dans l'eau. Notons que la présence de colloïdes dans les eaux de surface peut complexer le Th. Les eaux naturelles pauvres en colloïdes contiennent donc des traces d'U, mais sont pratiquement exemptes de Th et de Pa. Les minéraux précipitant à partir de l'eau tels que les carbonates secondaires (spéléothèmes, travertins, coquilles, coraux etc.) contiennent de l'uranium, mais aucun Th et Pa. Par conséquent, en l'absence de particules minérales détritiques, le taux d'activité du ^{230}Th/^{234}U dans la chaîne de désintégration de l'^{238}U ainsi que celui du ^{231}Pa/^{235}U de la chaîne de désintégration de l'^{235}U sont à zéro au moment de la formation (t=0). Avec le temps, les isotopes des chaînes de désintégration sont produits afin d'atteindre ultimement l'équilibre séculaire, c'est-à-dire tous les taux d'activité sont à 1 (fig. 3).

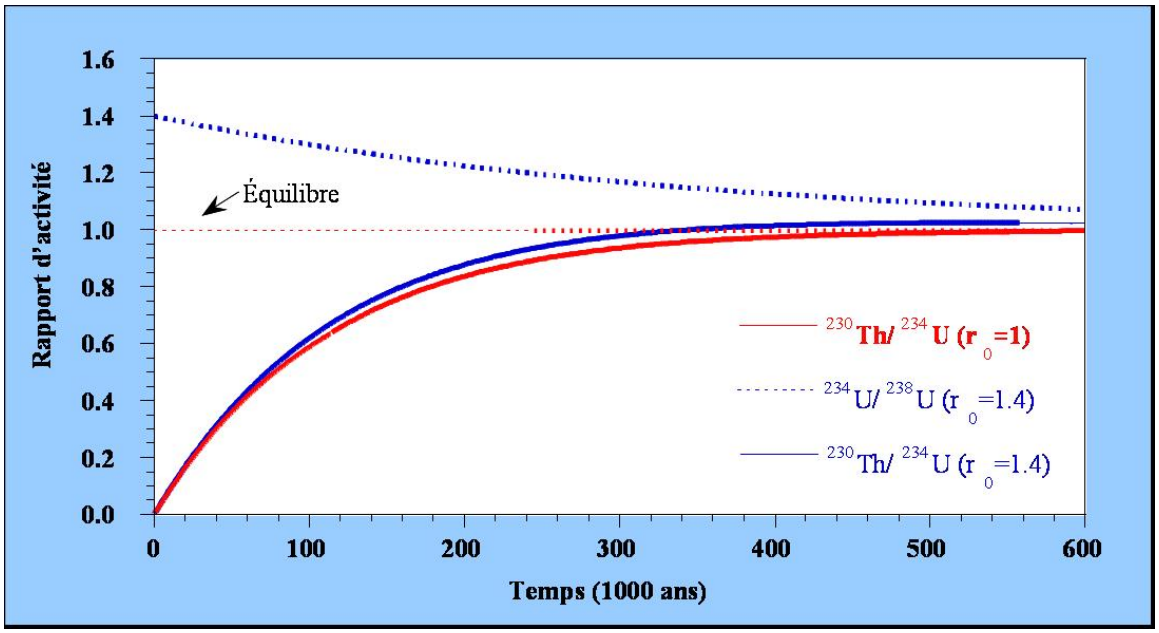

Figure 3. L'accumulation du ^{230}Th radioactif résulte de la désintégration de l'^{234}U. Ce dernier est lui-même en équilibre radioactif avec son isotope père, l'^{238}U. Les concentrations en ^{230}Th augmentent jusqu'à ce que le nombre de noyaux qui se désintègrent équilibre le nombre de noyaux qui se forment.

Si, initialement, aucun atome d'un isotope fils n'est présent, l'activité du rejeton, A_r est exprimée par :

$$A_r = A_p\left(1 - e^{(-\lambda_d t)}\right) \tag{1}$$

où A_p représente l'activité de l'isotope père et λ_d représente la constante de désintégration de l'isotope fils. L'activité du ^{231}Pa est exprimée par :

$$^{231}Pa = {}^{235}U\left(1 - e^{(-\lambda_{231} t)}\right) \tag{2}$$

où λ_{231} représente la constante de désintégration de ^{231}Pa. L'activité du ^{230}Th est exprimée par :

$$^{230}Th = {}^{234}U\left(1 - e^{(-\lambda_{230} t)}\right) = {}^{238}U\left(1 - e^{(-\lambda_{230} t)}\right); si \frac{^{234}U}{^{238}U} = 1 \tag{3}$$

où λ_{230} représente la constante de désintégration du ^{230}Th. L'équation (3) requiert que l'^{234}U et l'^{238}U soient à équilibre séculaire à t = 0 (i.e. quand l'uranium est incorporé dans l'échantillon). Ce n'est habituellement pas le cas, car la plupart des eaux naturelles ont un excès en ^{234}U comparativement à l'^{238}U. À cause de sa longue demi-vie, l'excès en ^{234}U doit être pris en considération :

$$\frac{^{230}Th}{^{238}U} = \left(1 - e^{(-\lambda_{230} t)}\right) + \frac{\lambda_{230}}{\left(\lambda_{230} - \lambda_{234}\right)}\left(\frac{^{234}U}{^{238}U} - 1\right)\left(1 - e^{-(\lambda_{230} - \lambda_{234})t}\right) \qquad (4)$$

où λ_{234} est la constante de désintégration de l'^{234}U. S'il y a excès en ^{234}U, le ratio d'activité ^{230}Th/^{238}U peut temporairement dépasser 1 ; néanmoins, il va éventuellement diminuer pour atteindre l'équilibre séculaire en accord avec l'équation (1). Dans les publications récentes, le ratio d'activité ^{234}U/^{238}U est exprimé en notation δ^{234}U, où δ^{234}U = (^{234}U/^{238}U - 1) x 1000 (i.e. un ratio d'activité ^{234}U/^{238}U de 1.15 équivaut à une valeur δ^{234}U de 150). En raison de la complexité de l'équation (4), le calcul d'une évaluation d'âge des séries-U exige des procédures mathématiques itératives. Pour faciliter la visualisation des âges, des diagrammes d'évolution isotopique sont donc employés pour la présentation des âges Th/U (fig. 4).

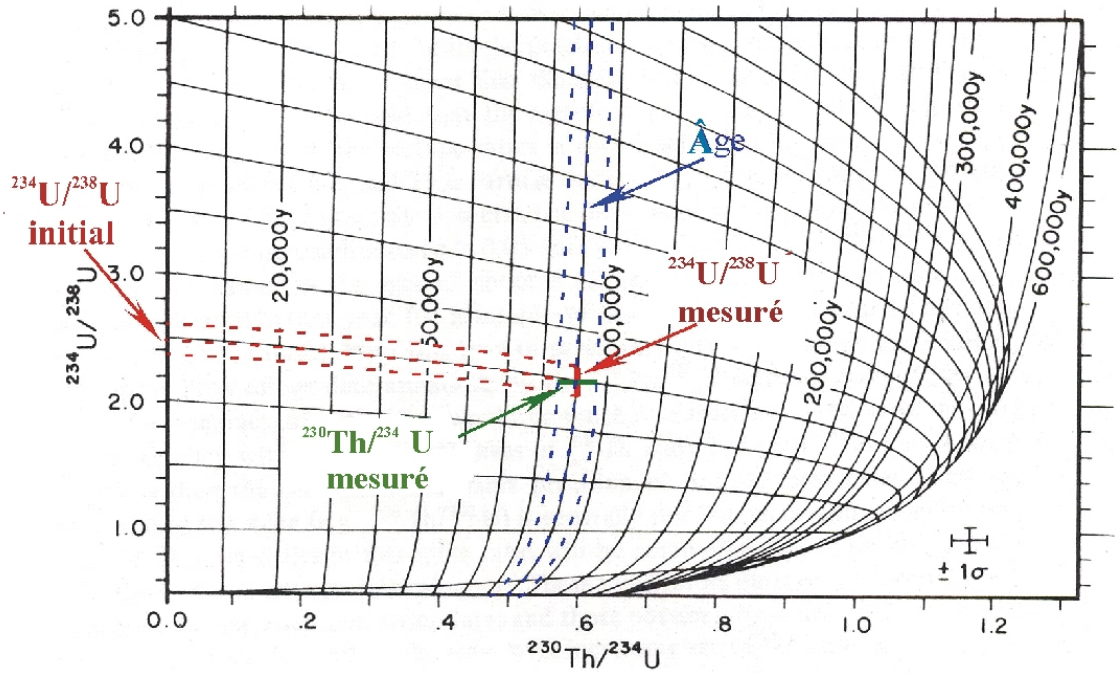

Figure 4. Exemple d'un diagramme d'évolution isotopique.

2.3 Mesure

Les techniques de mesure pour dater des échantillons par les séries-U ont été récemment passées en revue par Goldstein et Sterling (2003). Jusqu'à la fin des années 1980, les isotopes des séries-U étaient mesurés par spectrométrie alpha. Une autre alternative, la spectrométrie gamma (Yokoyama et Nguyen 1980) a pour inconvénient que les rayons gamma sont émis en très faibles quantités résultant en des erreurs analytiques considérablement plus grandes que pour la spectrométrie alpha. Cependant, la spectrométrie gamma a l'avantage d'être non destructive et les échantillons ne nécessitent aucune préparation.

Edwards *et al.* (1987a,b) furent les premiers à employer la spectrométrie de masse pour la mesure combinée de l'^{238}U, de l'^{234}U, et du ^{230}Th. Semblables aux mesures par AMS pour le radiocarbone, les mesures isotopiques par spectrométrie de masse sont beaucoup plus précises que les spectrométries alpha et gamma. Par conséquent, la limite d'âge calculée est passée d'environ 350 ka à environ 500 ka. De plus, des échantillons beaucoup plus petits peuvent être analysés. Edwards *et al.* (1997) ont démontré que le ^{231}Pa pouvait également être mesuré par

spectrométrie de masse. Les développements récents dans les techniques d'ablation laser et d'ICP-MS à haute résolution ont démontré que l'analyse *in situ* des isotopes des séries-U dans les os et les dents est réalisable (Eggins *et al.* 2003). Le spectromètre de masse utilisé pour cette recherche fait l'objet de l'item 2.8 de ce chapitre.

2.4 Isochrones

Beaucoup de carbonates en particulier les spéléothèmes et les travertins peuvent contenir du matériel détritique dans lequel les chaînes de désintégration de l'uranium sont en équilibre. Lors de la préparation chimique des échantillons en laboratoire, le Th et l'U sont non seulement dérivés de la matrice de calcite, mais également du matériel détritique compris dans les inclusions ou en périphérie des grains de carbonate. Ainsi, l'hypothèse de base assumant que l'échantillon ne contient aucun ^{230}Th à t = 0 est fausse. Cependant, le matériel détritique contient également du ^{232}Th qui n'est pas présent dans la structure cristalline de la calcite. Puisque le comportement chimique des deux isotopes de Th est identique, le ^{232}Th peut être employé pour estimer la quantité initiale de ^{230}Th dans l'échantillon par l'utilisation d'isochrones. Les données pour les isochrones peuvent être obtenues en dissolvant partiellement l'échantillon avec des solutions acides de concentrations croissantes ou en choisissant des échantillons contemporains contenant différentes quantités de matériel détritique (pour les détails voir Ku et Liang 1984, Schwarcz et Latham 1989, Przybylowicz *et al.* 1991). Cela mène à des quantités variables de ^{232}Th dissous (et de ^{230}Th détritique) dans les solutions à analyser.

2.5 Limite de la méthode

La limite d'âge atteinte par la méthode de datation par les séries-U dépend de la capacité à mesurer précisément les rapports isotopiques près de l'équilibre. Cela dépend de la taille des erreurs qui est fonction des concentrations dans l'échantillon et du système de détection utilisé. Pour le système ^{230}Th/^{234}U, le MC-ICP-MS et le TIMS peuvent être utilisés pour estimer des âges jusqu'à environ 500 ka, la spectrométrie alpha à environ 350 ka et la spectrométrie gamma à environ 250 ka. Pour le système ^{231}Pa/^{235}U, les âges limites sont approximativement de 200, 130 et 100 ka pour le MC-ICP-MS/TIMS, la spectrométrie alpha et la spectrométrie gamma.

2.6 Erreurs analytiques et précision +/-

En raison de la nature exponentielle de la fonction d'âge, les erreurs d'âges des séries-U sont nécessairement asymétriques. Des âges peuvent être calculés aussi longtemps que le rapport mesuré $^{230}Th/^{234}U$ est statistiquement distinct de l'équilibre. Ludwig (2003) a décrit les détails de la propagation d'erreurs. Le programme Isoplot (Ludwig 2001) qui peut être obtenu directement de Kenneth Ludwig (kludwig@bgc.org) offre des procédures complètes pour le calcul d'erreur. Près de l'équilibre, les stratégies de modélisation Monte-Carlo sont préférées pour estimer les erreurs. À ce propos, les principales sources d'erreur pour les datations par les séries-U concernent la mobilité de l'uranium, cette situation empêchant entre autres la datation des coquilles de mollusque (Kaufman et al 1971). Les coraux sont également enclins à la recristallisation et à la migration de l'uranium après déposition. Certains de ces effets peuvent être identifiés en mesurant le rapport $^{234}U/^{238}U$ et en les comparant à la valeur $^{234}U/^{238}U$ de l'eau de mer moderne qui est de 1,144±0,002 (Chen *et al.* 1986). Étant donné la nature variable du rapport $^{234}U/^{238}U$ des eaux terrestres, ce contrôle de qualité ne peut pas être appliqué aux échantillons terrestres.

2.7 Préparation des échantillons

Comme la préparation des échantillons est laborieuse et que le recouvrement chimique peut varier considérablement d'un échantillon à l'autre, les concentrations élémentaires précises sont déterminées avec l'aide de méthodes de dilution isotopique. Cette technique est basée sur la détermination de la composition isotopique d'un élément dans un mélange contenant une quantité connue d'un traceur isotopique et une quantité inconnue de l'élément à analyser. Le traceur est une solution contenant une concentration connue d'un ou plusieurs éléments pour lesquels la composition isotopique a été changée par l'enrichissement de un ou de plusieurs de ses isotopes.

Afin d'éliminer les interférences sur la masse ou sur le spectre de désintégration énergétique des éléments des séries-U, il est nécessaire de les purifier. Cette manipulation est également requise afin d'optimiser l'ionisation. Les résines d'extraction chromatographique sont faites de grains inertes recouverts d'un extractant organique qui peut être sélectif pour une série d'éléments en

solution (fig. 5). Pour cette recherche, la résine Tru.spec fut utilisée, celle-ci ayant l'avantage de nécessiter beaucoup moins de solutions acides que les résines conventionnelles comme la Downex. Le protocole utilisé est détaillé au tableau 3.

Figure 5. **Photo montrant le montage utilisé pour l'extraction chromatographique sur colonnes.**

2.8 Spectrométrie de masse à source plasma à couplage inductif et multicollection

Afin de déterminer les ratios isotopiques d'uranium et de thorium, un spectromètre de masse à plasma induit à haute résolution et équipé de multicollecteurs (Neptune MC-ICP-MS) a été utilisé, le prototype employé ayant été fabriqué par Thermo Corporation (fig. 6). Le Neptune est un spectromètre à multicollecteurs de haute résolution à double focalisation utilisé pour l'analyse des rapports isotopiques à haute précision. Un diagramme simplifié est présenté à la figure 7.

Figure 6. **Le Neptune MC-HR-ICP-MS dans le laboratoire de la Research School of Earth Sciences (Australian National University).**

L'échantillon est introduit sous forme d'aérosol à pression atmosphérique. Les éléments sont ensuite vaporisés, atomisés et ionisés. Une partie infime de ces ions est introduite dans le spectromètre par le biais d'une série de cônes qui modifient le faisceau ionique en générant une basse pression (< 10^{-7} mBar), cette dernière étant requise pour une transmission efficace dans le spectromètre. Le faisceau ionique est ensuite focalisé et modelé (d'un rayon circulaire à rectangulaire) et accéléré via une série de lentilles et ce, avant d'être introduit dans l'analyseur électrostatique (ESA) qui crée un faisceau ionique ayant une distribution énergétique homogène. Cette opération est importante car, même si la source plasma à couplage inductif (ICP) est une source ionique très efficace, elle produit des ions ayant une large diffusion énergétique (15-20 V). Cette action a pour but de réduire le niveau d'interférence ionique polyatomique introduit dans le spectromètre de masse par l'ICP. L'analyseur électrostatique focalise ensuite le rayon ionique constitué d'énergie cinétique filtrée vers le secteur magnétique. Lorsqu'un analyseur électrostatique est installé devant le secteur magnétique, l'appareil est dit à double focalisation.

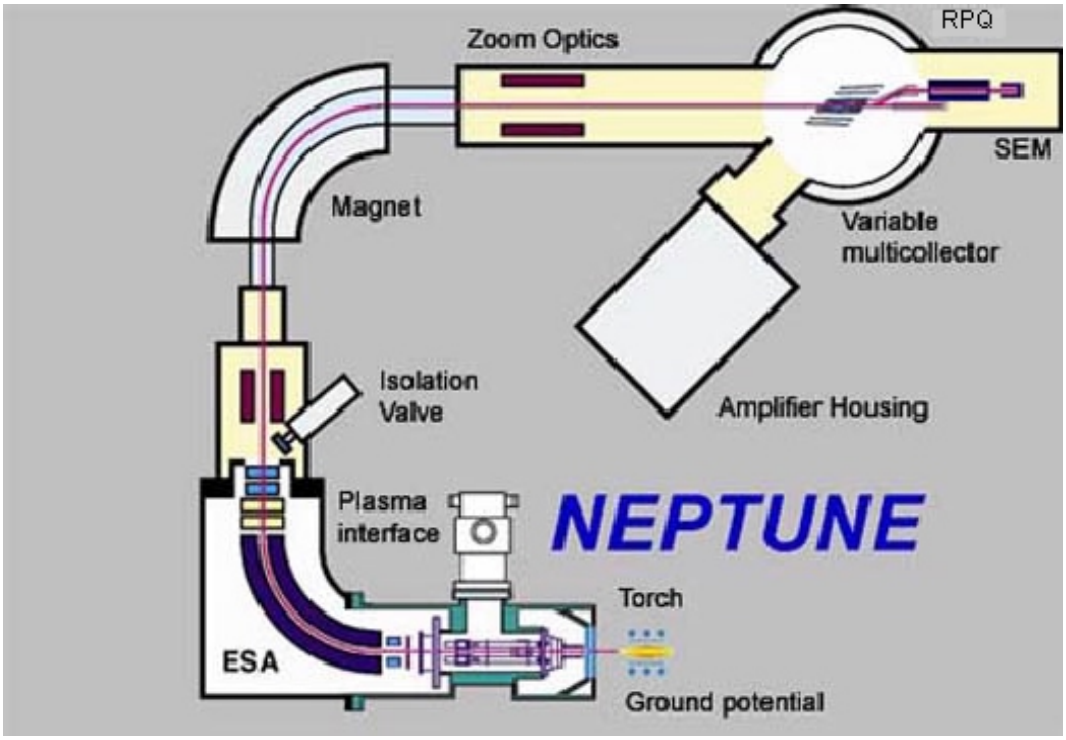

Figure 7. Diagramme simplifié du Neptune MC-HR-ICP-MS utilisé pour cette recherche. Source Thermo Electron Corporation.

Le faisceau ionique est donc subséquemment dispersé dans le secteur magnétique qui discrimine les ions selon leur ratio masse/charge (m/z). Ce faisceau ionique dispersé entre les pôles d'un aimant est ensuite projeté sur une rangée de cages de Faraday mobiles où la détection des ions et le comptage sont faits en mode multicollection, i.e. par détection simultanée des faisceaux dispersés. Le mode multicollection a l'avantage d'éliminer les petites fluctuations dans l'intensité du faisceau ionique causées par la relative instabilité de la source plasma à couplage inductif (ICP), améliorant ainsi la précision pour la mesure des ratios isotopiques. Le Neptune est équipé de huit (8) plates-formes de détecteurs mobiles et d'une autre fixe (fig. 8), chacune comportant une cage de Faraday et un détecteur à comptage ionique miniature. Les cages de Faraday sont connectées individuellement à un amplificateur de courant.

En plus des cages de Faraday, le faisceau ionique central peut être divergé vers un Secondary Electron Multiplier (SEM) permettant la détection des ions de basse intensité comme ceux qui sont produits par les isotopes de faible concentration tels l'^{234}U et le ^{230}Th (fig. 9). Le SEM multiplie le courant dans un faisceau d'électrons par l'incidence d'électrons accélérés sur la surface d'électrodes décentrées et, quand elles sont heurtées par un ion, ces électrodes décentrées éjectent des électrons secondaires multipliant ainsi le courant ionique. Comme les cages de Faraday ne peuvent être utilisées qu'en mode analogue, elles sont beaucoup moins sensibles que le SEM qui peut opérer en mode de comptage d'impulsions (mode digital). Un deuxième SEM sera bientôt installé sur le Neptune et permettra la détection simultanée de l'^{234}U et du ^{230}Th.

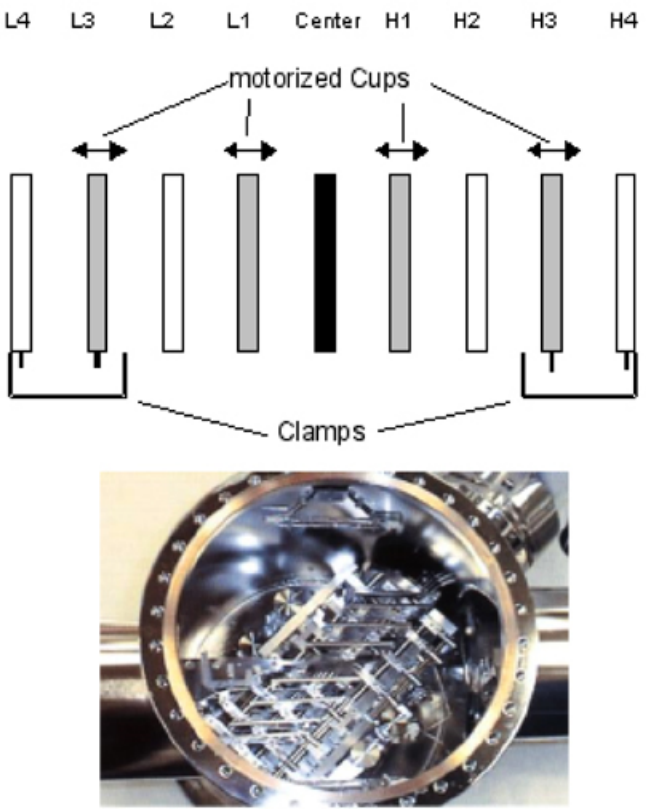

Figure 8. **Le système à multicollection comprend neuf (9) cages de Faraday (huit mobiles plus une fixe) et un Secondary Electron Multiplier (SEM) orienté vers le canal central. Source: Thermo Electron Corporation.**

Afin de diminuer les contributions des queues des faisceaux ioniques de haute intensité sur les signaux voisins de basse intensité (e.g, ^{232}Th sur ^{230}Th ou ^{238}U sur ^{234}U), un Retardation Potential Quadrupole (RPQ) est installé devant le SEM (fig. 10.). Le RPQ augmente de manière significative la sensibilité de l'instrument parce qu'il rejette toutes les particules ayant subi des pertes énergétiques causées par la dispersion du signal.

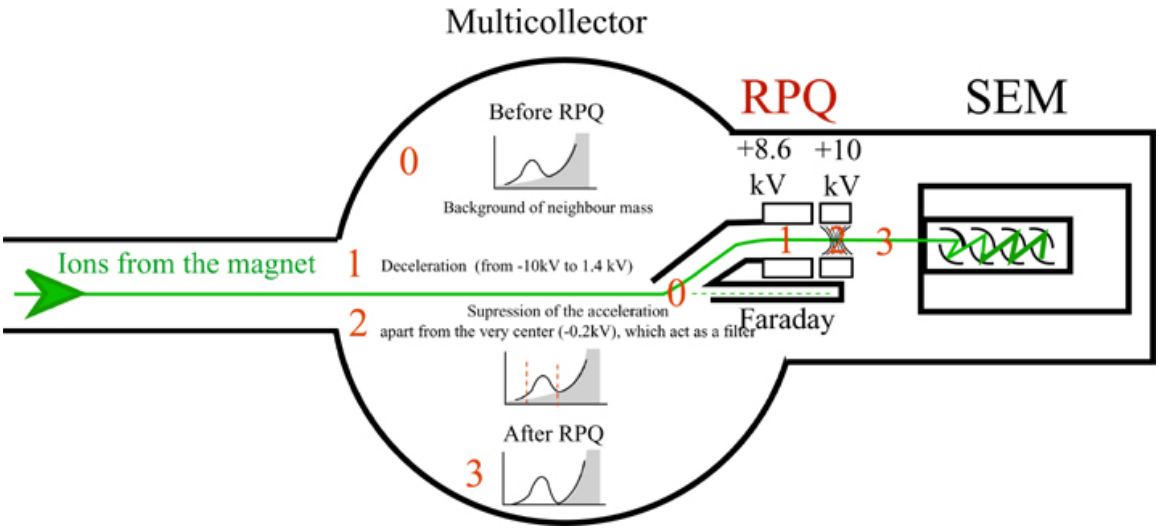

Figure 9. **Schéma montrant l'efficacité du Retardation Potential Quadrupole (RPQ). Source: Thermo Electron Corporation.**

3 DÉVELOPPEMENT DE TECHNIQUES DE DATATION PAR LES SÉRIES DE L'URANIUM *IN SITU* (ABLATION LASER MC-ICP-MS)

L'analyse des séries de l'uranium est présentement limitée par la nécessité d'utiliser des laboratoires équipés de salles blanches et requiert une préparation laborieuse des échantillons impliquant la dissolution, le dosage isotopique 'spiking', l'extraction et la concentration des isotopes sur colonnes. L'analyse *in situ* des isotopes des séries-U utilisant un système à ablation laser couplé à un spectromètre de masse à plasma induit à haute résolution et équipé de multicollecteurs (Neptune MC-ICP-MS) offre plusieurs avantages par rapport aux méthodes conventionnelles. Cette technique permet (i) l'analyse de la distribution des isotopes des séries-U (^{238}U, ^{234}U et ^{230}Th) à une résolution spatiale à l'échelle de 10–100 μm, (ii) n'exige aucune préparation chimique des échantillons et (iii) permet une mesure rapide. Même si ces avantages compensent largement la perte de sensibilité et de précision obtenues avec les techniques conventionnelles, cette technique nécessite au moins 1 ppm d'uranium et l'échantillon doit être relativement pur (faible en matière détritique).

3.1 Instrumentation

Le système présentement utilisé à la Research School of Earth Sciences/Australian National University comprend un laser Excimer HelEx ArF de 193 nm couplé soit à un ICP-MS à quadrupole (Varian 810-MS) ou soit à un Neptune MC-ICP-MS (Finnigan MAT). Le système a été optimisé pour l'analyse en haute résolution et utilise un design de chambre d'ablation unique (fig. 10). Par exemple, afin de réduire la déposition de condensation autour du site d'ablation, l'hélium au lieu de l'argon est utilisé comme médium d'ablation. Ceci permet également d'augmenter le flux de matière vers l'ICP. La chambre d'ablation a un volume d'environ 2,5 cm^3 minimisant ainsi le temps de résidence des particules vaporisées (~0.5 seconde). Quant aux échantillons, ils sont placés dans une autre chambre, celle-ci pouvant contenir des échantillons de différentes tailles (maximum 100 cm^2).

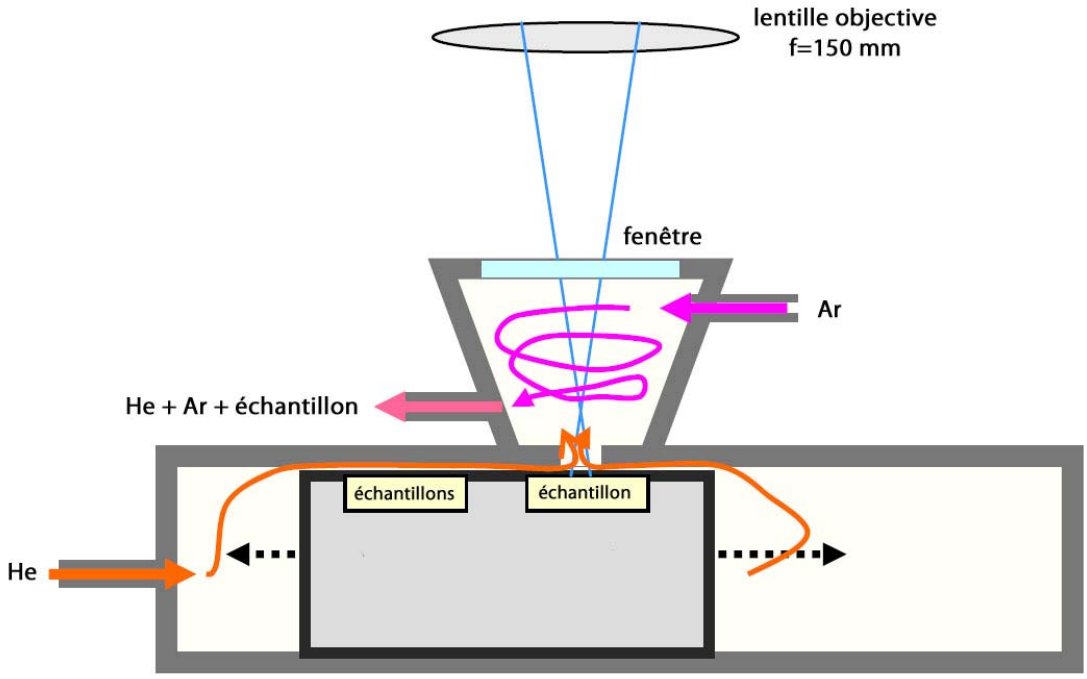

Figure 10. Le système à ablation laser utilisé à la Research School of Earth Sciences/Australian National University.

3.2 Datation des os et des dents archéologiques par les séries de l'uranium

Lorsqu'on tente de reconstruire l'évolution de l'Homme, il est absolument nécessaire de connaître l'âge des fossiles humains. Jusqu'à récemment, ces derniers ne pouvaient être datés directement que par le radiocarbone, cette méthode de datation ayant une limite d'environ cinquante mille ans. Ainsi, les vieux fossiles (plus de cinquante mille ans) ne peuvent pas être utilisés pour traiter de l'évolution humaine. De plus, la plupart des méthodes de datation détériorent les fossiles qui sont précieux et très rares. Pour l'analyse des vestiges humains de plus de cinquante mille ans, il est impératif de développer et d'appliquer des méthodes qui ne les endommagent pas ou très peu.

Il n'est pas facile de dater des os et des dents de la préhistoire par les séries de l'uranium sachant que ces vestiges ne se conforment pas aux présuppositions de la méthode affirmant que l'uranium doit être présent dès la formation et qu'il ne doit être ni gagné ni perdu sauf par désintégration radioactive. Les os et les dents accumulent l'uranium depuis les sites d'enfouissement et notre habileté à les dater repose entièrement sur notre compréhension et sur la modélisation de cette incorporation en uranium.

Les os et les dents contemporains ne contiennent que de très faibles concentrations en uranium (< 1 à 50 ppb, Tandon *et al.* 1998) en comparaison avec les spécimens archéologiques qui peuvent contenir plusieurs centaines de ppm d'uranium. Afin de dater ces os et ces dents fossiles, l'incorporation temporelle en uranium doit être reconstruite (fig. 11). Et, si cette intrusion en uranium est le principal processus géochimique, l'âge des séries-U calculé (selon l'hypothèse d'un système fermé) sous-évaluera l'âge réel de l'os ou de la dent. L'âge réel sera également sous-évalué si le thorium est lessivé hors du système. Il faut dire cependant que, dans la nature, ce phénomène de lessivage n'a jamais été observé. Par contre, si l'uranium présent dans les os et les dents originalement a subi le phénomène de lessivage hors du système, l'âge des séries-U sera surestimé. Cet âge sera également surestimé si l'os ou la dent contient du thorium détritique, quoiqu'il peut être détecté par la présence de ^{232}Th.

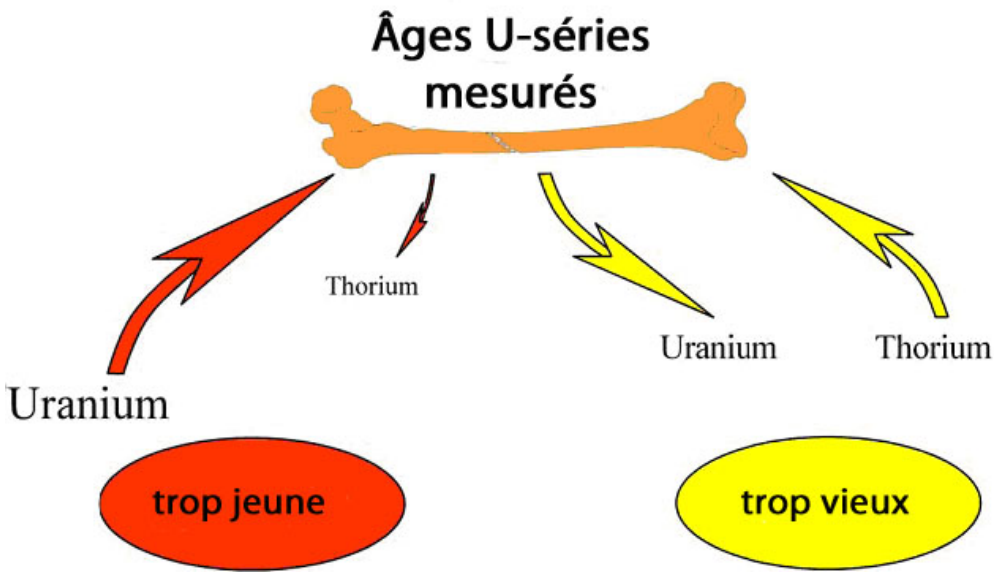

Figure 11. L'effet de la mobilité de l'uranium et du thorium sur l'âge des séries-U mesuré.

Le mécanisme favorisant l'intrusion d'uranium dans les os et les dents archéologiques implique la diffusion d'uranyle (UO_2^{2+}) suivie d'une adsorption sur la surface constituée d'hydroxyapatite minérale (Millard 1996; Millard et Hedges 1996; Pike *et al.* 2002). Le modèle de diffusion-adsorption (D-A) proposé par ces auteurs prédit la distribution spatiale de l'uranium et des isotopes des séries-U à travers un os ou une section d'émail dentaire. La diffusion constante d'uranium provenant des surfaces extérieures vers l'intérieur mène au développement de profils d'uranium en forme de ∪. Avec le temps, ces profils vont graduellement s'aplatir lorsque l'os s'équilibre avec l'uranium en solution (fig. 12A). La distribution des âges des séries-U suit un modèle semblable avec des âges de plus en plus jeunes vers le centre de l'os (fig. 12B). Si l'adsorption en uranium est un processus constant sans aucun changement dans le taux d'adsorption, les âges des séries-U modelés (selon le modèle de diffusion-adsorption (D-A) seront consistants dans tout l'os.

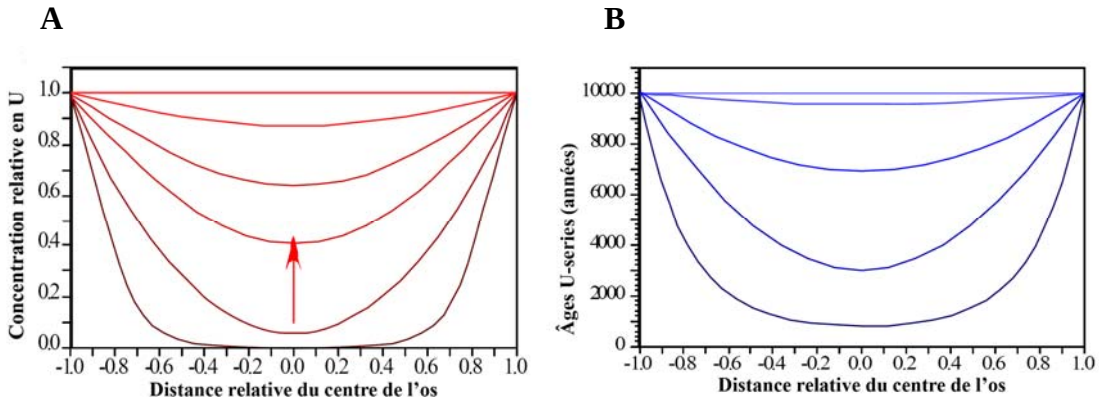

Figure 12. Le modèle de diffusion-adsorption de Millard et Hedges (1996).

A: Développement d'un profil de concentration en uranium normalisé selon le modèle D-A.
B: Âges des séries-U mesurés sur un os de 10 ka. Les âges sont modelés selon différents paramètres de diffusion-adsorption.

Le modèle D-A permet d'identifier les situations où il y a lessivage d'uranium hors du système. Ainsi, les concentrations en uranium à travers l'os ne seront pas constantes et les profils d'uranium n'auront pas la forme de ∪. Après avoir identifié ce problème, ces os sont tout simplement rejetés et ne sont pas soumis aux processus de datation. Le modèle D-A a également l'avantage de permettre l'identification des os ayant un historique complexe d'intrusion en

uranium. Par exemple, si l'intrusion en uranium s'est produite en deux épisodes distincts (fig. 13A), il est possible que le profil d'uranium ait une forme de ∪. Néanmoins, la distribution des âges des séries-U suivra un modèle inversé avec des âges de plus en plus vieux vers le centre de l'os (fig. 13B).

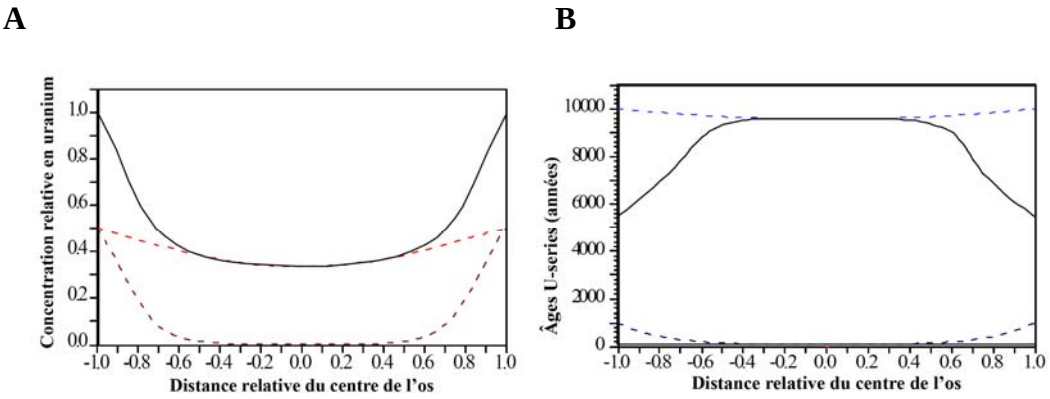

Figure 13. Incorporation d'uranium en deux phases distinctes. Le profil d'uranium semble se conformer au modèle ayant une forme de ∪ (A). Néanmoins, la distribution des âges des séries-U montre un modèle inversé avec des âges de plus en plus jeunes vers la surface de l'os (B).

Le lessivage de l'uranium hors du système peut également produire une concentration en uranium décroissante vers la surface de l'os (fig. 14A). Les âges des séries-U mesurés seront ainsi surestimés vers la surface de l'os (fig. 14B). Pour plus de détails, voir Pike *et al.* 2002.

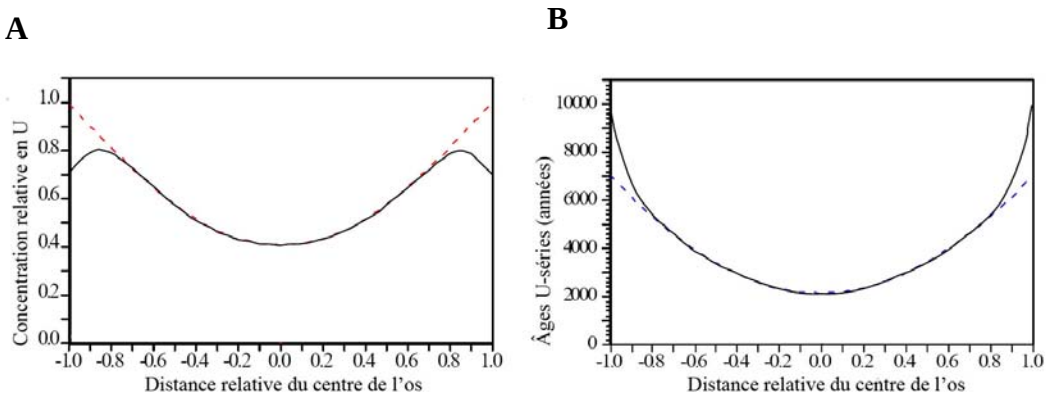

Figure 14. Le lessivage de l'uranium est démontrée par une concentration en uranium décroissante vers la surface de l'os (A). Les âges des séries-U mesurés seront surestimés vers la surface de l'os (B).

Il y a peut-être une situation où le modèle D-A ne peut pas être utilisé pour dater les os et dents fossiles. Des os peuvent avoir été enfouis pendant une longue période de temps sans accumuler d'uranium. Ultérieurement, à cause de changements dans les conditions hydrologiques locales, l'uranium devient mobile dans les environs du site et s'accumule dans les os. Cette situation est semblable au scénario présenté à la figure 13A, mais la quantité d'uranium accumulée lors de la deuxième phase d'incorporation est beaucoup plus grande que lors de la première phase. Ainsi, le modèle D-A peut donner des âges significativement sous-estimés sans nécessairement présenter une distribution d'âges des séries-U inversée (voir 13B).

3.3 Datation des os et des dents archéologiques par les séries de l'uranium *in situ* (ablation laser MC-ICP-MS)

Le modèle D-A a été établi en utilisant une méthodologie conventionnelle. Les échantillons provenant de différents emplacements dans l'os ou la dent étudiés ont été obtenus avec l'aide d'une micro-foreuse. Les concentrations en uranium ont ensuite été établies avec l'aide d'un ICP-MS en mode solution. Les os et les dents ayant un profil d'uranium en forme de ∪ sont ensuite soumis aux processus de datation. Ce processus comprend l'extraction chromatographique sur colonne et l'analyse des isotopes des séries-U avec l'aide d'un TIMS ou d`un MC-ICP-MS. L'analyse d'un seul os est un exercice laborieux et nécessite plusieurs semaines, voire plusieurs mois de travail.

Les récents développements dans le domaine des analyses *in situ* utilisant un système à ablation laser offrent plusieurs avantages. La préparation des échantillons se résume à couper l'os ou la dent de façon à exposer une surface plane pour le laser. Les échantillons sont d'abord analysés avec un ICP-MS à quadrupole et les échantillons ne présentant pas un profil en forme de $\cup$ et dont la concentration en uranium est inférieure à 1 ppm sont tout simplement rejetés (fig. 15). Ensuite, les échantillons retenus sont analysés avec un MC-ICP-MS. La collecte de données est relativement rapide et offre une résolution spatiale sans précédent.

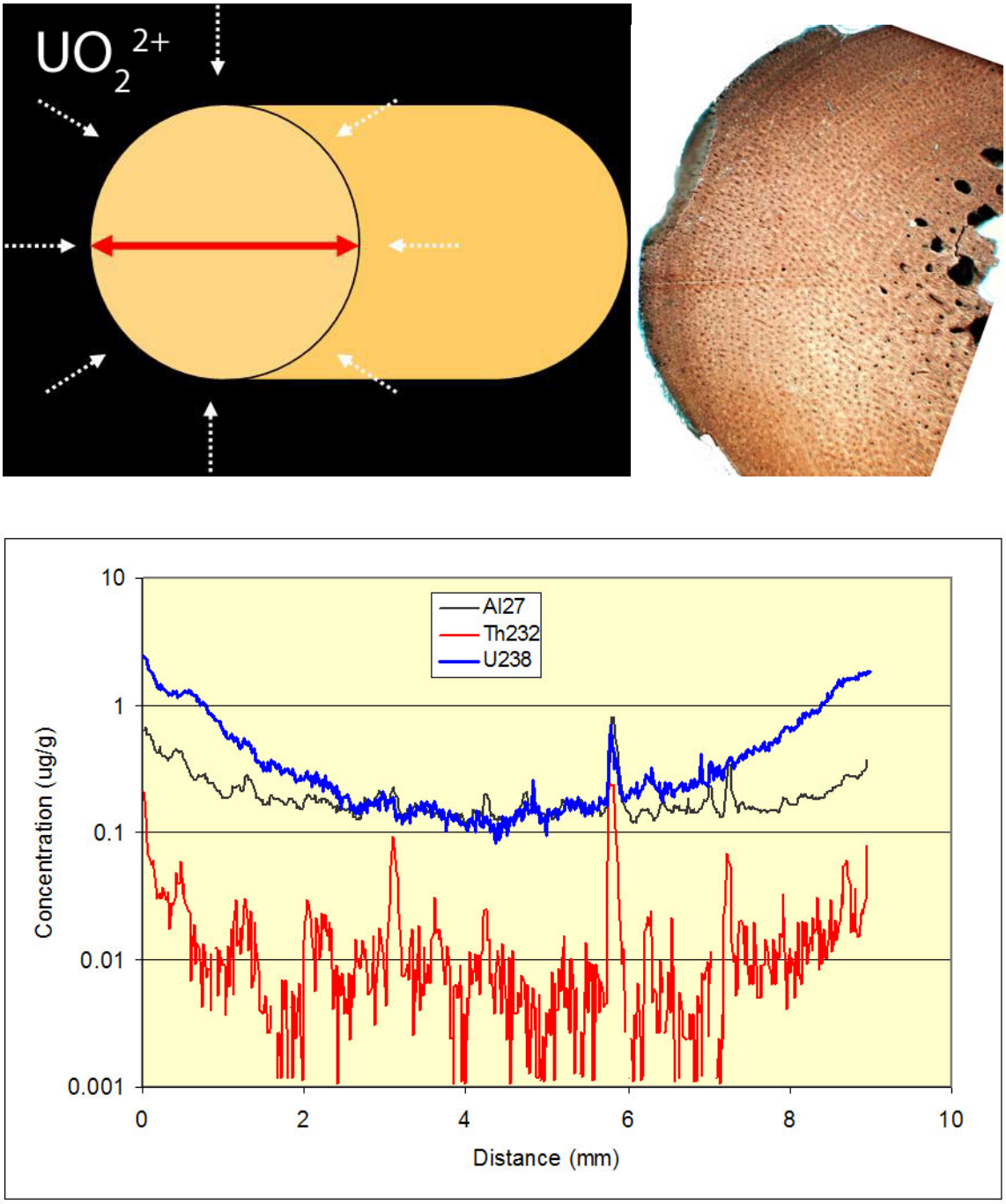

Figure 15. **Tibia de macropode provenant de Cuddie Springs, Australie. Les concentrations ont été obtenues à l'aide d'un ICP-MS à quadrupole équipé d'un système à ablation laser. Le profil d'uranium est en forme de ∪, mais la concentration en uranium est trop faible pour la datation *in situ*.**

Pour les datations *in situ*, les isotopes de faible abondance (^{234}U et ^{230}Th) peuvent être mesurés soit de manière dynamique ou soit statique, la première nécessitant la constante alternance du canal central entre les masses 230 et 234. Pour la seconde méthode, le ^{230}Th est d'abord mesuré dans le canal central. Ensuite, l'^{234}U est mesuré en répétant le trajet effectué pour le ^{230}Th (fig. 16). L'approche statique nécessite l'homogénéité de l'échantillon. Heureusement, le laser n'enlève qu'entre 10 et 40 µm d'épaisseur minimisant ainsi le risque d'hétérogénéité. Un deuxième SEM sera bientôt installé sur le Neptune et permettra la détection simultanée de l'^{234}U et du ^{230}Th.

	L1	C	H1	H2	H3	H4
Ligne 1		**230Th**		**234U**	**235U**	**238U**
Ligne 2	**232Th**	**234U**	**235U**	**238U**		

Figure 16. Position des différents isotopes mesurés de manière statique. Le ^{230}Th est d'abord mesuré dans le canal central (ligne 1). Ensuite, l'^{234}U est mesuré en répétant le trajet effectué pour le ^{230}Th (ligne 2).

Présentement, la précarité de la plupart des âges mesurés provient des incertitudes reliées au fractionnement élémentaire du thorium et de l'uranium. En effet, les taux de production d'U^+ et de Th^+ dépendent de la matrice analysée et ils ont tendance à dériver de façon monotone au cours de la session. Lors de l'analyse, un échantillon témoin est préalablement analysé pour rectifier les mesures pouvant être faussées par l'effet de matrice. Pour la datation des os et des dents fossiles, une dent de rhinocéros fossile dont la composition des séries-U a été déterminée par TIMS sert d'échantillon témoin (fig. 17).

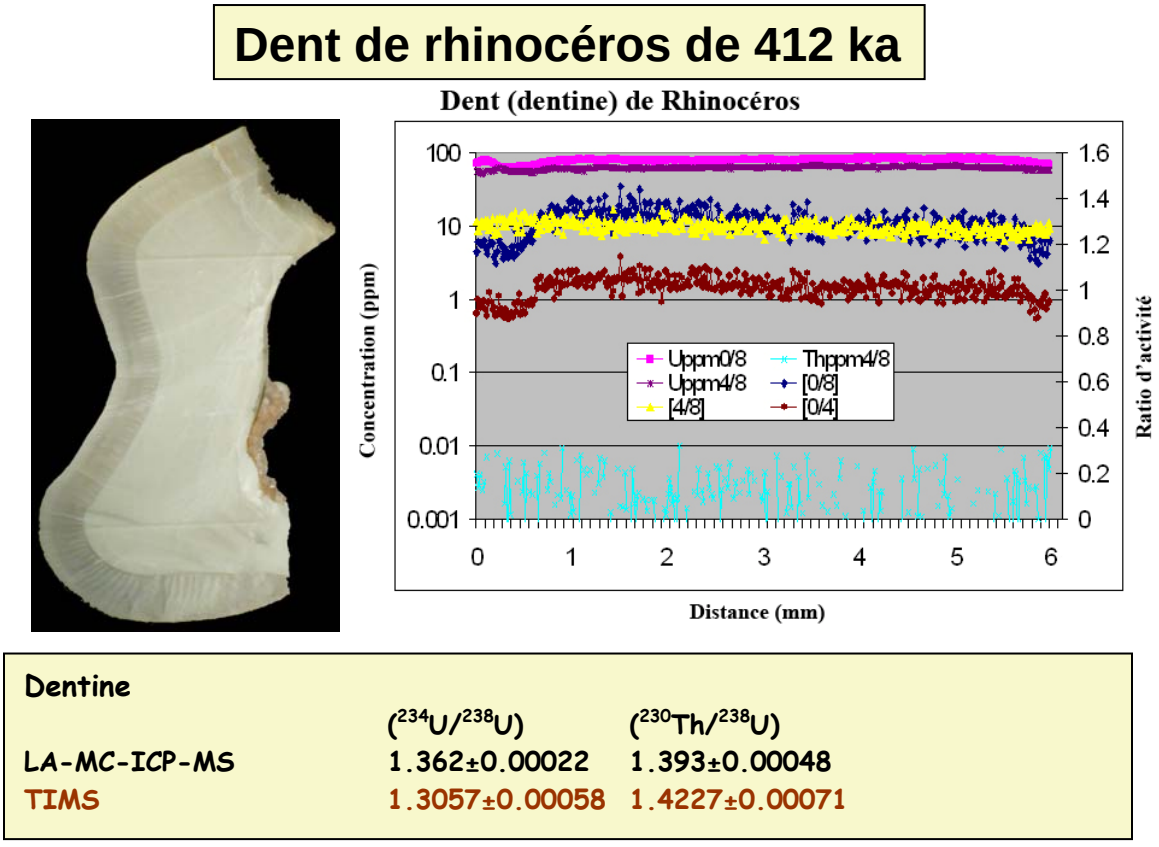

Dentine	($^{234}U/^{238}U$)	($^{230}Th/^{238}U$)
LA-MC-ICP-MS	1.362±0.00022	1.393±0.00048
TIMS	1.3057±0.00058	1.4227±0.00071

Figure 17. Dent de rhinocéros de 412 ka mesurée à l'aide du LA-MC-ICP-MS et comparée aux données obtenues par TIMS.

3.4 Carte de distribution isotopique d'une dent de Néanderthalien du site de Payre, France

Afin d'étudier plus en détail l'intrusion, la diffusion et le lessivage d'uranium et de thorium dans les dents archéologiques, à l'aide de l'ICP-MS à ablation laser, les premières cartes de concentration et de distribution istotopiques furent mises au point. Les données démontrent que pour modéliser cette incorporation et diffusion, il est absolument nécessaire de produire de telles cartes. En effet, l'analyse d'une seule traverse n'est pas nécessairement représentative de ce phénomène pour l'ensemble de la dent. Les cartes nous apprennent que l'uranium migre depuis le canal vers la dentine et l'émail. La migration dans l'émail dépend de la structure minéralogique et de la présence de fissures.

La dent étudiée, une molaire de Néanderthalien, provient du site de Payre situé dans la vallée du Rhône en France. Les données obtenues nous apprennent que l'uranium a été accumulé rapidement après la mort de l'individu, mais l'on observe néanmoins des accumulations tardives reliées aux fissures. Les cartes de distribution isotopiques démontrent que la dent est âgée d'au moins deux cent mille ans, cet âge correspondant à celle de la couche archéologique dans laquelle elle a été trouvée. Pour plus de détails, voir le chapitre 7.

4 FORMATION ET DATATION DES ENDUITS MINÉRAUX SUR LES SITES D'ART RUPESTRE

4.1 Travertin

Tout comme les spéléothèmes, les travertins sont des dépôts de carbonate formés à partir de la déposition du bicarbonate de calcium dissous dans l'eau douce froide. Le processus de précipitation du carbonate de calcium dépend des conditions physico-chimiques (température, pH, alcalinité, concentration de calcium, magnésium et dioxyde de carbone dissous (CO_2) dans l'eau) et des conditions biologiques, hydrologiques et climatologiques. Lors de la précipitation du carbonate de calcium à partir de l'eau douce, des traces d'ions d'uranium solubles (en particulier l'isotope ^{234}U) sont incorporées dans le dépôt de carbonate. Ainsi, dans la chaîne de désintégration de l'^{238}U, seuls les isotopes ^{238}U et ^{234}U sont solubles dans les solutions aqueuses contenant du bicarbonate de calcium ($Ca(HCO_3)_2$). Ensuite, ils sont précipités en cristaux de carbonate de calcium ($CaCO_3$) sous la forme de travertins et de spéléothèmes (Richards 1998). Les ions insolubles de thorium ne sont pas déposés à ce moment-là. L'uranium commence alors à se désintégrer exponentiellement pour produire le thorium nécessaire afin de recréer les conditions d'équilibre. Connaissant la demi-vie de l'uranium et en mesurant la quantité d'isotopes de thorium (^{230}Th) qui s'est accumulée *in situ*, il est possible théoriquement de calculer le temps écoulé depuis la déposition de l'uranium. L'intervalle de temps couvert par cette méthode de datation s'étend de quelques décennies à ~500 ka (Bourdon *et al.* 2003).

Afin de valider les dates obtenues, il faut s'assurer que le Th et l'U appartiennent à un système fermé. Cela signifie qu'aucun isotope de ces éléments ne doit être entré ou sorti du cristal de $CaCO_3$ depuis sa formation. Dans la nature, il est possible qu'une proportion significative d'uranium se dissolve hors des spéléothèmes et/ou des travertins. La mobilité de l'uranium et de ses isotopes est alors conditionnées par les propriétés chimiques de la solution aqueuse ainsi que par les propriétés physiques du dépôt de carbonate (porosité et perméabilité), ces situations ayant comme conséquence une surestimation de l'âge de précipitation des carbonates. Afin de solutionner ce problème, un système ICP-MS à ablation laser sera employé pour profiler la distribution de l'uranium le long de chacune des couches de déposition. Les fluctuations significatives dans la concentration en uranium indiqueront la possibilité d'un système ouvert.

Des fluctuations dans le transport des eaux souterraines ou des perturbations climatiques peuvent également modifier le cycle de l'uranium. Les rapports isotopiques seront quant à eux mesurés avec un MC-ICP-MS.

4.1.1 Lene Hare, Timor Leste

Établir les âges des routes migratoires potentielles empruntées par l'Homo Sapiens au Pléistocène pour se rendre au paléo-continent Sahul (Nouvelle-Guinée et Australie) depuis l'arc insulaire volcanique de Sunda (Asie du Sud-Est) est d'une importance capitale afin de comprendre l'évolution et la diaspora humaines. Celui de 55-65 ka (Roberts et al 1994; Thorne *et al.* 1999) est généralement accepté comme première phase de colonisation de l'Australie, les îles de Wallacee ayant été reconnues comme routes migratoires probables impliquant de courtes traversées maritimes (Birdsell 1977) (fig.18). Par contre, les études archéologiques faites sur ces îles n'ont pas encore donné des âges d'occupation humaine aussi anciens que ceux obtenus en Australie. Cette situation pourrait s'expliquer par le manque de recherche dans le secteur et pourrait également être attribuée au fait que les méthodes de datation alternatives au ^{14}C (dont la limite est d'environ 50 ka) n'ont pas été employées aussi fréquemment qu'en Australie.

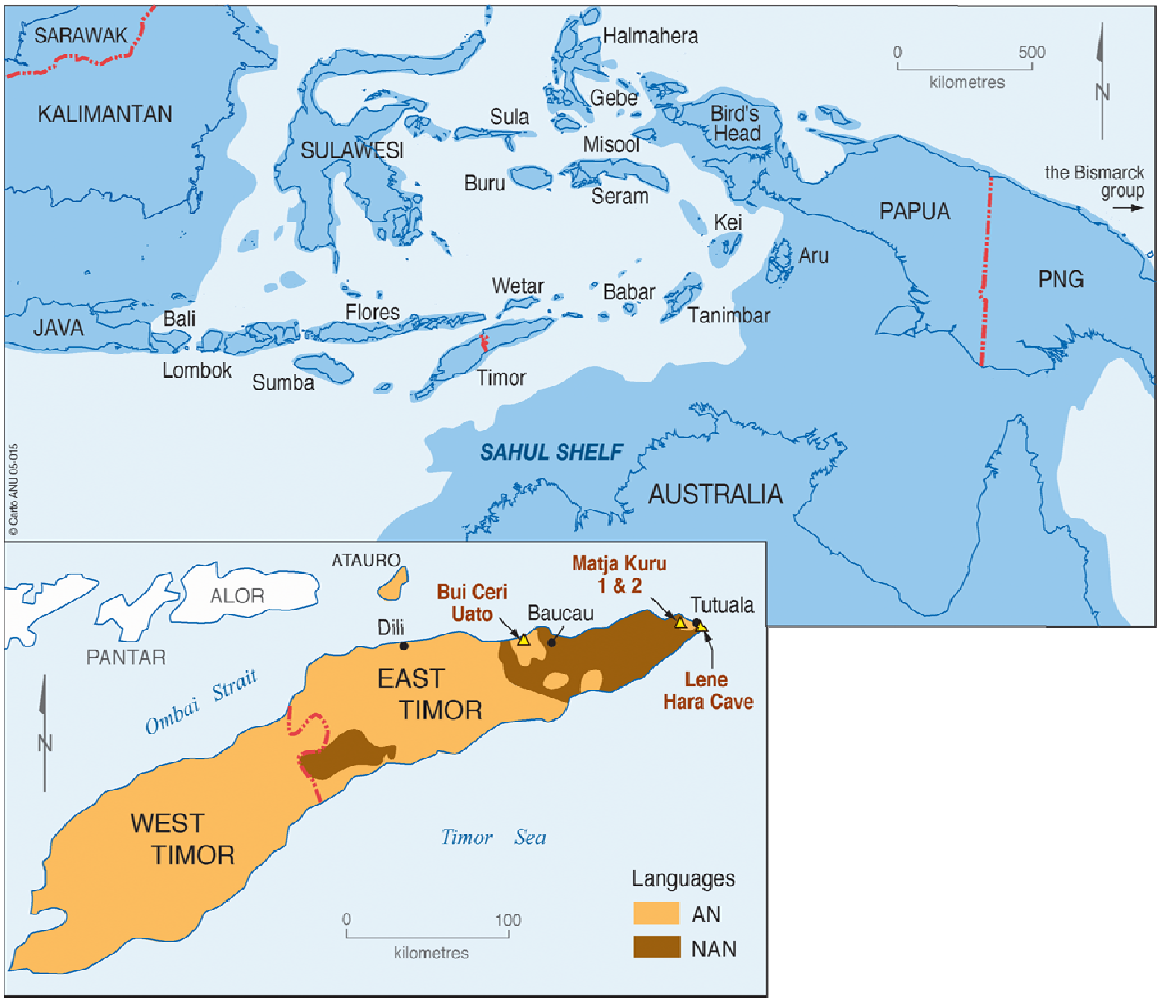

Figure 18. **Schéma montrant les paléo-continents Sunda et Sahul et les îles de Wallacee. L'encadré montre la localisation de la grotte de Lene Hara au Timor. Source: ANU maps.**

L'un des sites les plus anciens de Wallacee est situé au Timor Leste. Des fouilles archéologiques dans la grotte de Lene Hara ont permis d'établir plusieurs niveaux d'occupation humaine entre autres, le premier niveau contenant des coquillages datés au ^{14}C entre ~35 ka et ~30 ka et un deuxième avec des dépôts néolithiques contenant des poteries datant d'environ 3 ka (O'Connor *et al.* 2002). Plusieurs peintures rupestres présentement visibles dans la grotte sont de la deuxième phase d'occupation et, comme les poteries, d'origine austronésienne. Les Austronésiens proviennent d'un groupe localisé dans le sud de la Chine (proto-Austronésiens)

qui, en possession d'une technologie maritime très avancée, ont commencé à émigrer il y a six mille ans en direction du sud-ouest.

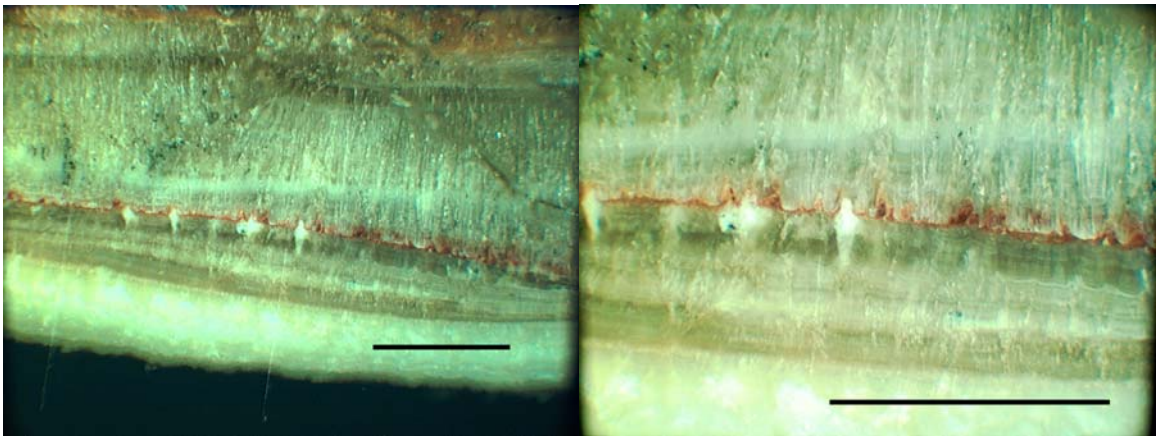

Figure 19. Photos montrant les couches de déposition de carbonate et la couche rouge hématisée présente dans le dépôt de travertin du site de Lene Hara. Échelle 1 mm.

Des dépôts de travertin tapissent les parois de la caverne et certains recouvrent partiellement les peintures rupestres. De nombreux spéléothèmes y sont également présents. Ayant environ 2,5 millimètres d'épaisseur et comprenant plusieurs couches, un échantillon de travertin n'étant pas directement associé aux œuvres rupestres a été amassé afin de tester le potentiel de datation (séries-U). Les résultats de l'analyse étant positifs, ils nous indiquent que les peintures visibles dans la grotte sont plus jeunes que 6,3 ka. De plus, une fine couche rouge unique a été observée entre les dépôts de carbonate (fig. 19) pouvant possiblement être attribuée à un précédent épisode de peinture. En échantillonnant et en datant des couches de déposition de carbonate de moins de 0,25 millimètres d'épaisseur situées immédiatement au-dessus et en dessous de cette couche rouge, il a été possible d'établir sa présence entre vingt-quatre et vingt-neuf mille ans (fig.20). Ces dates concordent avec le premier niveau d'occupation humaine suggéré dans les travaux de O'Connor *et al.* (2001).

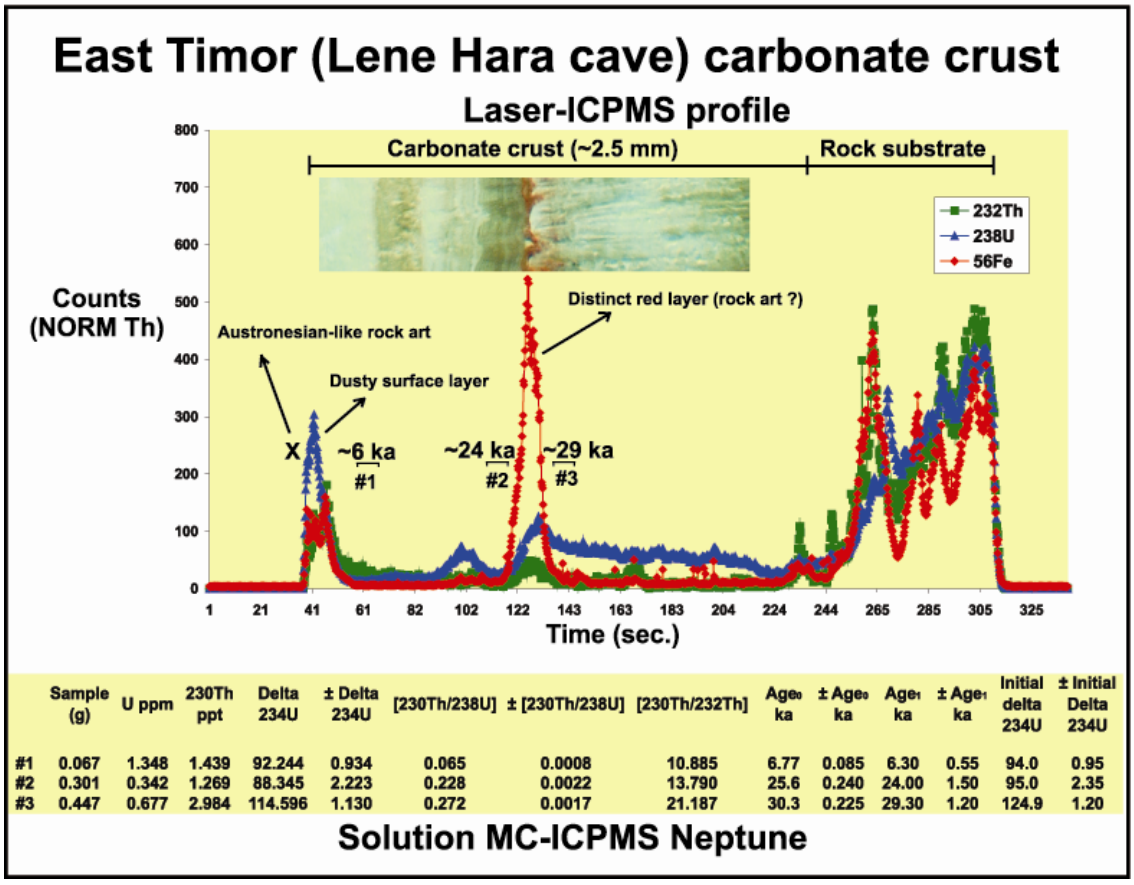

	Sample (g)	U ppm	230Th ppt	Delta 234U	± Delta 234U	[230Th/238U]	± [230Th/238U]	[230Th/232Th]	Age$_0$ ka	± Age$_0$ ka	Age$_1$ ka	± Age$_1$ ka	Initial delta 234U	± Initial Delta 234U
#1	0.067	1.348	1.439	92.244	0.934	0.065	0.0008	10.885	6.77	0.085	6.30	0.55	94.0	0.95
#2	0.301	0.342	1.269	88.345	2.223	0.228	0.0022	13.790	25.6	0.240	24.00	1.50	95.0	2.35
#3	0.447	0.677	2.984	114.596	1.130	0.272	0.0017	21.187	30.3	0.225	29.30	1.20	124.9	1.20

Figure 20. Spectre chimique obtenu par ICP-MS à ablation laser montrant les concentrations en uranium, en thorium et en fer présentes dans les couches de déposition de carbonate du site de Lene Hara. Le tableau présente les rapports isotopiques et l'âge des échantillons récoltés par microexcavation et obtenus par MC-ICP-MS. Les âges (Ages$_1$) ont été corrigés en assumant un ratio ^{230}Th/^{232}Th initial de 0,8 ± 0,8 pour les valeurs planétaires actuelles (Bulk Earth) à équilibre séculaire.

Les résultats obtenus démontrent avec efficacité la possibilité d'utiliser d'infimes dépôts de travertin pour dater les œuvres rupestres préhistoriques. De plus, il devrait être possible d'obtenir d'autres données isotopiques et élémentaires permettant d'étudier les paléoclimats. En effet, tout comme les spéléothèmes, les travertins peuvent indiquer les conditions hydrologiques passées parce que leurs phases de croissance correspondent aux périodes de précipitation et d'infiltration d'eau dans les grottes. De plus, comme les travertins se déposent généralement sous des conditions de précipitations hydrologiques relativement plus faibles que pour les spéléothèmes, ils sont susceptibles d'inclure des périodes de croissance pendant lesquelles les spéléothèmes

étaient inactifs (Wang *et al.* 2004). Les données obtenues pourraient alors compléter celles fournies par les spéléothèmes.

4.2 Vernis minéral

Le vernis minéral se compose d'argile (approximativement 70%) et autres détritus d'origine éolienne, comme de la silice, des hydroxydes et du carbonate de calcium, le tout cimenté à la surface rocheuse par des oxydes de fer et de manganèse. Les concentrations en manganèse peuvent excéder jusqu'à cent fois les niveaux ambiants, (Dorn 1991). Quant à l'épaisseur des vernis, elle peut varier de un à plusieurs dixièmes de microns. La plupart des échantillons montrent des stratifications internes. Toutefois, le processus de formation n'étant pas complètement connu, il est néanmoins généralement admis que cet enrichissement en manganèse représente la clef pour comprendre la formation du vernis (e.g. von Humboldt 1812; Lucas 1905; Engel and Sharp 1958; Jones 1991).

La théorie la plus acceptée suggère l'intervention de microbes. En effet, on a observé que certaines communautés bactériennes vivant sur les surfaces rocheuses facilitent la formation du vernis (Dorn 1991 ; Palmer *et al.* 1986 ; Nagy 1991). Bien que les bactéries puissent vivre dans des climats arides, elles fixent de plus grandes quantités de manganèse quand l'humidité augmente (Palmer *et al.* 1986 ; Fleisher *et al.* 1999, Liu et Broecker 2000). On croit que ces micro-organismes concentrent le manganèse (et autres métaux) par consommation et excrétion (Krinsley 1998). Les détritus d'origine éolienne adhèrent alors au biofilm afin de créer le vernis (fig. 21).

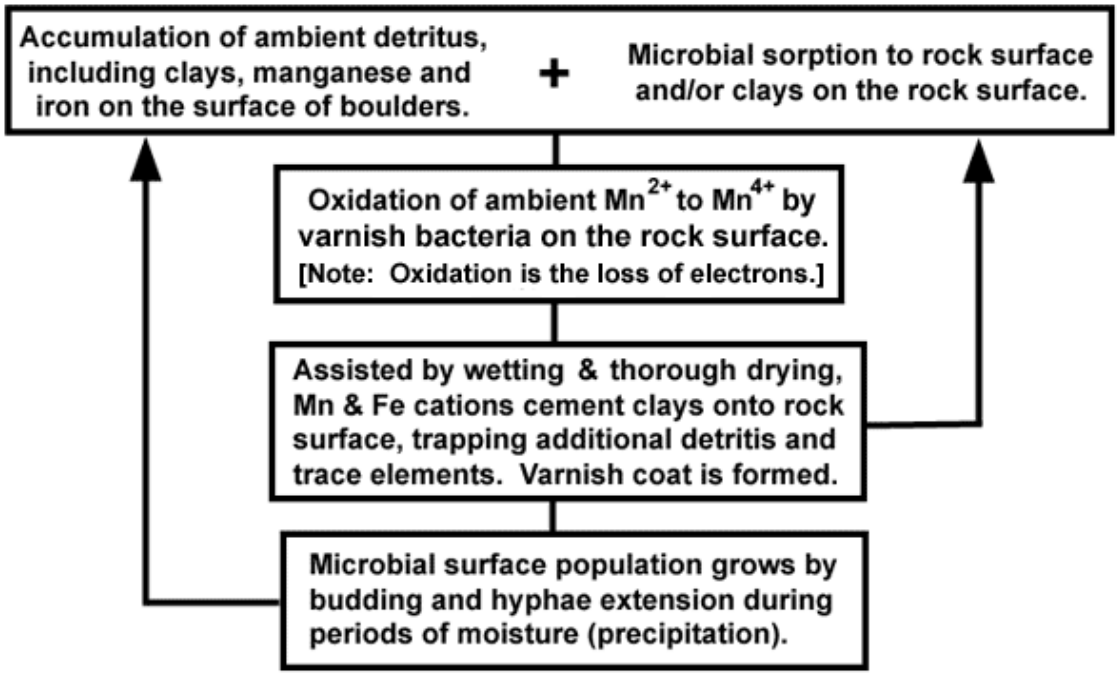

Figure 21. Schéma simplifié montrant le processus suggéré pour la formation du vernis minéral. Source Dorn et Oberlander, 1982.

4.2.1 Datation

Dans les années 1980, Knauss et Ku (1980) ont suggéré que dans les vernis minéraux, la fraction minérale contenant les hydroxydes de fer et de manganèse pourrait former un système fermé pour l'uranium, le thorium et le protactinium. La contamination par le ^{232}Th était un problème de taille et l'approche fut abandonnée. D'autres méthodes de datation ont été proposées, mais aucune ne fait l'unanimité. Pour en connaître davantage, il faut se référer à Watchman (2000a) qui a passé en revue l'histoire de la datation du vernis minéral.

Pour cette recherche doctorale, ce sont les techniques d'extractions séquentielles développées pour les études environnementales (Tessier 1979) et modifiées pour permettre l'analyse des lanthanides, actinides et autres éléments qui ont été retenues (Land *et al.* 1999). Ces techniques permettent de déterminer le mode et l'occurrence de métaux traces dans les sols et les sédiments. Après avoir séparé le vernis en différentes fractions, on déterminera les concentrations élémentaires et isotopiques dans chacune d'entre-elles. Cette opération apportera sans doute des

indices sur le ou les modes de formation et permettra peut-être de dater l'échantillon en déterminant les ratios isotopiques d'uranium et de thorium dans les fractions minérales les moins assujetties à l'incorporation de thorium et d'uranium de sources détritiques.

4.2.1.1 Cation-ratio

En 1983, s'appuyant sur la variation des ratios élémentaires, Dorn (1983) proposa une méthode de datation pour le vernis minéral. Il était suggéré qu'avec le temps certains éléments mineurs solubles étaient lessivés hors du vernis et que ces variations n'étaient pas sensibles aux facteurs affectant la déposition du manganèse:

''The premise of cation-ratio dating is that with time the leachable cations in varnishes, such as Na, Mg, K, and Ca, are gradually replaced by and/or depleted relative to less mobile cations, such as Ti. The decreasing cation ratio of Na + Mg + K + Ca: Ti, or any component thereof (e.g., Ca:Ti), provides an indication of the length of time that the varnish has been exposed to cation leaching'' (Dorn 1983: p. 50).

La datation cation-ratio suppose que lors de la fixation du vernis aux surfaces rocheuses stables, les cations solubles sont graduellement lessivés hors du vernis. Cependant, il n'existe aucune preuve démontrant ce phénomène. Ce serait plutôt la solubilité du minéral dans lequel ils sont présents qui expliquerait les variations des ratios observées dans certains vernis (Renaud et Raymond 1991). De plus, tous les facteurs pouvant affecter la variation des ratios sont localement variables (Dragovich 1988; Clarke 1989; Krinsley et Anderson 1989). Par exemple, les composantes du vernis n'ont pas nécessairement la même source et peuvent avoir une composition élémentaire totalement différente. Plusieurs autres facteurs, tel le pH, peuvent également modifier la mobilisation relative de certains éléments. Après avoir reçu maintes critiques, la méthode fut finalement abandonnée par Dorn (1996).

4.2.1.2 Carbone-14

Afin d'obtenir des courbes de calibration pour la datation cation-ratio, Dorn utilisa la spectrométrie de masse à accélérateur pour dater la matière organique dans les vernis (Dorn *et al.* 1992a; Dorn *et al.* 1992b; Nobbs et Dorn 1993). En mesurant l'activité du carbone-14 de la matière organique emprisonnée dans les couches de 'rock varnish' à la surface d'une gravure, en

théorie, il est possible de dater indirectement l'œuvre rupestre. Cette méthode de datation repose en partie sur les deux conditions suivantes, à savoir que (a) le carbone organique ancien n'est pas un contaminant et (b) que les composantes organiques sont physiquement stables, chimiquement immobiles et n'échangent pas d'atomes de carbone avec d'autres sources de carbone (hydrosphère, biosphère).

On doit également être capable d'identifier et d'amasser des substances datables qui sont directement associées à l'œuvre rupestre. Afin d'obtenir une date archéologiquement acceptable, l'association entre les substances organiques datées et la gravure doit être clairement démontrée. Un tel objectif n'est pas toujours facile à atteindre. Pour plus de détails voir le chapitre 1.3.1.

L'avènement de la datation AMS ^{14}C pour dater la formation des vernis minéraux a souffert du même manque de rigueur scientifique qu'a connu le développement de la méthode cation-ratio. Et ce, parce qu'aucune recherche fondamentale portant sur la nature et les propriétés des principaux composés organiques utilisés à la base de cette méthode n'a été effectuée. Des composés organiques non identifiés ont été datés sur la présomption qu'ils étaient directement reliés à la formation du vernis ; des recherches ultérieures ont démontré l'inexactitude de cette hypothèse (Watchman 1992a, Watchman 1992b, et Watchman 1993).

4.2.2 Karolta, South Australia

Localisé à environ 150 km au sud-ouest de Broken Hill, Karolta est l'un des plus importants sites à pétroglyphes en Australie, le style des gravures (*Panaramitee style*) étant considéré par les archéologues comme l'un des plus vieux du continent (Dorn *et al.* 1988). Recouvrant les surfaces rocheuses et les pétroglyphes (fig.22), le vernis minéral 'rock varnish' présent à ce site est l'un des plus épais jamais observé sur des sites d'art rupestre.

Figure 22. **Pétroglyphes du site de Karolta. Le substrat rocheux et les pétroglyphes sont recouverts de vernis minéral de couleur noire.**

Lors d'une visite à cet endroit, des échantillons non directement accolés aux gravures furent recueillis, le vernis ayant environ 80 microns d'épaisseur réparti sur plusieurs couches de déposition (fig.23). À l'aide d'une microforeuse équipée d'une fraise à dentisterie (microexcavation), un échantillonnage de quelques milligrammes de vernis a été prélevé sur la surface rocheuse, de même que de la roche altérée et du substrat rocheux. Par la suite, ces trois échantillons ont été soumis au protocole d'extraction du manganèse, du fer, des terres rares et des isotopes d'uranium et de thorium.

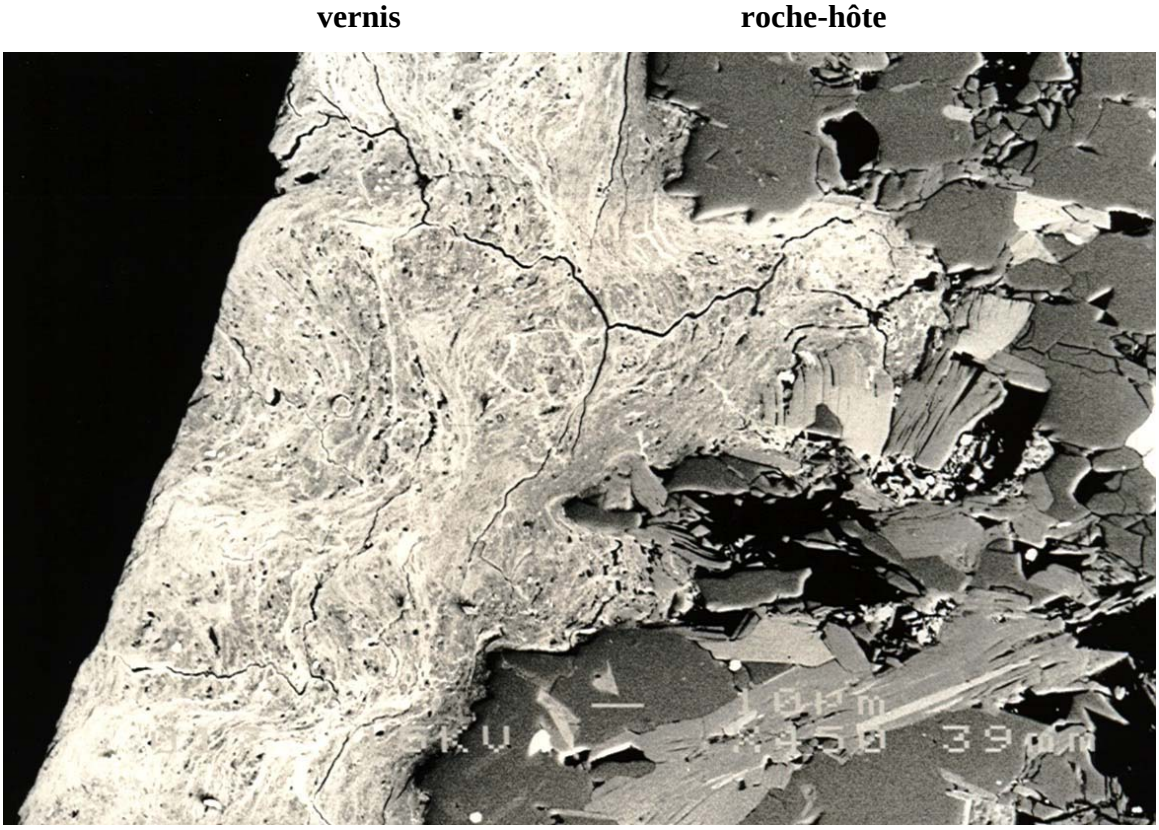

Figure 23. Photographie prise au microscope électronique à balayage montrant les couches de déposition de vernis et le substrat rocheux. Les zones blanches sur la photo indiquent la présence d'éléments à numéros atomiques plus élevés (Mn, Fe). La partie droite de la photo présente la roche hôte constituée de quartz, feldspaths, micas, etc.

Les techniques d'extraction séquentielles sont proposées ici comme méthode permettant d'éliminer le matériel détritique contaminant les échantillons de vernis. Dans le passé, on a essayé sans succès de dater des carbonates impurs en dissolvant l'échantillon à l'aide de solutions d'acide nitrique variablement diluées, le but étant de dissoudre la fraction de carbonate sans perturber la fraction détritique. Sachant qu'il avait été démontré que la dissolution préférentielle de l'uranium relativement au thorium se produit dans la phase détritique (Bischoff et Fitzpatrick 1991; Luo et Ku 1991; Kaufman 1993), pourquoi ne pas essayé de dater la météorisation de concrétions ferrugineuses en dissolvant le matériel pédogénique (i.e. les oxy/hydroxydes de fer) de l'échantillon à l'aide de 'dithionite-citrate' (Augustinus *et al.* 1997; Augustinus 1999) ? Cependant, cette méthode s'est avérée inefficace car elle dissout d'autres phases minérales non ciblées par la solution de 'dithionite-citrate' (Shulmeinster *et al.* 1993).

Tableau 2 : Protocole de microextraction séquentielle utilisé dans ce projet de recherche. Protocole modifié des travaux de Land *et al.*1999.

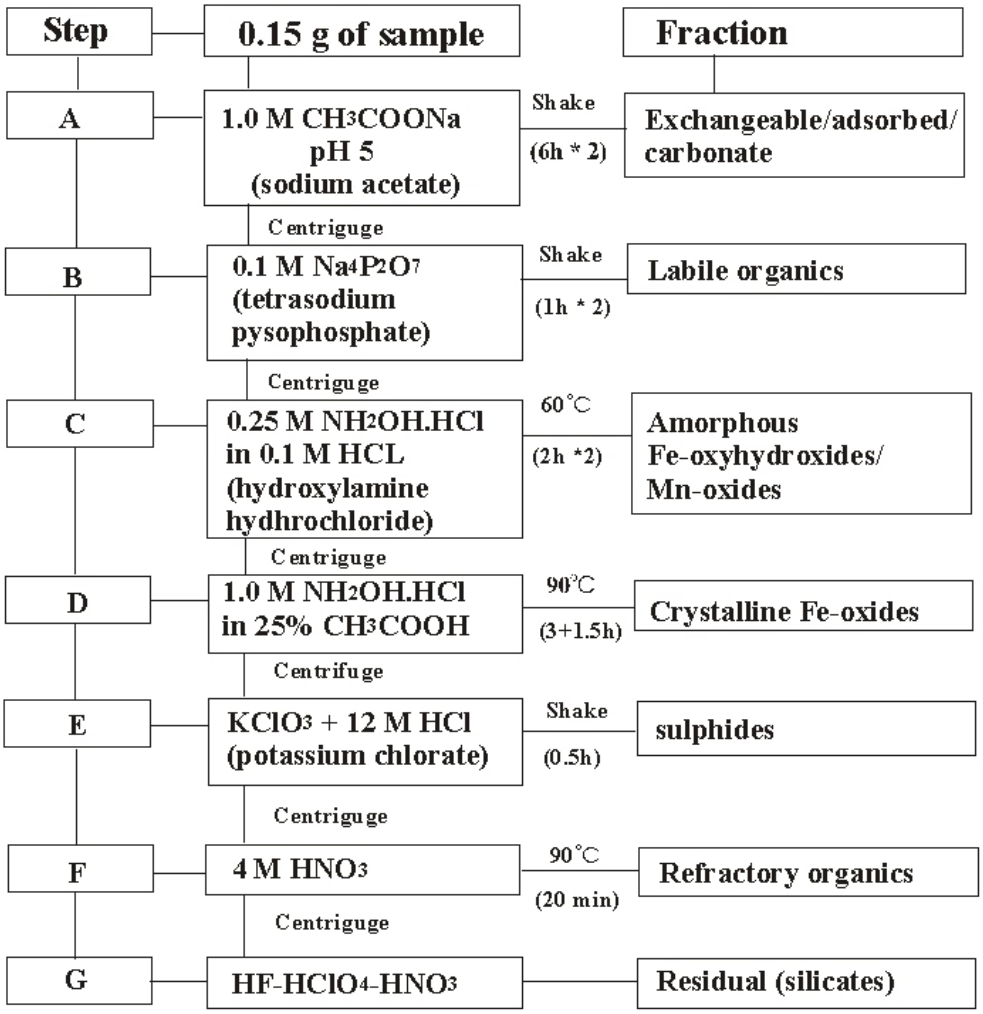

Les échantillons de vernis minéral étudiés ici ont donc été soumis au protocole de microextraction chimique séquentielle dans l'espoir d'éviter ainsi les problèmes de dissolution partielle et de fractionnement isotopique présentés plus haut. Cette technique modifiée de Land *et al.* (1999) a été développée afin d'étudier la mobilité et le fractionnement naturel des terres rares dans les sols. Ce protocole a été choisi parce que les actinides et les terres rares ont un comportement chimique similaire (Land *et al.* 1999).

Les données obtenues montrent que, dans le vernis de Karolta, l'enrichissement en manganèse et en terres rares est un processus complexe caractérisé par deux étapes distinctes. La surface rocheuse altérée est d'abord considérablement enrichie en manganèse (avec un facteur de 13) comparativement à la roche hôte non altérée. Ce phénomène peut s'expliquer par la météorisation chimique de la roche-hôte en contact avec l'eau de surface. Comme le manganèse est beaucoup plus soluble que le fer dans les conditions de Ph/Eh typiquement désertiques (Engel et Sharp 1958), le manganèse va être lessivé hors de la roche hôte et se concentrer à la surface dans la zone de transition anoxique/oxique.

La surface rocheuse subit également les effets de l'altération mécanique. Il s'y dégagera des particules volatiles riches en manganèse qui seront transportées dans l'air et déposées sur la surface rocheuse altérée, s'accumulant dans les dépressions naturelles. En contact avec l'eau de surface s'accumulant dans les mêmes dépressions, le manganèse sera dissous et éventuellement fixé par les oxydes et hydroxydes cimentant les particules résiduelles et autres débris. Le vernis sera alors enrichi en manganèse comparativement à la croûte altérée (avec un facteur de 4).

Les données provenant de l'extraction séquentielle nous apprennent également qu'une proportion significative d'uranium est concentrée dans la phase des silicates résiduels et est probablement associée aux minéraux accessoires comme les zircons. Dans le vernis, il y a néanmoins une proportion importante d'uranium de source authigénique. Par contre, les concentrations en thorium de source allogénique augmentent considérablement. De plus, il semble que la technique d'extraction séquentielle est inefficace pour extraire séquentiellement le thorium. Conséquemment, il est impossible de dater le vernis par les séries de l'uranium. Pour plus de détails voir le chapitre 6.

5 URANIUM-SERIES DATING ROCK ART IN EAST TIMOR

Maxime Aubert[1,2,3], Sue O'Connor[2], Malcolm McCulloch[3], Graham Mortimer[3], Alan Watchman[4] & Marc Richer-LaFlèche[1]

[1] Eau, Terre & Environnement, Institut National de la Recherche Scientifique, G1K 9A9, Québec, Canada

[2] Department of Archaeology and Natural History, Research School of Pacific and Asian Studies, Australian National University, Canberra, Australian Capital Territory 0200, Australia

[3] Research School of Earth Sciences, Australian National University, Canberra, Australian Capital Territory 0200, Australia

[4] 1723 Stellar Place, Montrose, Colorado, 81401, United States of America

Abstract

At many sites throughout the world rock art paintings have been covered by naturally deposited calcite laminations which we demonstrate can be individually dated by recently improved uranium-series methods. Here we report the application of multi-collector inductively coupled plasma mass spectrometry to measure the ages for carbonate coatings that bracket red pigment at Lene Hara cave, East Timor, which could be evidence of human painting. These analyses establish the feasibility of dating milligram samples of finely layered calcite deposits associated with archaeological evidence of human occupation. In addition to confirming an age of less then 6,300 yrs for the visible red paintings on the carbonate surface we also report a substantially older age of 24,000 to 29,300 yrs for a similar, older red pigment lamination providing possible evidence for an earlier painting episode.

5.1 Introduction

Rock art is one of the most cogent signatures in the archaeological record documenting the appearance of modern humans (i.e. *Homo sapiens*). Artefacts (such as flaked stones) appear early in the record alongside the remains of pre-modern hominids, but even when found in clear association with modern humans, do not generally appear to be sensitive indicators of cognitive attainment. Furthermore, rock art has the unique potential to inform on symbolic expressions and cultural practices, and therefore provides one of the few 'windows' into the way people thought in non-literate societies. Until the pioneering application of dating carbon in amorphous silica coatings (Watchman 1994) and layered oxalate-rich crusts (Watchman 1993), the study of rock art was treated more as an aesthetic pursuit rather than a facet of scientific archaeology, as it had been considered impossible to date, and hence, could not be integrated with other archaeological and environmental records.

Improvements in radiocarbon dating techniques in the last twelve years have facilitated the chronometric dating of charcoal and other organic materials in painted rock art (Watchman *et al.* 1993; Tuniz and Watchman 1994). However, red pigment art is usually produced using finely ground hematite mixed with water (Ward *et al.* 2001), and has rarely been found to incorporate contemporaneous organic materials (Watchman and Cole 1992). Consequently, the dates obtained on hematite images can give apparent ages that are inconsistent with existing archaeological data, and raise doubts about whether or not the small quantity of organic extracts are associated with the painting episode or are later contaminants (Smith and Rosenfeld 1997). Natural calcite deposits that sequentially interlay some rock paintings provide the opportunity for using uranium-series dating techniques to determine precisely when the coatings were deposited and hence bracket the timing of painting events.

5.2 Background context

Rock art complexes exist on a number of islands in South-East Asia (Kosasih 1991; Ballard 1992; Chazine 2003; O'Connor and Oliveira 2007), but certainly one of the largest and most diverse concentrations of painted rock art yet found is near the small village of Tutuala, at the eastern end of East Timor (fig. 24). Rock art in this area is similar to that in other parts of

South-East Asia and the western Pacific (O'Connor 2003). Ballard (1992) has proposed an 'Austronesian' origin for the painted rock art in the area stretching from Timor in the west to Vanuatu in the east. He suggested an antiquity of no more than 3,500 years. With the exception of Vanuatu (Wilson *et al.* 2001), direct dating of the rock art has not been attempted throughout most of this region. Dates from Vanuatu confirm that the earliest artistic expression was about 3,000 years BP which agrees well with dates for the earliest occupation of this region. Earlier art, pre-dating Austronesian expansion, could be found in South-East Asia and the Melanesia islands because they have far longer records of human occupation. Except for Flores (Morwood *et al.* 2004), most islands investigated appear to have been occupied by modern humans for at least 28,000 years (Bellwood 1997; O'Connor *et al.* 2005). Sites containing painted art on East Timor have produced occupation ages as old as 35,000 BP (O'Connor *et al.* 2002). The recent dating of rock art in southeastern Borneo has produced a range of Th/U and ^{14}C ages with a minimum age of ca. 9,800 BP (Plagnes *et al.* 2003). These latest results demonstrate the presence of a painting tradition on the then Asian mainland during terminal Pleistocene times, and confirm that in some circumstances painting can endure in limestone caves in tropical environments for many thousands of years. Estimating the age of the East Timor paintings by measuring uranium-thorium values in calcite with which they are associated is essential in order to confirm the temporal and geographic consistency of the Austronesian painting tradition.

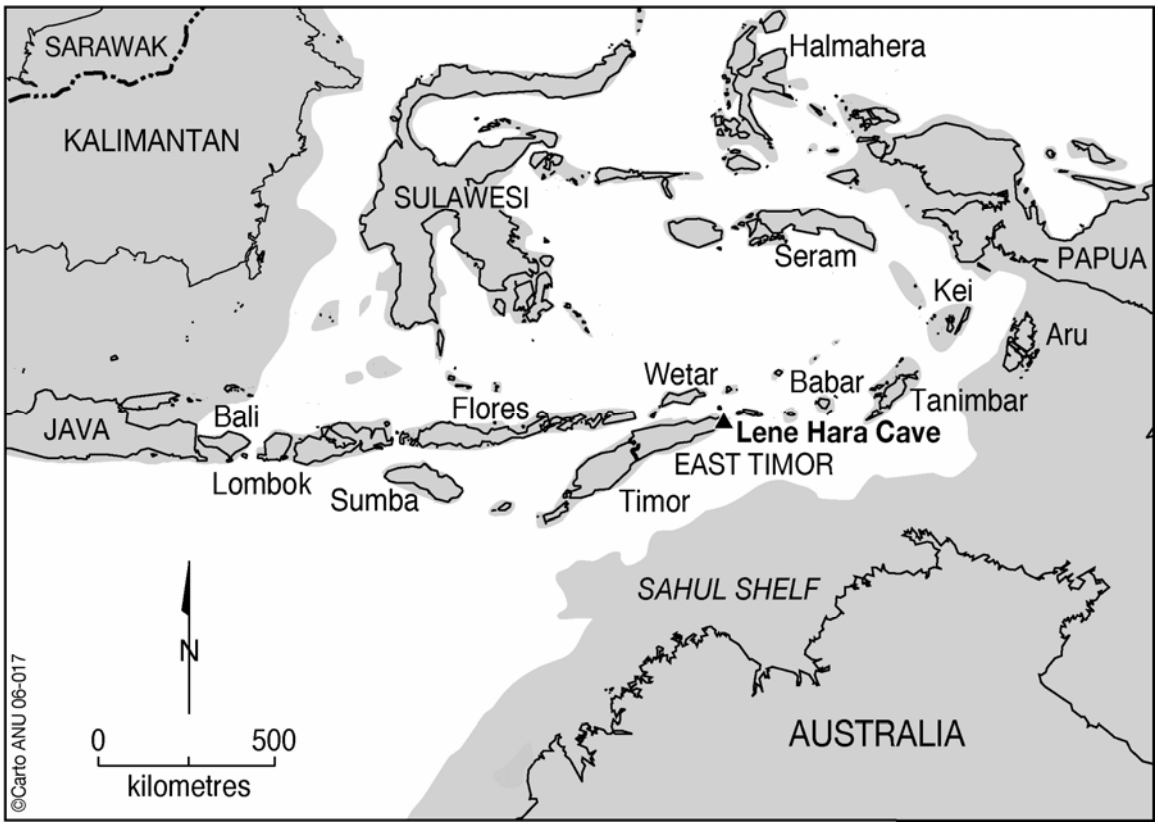

Figure 24. Map of the Australasian-South East Asian region, showing Timor and Lene Hara Cave.

5.3 Site description

Lene Hara is a large limestone solution cave at the extreme eastern tip of East Timor (fig. 24). It is situated at an altitude of about 100 m in an uplifted limestone marine terrace, which is less than 1 km from the current coastline. The limestone bedrock of the cave is well bedded, with folding in the limestone providing a structural control on much of the curvature of the walls and the arched cave roof. The overall architecture of the cave is open, and elliptical in cross-section, possibly reflecting an early phreatic origin (fig. 25). Relatively thick calcite deposits cover the cave walls. Isolated large speleothem deposits occur as 2-4 m and 1-2 m high mounds within the interior of the cave, and as both thin columns and massive columnar complexes that are overlain by more recent flowstone. Active speleothem growth is restricted to minor stalactite formation.

Between 2000 and 2002, the archaeological excavations at the site have revealed that discrete time slices of the human occupation record are preserved in different parts of the cave. Test Pit A, excavated in 2000 has a basal deposit dating between 35,000 BP and ~30,000 BP (O'Connor *et al.* 2002), and a thin upper level with Neolithic deposits containing pottery dating to ~2 000 years BP. Test Pit B was located about 4 m east of the large (9 m diameter) speleothem column, and while its depositional sequence and depth are broadly similar to Pit A, its sediments are younger. Radiocarbon dating indicates that this deposit accumulated mostly between 26,000 BP and ~18,000 BP. Test Pits D and F were located 1 m apart and 4 m out from the northern wall (fig. 25). The chronologies of the stratigraphy from Pits D and F demonstrate that all of the sampled sequence is of Holocene age dating between 1,000 and 10,000 BP (O'Connor and Veth 2005).

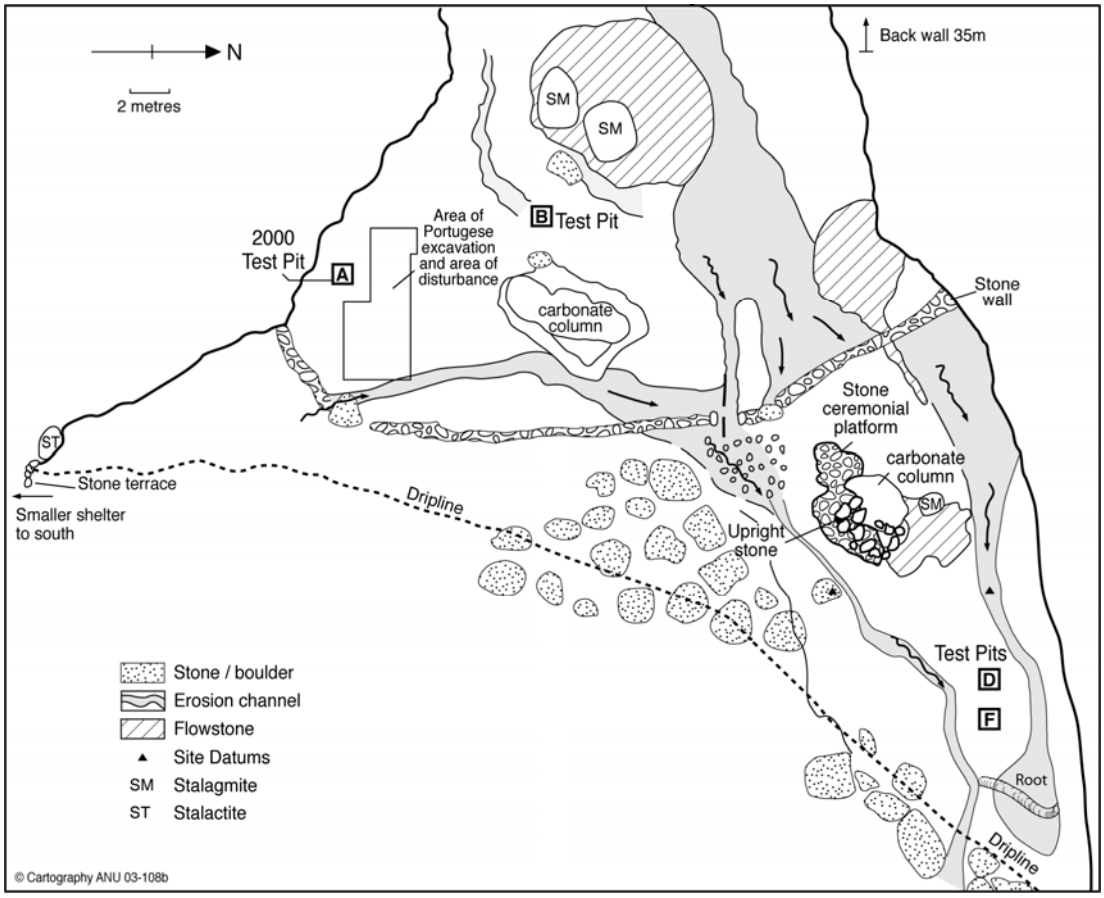

Figure 25. Plan of Lene Hara cave.

Rock paintings are visible today on the limestone cave walls and most are attributed to the post pottery Neolithic phase of occupation on the basis of stylistic similarities with relatively dated images from elsewhere in the western Pacific (O'Connor 2003). Figurative motifs include small anthropomorphic figures depicted carrying objects, apparently weapons (fig. 26). Other figurative motifs include boats, animals, such as fish shown in X-ray style and birds. Some images are zoomorphic combining human and animal features, whereas others are mixtures of geometric shapes and human features. The most common motifs in Lene Hara are non-figurative forms such as star/sun images, circles and scrolled or linear geometric forms. Hand stencils also feature. Most motifs are monochrome red pigment, but black, yellow and brown pigments occur, sometimes as polychrome motifs. One of the linear motifs in red and black includes a faded green infill (O'Connor 2003).

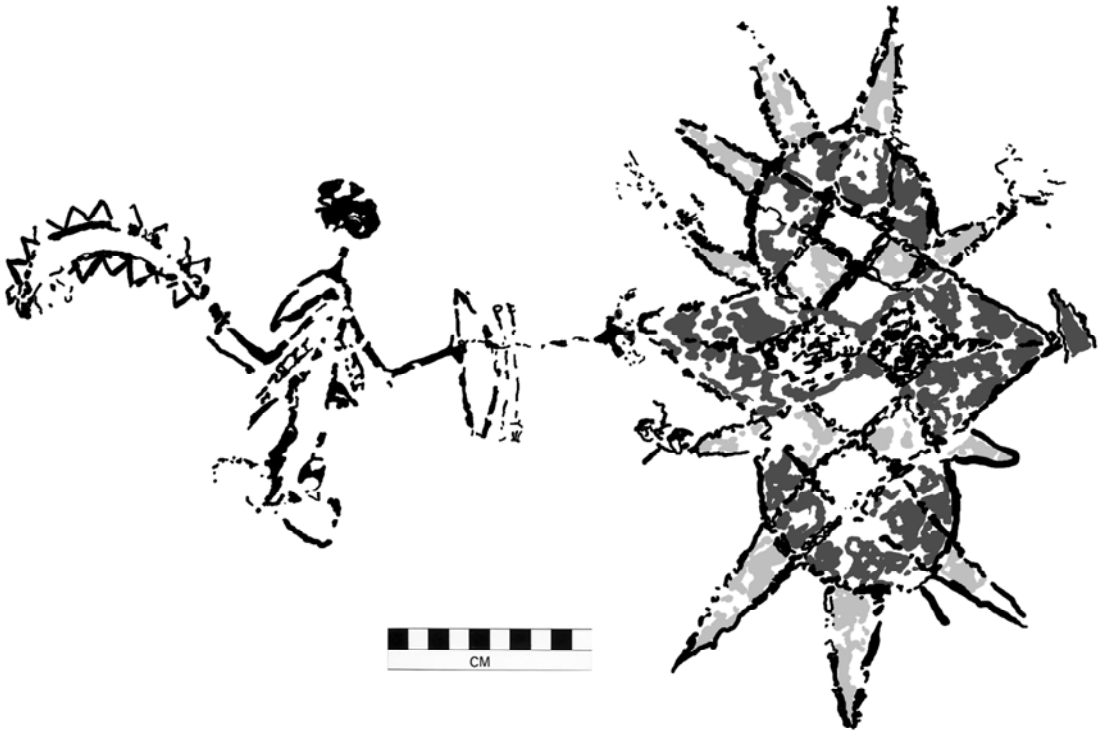

Figure 26. Small red anthropomorph with weapons and linear geometric motif in red, black and green in style thought to post date Austronesian settlement.

5.4 Materials and methods

Calcite coatings are formed from the deposition of dissolved calcium bicarbonate from saturated solutions that flow across the surfaces. These solutions contain small quantities of dissolved uranium and this element when deposited in a calcite coating provides the ingredient for uranium-series dating. This dating method is based on the radioactive decay chain which includes the parent ^{238}U, the intermediary isotope ^{234}U and the daughter ^{230}Th (Bourdon *et al.* 2003). Because ^{238}U and ^{234}U isotopes are soluble in aqueous solutions but ^{230}Th is not, calcium carbonate ($CaCO_3$) crystals that are precipitated in calcite coatings will initially contain ^{238}U and ^{234}U, but generally not ^{230}Th. Subsequently, ^{234}U decays to ^{230}Th. The measurement of the ^{230}Th, ^{238}U, and ^{234}U isotopes allows calculation of the age of the carbonate host because the decay rate is known. The uranium-series dating method enables the determination of ages of several hundred thousand years and covers the whole time span of human history in which rock art was created.

A test specimen (off-art) was collected from the cave wall near a painted figure. This sample contains the limestone bedrock covered by a ~2.5 mm thick calcite coating. The calcite crystal fabric covering the limestone is open columnar crystallites (Kendall and Broughton 1978) and is characterized by a series of layers of different colours ranging from smoky grey-black to white. Those are themselves highly laminated. This fabric is ~1.5 mm thick and terminates at a horizon indicated by a distinct continuous red layer. Above this coloured layer is a dense, finely laminated fabric 1 mm thick containing multi-coloured layers ranging from translucent to grey-brown.

Laser ablation ICP-MS (Eggins *et al.* 2003) was used to profile a series of elements along individual layers of interest. Uranium concentration was measured to establish sample size requirements for the determination of the U and Th isotopic ratios. Under 30X magnification the fine carbonate laminations were ground into fine powders using a micro-drill and dental burrs, maintaining control over the micro-stratigraphic level (Watchman 2000). An area measuring approximately 1 cm x 1 cm was removed to a depth of about 0.1 mm per sample and the powder collected on aluminium foil.

Each sample was then dissolved in nitric acid, spiked and prepared according to the method described by Luo *et al.* (1997). Isotopic ratio measurements were made on a Finnigan Neptune multi-collector ICP-MS equipped with desolvating nebuliser. Due to its significantly higher ionisation efficiency than thermal ionization mass spectrometry (TIMS), MC-ICP-MS permits the analysis of samples with much lower U concentrations in smaller samples. For example, TIMS usually requires about 100 ng of Th while MC-ICP-MS needs less than 10 ng (Nakai *et al.* 2001). The method has therefore a much wider applicability on rock coatings, where often only minute sample masses are available. Furthermore, it allows for greater spatial resolution and minimises the visual aspect of sampling. This technology also enables the potential use of laser ablation for *in situ* uranium series dating of rock art where U concentrations are higher then 1 ppm (Eggins *et al.* 2005).

5.5 Results and discussion

Figure 27 illustrates the chemical spectrum and summarises the analytical data measured by solution MC-ICP-MS for a sectional profile through the calcite chip from Lene Hara cave. A small correction for initial ^{230}Th was made to each Th analysis on the basis of the ^{230}Th/^{232}Th ratio for Bulk Earth at secular Equilibrium (0.8 ± 0.8). This value is commonly used for initial Th corrections in the absence of independent data (Bourdon *et al.* 2003). For all our samples, this correction was small because of low ^{232}Th concentrations.

The spectrum, microstratigraphy and analytical measurements indicate that the visible paintings on the surface are younger than 6,300 years old. This suggests an Austronesian origin for the recent paintings, as previously argued on the basis of their formal attributes and associations based on style.

The distinct red layer observed within the pale carbonate deposit beneath the present red paintings at a depth of 1 mm is possibly the remnants of a much older painted image. This red layer was bracketed between 29,300 and 24,000 years old using laminations less than 0.1 mm-thick under and overlying the red layer (fig. 27). Such a painting is plausible because the Lene Hara cave is one of the oldest *Homo sapiens* sites in South-East Asia and was occupied at that time. Several pellets of red ochre found amongst other cultural material in the Pleistocene levels

of the archaeological excavations at Lene Hara must have been introduced into the cave by the human occupants for painting or other decorative purposes as no iron rich deposits occur within the cave. A significant flow of iron-rich water through the site would have been necessary to deposit a natural iron oxide layer on the cave walls and the effects of such an unusual stream should have been evident in the stratigraphy at the excavation pits. As no iron enrichment or natural iron deposit was found in the sediments and as no current iron-rich seepages exist on the cave walls or floor it seems doubtful that the red layer encapsulated in the calcite wall coatings is natural. Nevertheless, specialized analysis of the red layer is required to identify the constituents, such as organic binders and mineral phases to confirm its anthropogenic origin as paint. If this red layer is indeed a paint layer, and not a natural lamination (noting that nothing similar is seen on the adjacent rock surfaces), then its age challenges orthodox models for the age of the rock art and the makers of the rock art in Eastern South-East Asia. Thus the socio-cultural use and practice of rock art in the region, which have been previously attributed only to Austronesian influence, should be revised.

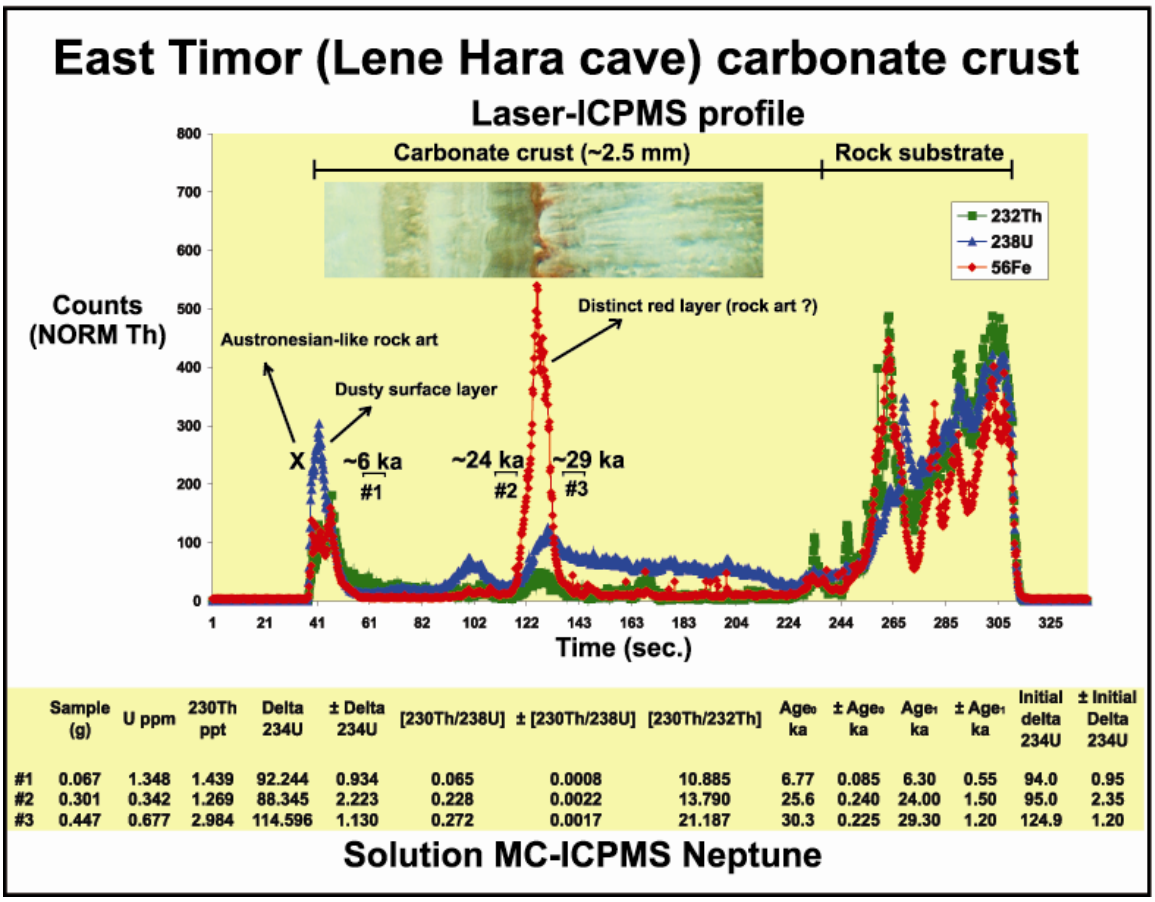

	Sample (g)	U ppm	230Th ppt	Delta 234U	± Delta 234U	[230Th/238U]	± [230Th/238U]	[230Th/232Th]	Age$_0$ ka	± Age$_0$ ka	Age$_1$ ka	± Age$_1$ ka	Initial delta 234U	± Initial Delta 234U
#1	0.067	1.348	1.439	92.244	0.934	0.065	0.0008	10.885	6.77	0.085	6.30	0.55	94.0	0.95
#2	0.301	0.342	1.269	88.345	2.223	0.228	0.0022	13.790	25.6	0.240	24.00	1.50	95.0	2.35
#3	0.447	0.677	2.984	114.596	1.130	0.272	0.0017	21.187	30.3	0.225	29.30	1.20	124.9	1.20

Figure 27. Chemical spectrum obtained from the laser ablation ICP-MS analysis of a sectional profile across a small chip of calcite from Lene Hara Cave, East Timor. The surface layer of paint is younger than 6 ka, and the older red pigment layer, which could also be paint, is bracketed between 24 and 29 ka. The table summarises the analytical data measured by solution MC-ICP-MS. Values for Age_1 are corrected ages assuming an initial $^{230}Th/^{232}Th$ ratio for Bulk Earth at secular Equilibrium = 0.8 ± 0.8.

5.6 Conclusion and perspective

This study shows that natural calcite laminations covering rock paintings can provide the means for bracketing those anthropogenic artefacts in age. This is possible because each sub-millimetre-thick carbonate lamination can now be precisely and accurately studied, chemically and isotopically analysed, and dated at extraordinary and unprecedented spatial and temporal resolutions using multi-collector inductively coupled plasma mass spectrometry. Application of the uranium-series dating method at the sub-millimetre scale therefore enables the dating of

hematite paintings on carbonate deposits where the pigments have not been combined with organic binders, and where radiocarbon dating is unreliable because of mixing of carbon from different sources. We believe that this innovative technique provides a new level of sophistication in the research of rock art on a world scale, and can be used to enhance our understanding of the evolution of human symbolic thought and cognition.

6 INVESTIGATING ROCK VARNISH WITH SEQUENTIAL EXTRACTION: POTENTIAL FOR UNDERSTANDING PROCESSES OF FORMATION AND URANIUM-SERIES DATING

Maxime Aubert[1,2], Marc Richer-LaFlèche[1], Alan Watchman[3], Malcolm McCulloch[2] & Graham Mortimer[2]

[1] Eau, Terre & Environnement, Institut National de la Recherche Scientifique, G1K 9A9, Québec, Canada

[2] Research School of Earth Sciences, Australian National University, Canberra, Australian Capital Territory 0200, Australia

[3] 1723 Stellar Place, Montrose, Colorado, 81401, United States of America

Abstract

We have investigated how rock varnish forms by studying the speciation of manganese, iron and the distribution of rare earth elements in a varnish sample and its supporting weathered and unweathered bedrock from Karolta, South Australia. We have also examined the uranium-series systematics in order to explore the possibility for uranium-series dating of the varnish. It appears that the enrichment of manganese and rare earth elements is a two step process involving an initial enrichment in the weathered sandstone. While most of the uranium is bound to the residual silicate fraction, there is also a large proportion of authigenic uranium in the varnish. The varnish is noticeably enriched in allogenic thorium. The uranium-series dating process is further compromised by the inefficient extraction of thorium during the chemical sequential extraction procedures that we have employed.

6.1 Introduction

Rock varnishes are natural, thin (0.005-l mm) brown, black or grey coatings formed on rock surfaces (Dorn and Oberlander 1981) in a wide range of environmental settings (Dorn 1998: 191). These deposits are accumulations composed of clay, iron and manganese oxides and hydroxides, quartz, carbonates and other mineral particles, and organic debris which are cemented together in finely laminated films (Hunt 1954, 1961; Engel and Sharp 1958; Lakin *et al.* 1963; Hooke *et al.* 1969; Potter and Rossman 1977). The mode of varnish formation is a complex process and is not fully understood. One of the leading theories involves the intervention of microbes. Oxidizing micro-organisms that convert Mn^{2+} to Mn^{3+} and Mn^{4+} in solution (McKeown and Post 2001) have been proposed to concentrate manganese and likely much of the iron that is present in rock varnish. The inconsistency in varnish development in an environment type may be the result of the irregular onset of bacterial colonization (Krumbein and Jens 1981; Taylor-George *et al.* 1983). Other models for varnish formation have been reviewed by Thiagarajan and Lee (2004). Their total dissolution-ICP-MS elemental analyses of varnishes indicated that rock varnishes are probably formed by direct chemical precipitation of dissolved atmospheric components in rain water, fog droplets or aerosols.

Varnished rocks offer a potential way for dating exposed rock surfaces (Dorn 1994), archaeological events (such as the creation of petroglyphs) and the construction of stone structures because the process of varnish formation can only occur on stable surfaces where natural laminated coverings are deposited. Dating rock varnishes using cation-ratios (Dorn 1983) and accelerator mass spectrometry radiocarbon methods (Nobbs and Dorn 1993; Watchman 1992) was initially promising, but these techniques have subsequently been found to have serious geochemical and other limitations (Watchman 2000). In 1980, Knauss and Ku (1980) suggested that the authigenic oxides phases present in rock varnishes could form a closed system for uranium, thorium and protactinium. However, the presence of allogenic thorium from other mineral phases was found to be a major problem and the method was abandoned.

Possible applications of varnish chemistry include environmental monitoring (Liu 1994) and possibly mineral exploration. Varnish-like coatings may exist on Mars, as suggested by observations at Viking and Mars Pathfinder landing sites (Israel *et al.* 1997; DiGregorio 2000),

and a microbiological pathway for deposition of manganese would have significant implications for the existence of life on that planet.

In this paper, an approach involving sequential extraction techniques was used to study the mode of formation of a manganese rich rock varnish sample from Karolta, South Australia. This approach was also used to explore the feasibility of accurately dating the formation of the varnish by using uranium-series disequilibrium.

6.2 Site description

6.2.1 The rock art

Dating rock varnishes in the Yunta-Mannahill area of South Australia is important because of archaeological interest in determining the antiquity of the Aboriginal rock engravings. The style of the engravings (Panaramitee style), consisting of circles, arcs, lines and animal tracks (fig. 28), is thought to be one of the oldest in Australia (Horton 1994:842-843). Studies of Australian rock varnishes include the work by Francis (1921), Staley and others (1983), and Clarke (1977). Preliminary dating and electron probe studies of varnishes near Broken Hill (Dragovich 1986, 1988) have provided insight into the possible antiquity and variability of varnish compositions. Clarke (1989) also examined compositional variations in rock varnishes from a site north of Broken Hill and concluded that there was considerable variation in the concentrations of Ti, K and Ca with depth.

Figure 28. Panaramitee-style petroglyphs carved into dark, varnish-covered rock at Karolta, South Australia.

In the Olary area of South Australia, a calibration curve for cation-ratio dating engravings was established for rock varnish at Pepuarta Bluff using accelerator mass spectrometry (AMS) radiocarbon to date the unidentified organic matter extracted from the lowest 10% of a varnish (Dorn *et al.* 1988). In that work it was assumed that varnish was formed by microbial fixation of aeolian components and that the calibration sites on the slopes of Pepuarta Bluff were similar to micro-environments at a nearby Aboriginal engraving site (Karolta). The cation-ratio dating method was used to estimate minimum limiting ages ranging from 1400 to 31,500 years BP (before present) for twenty four engravings at Karolta (Nobbs and Dorn 1988). These results were received with mixed reactions by a geographer (Dragovich 1988c), archaeologists (Bednarik 1988; Clegg 1988; Lanteigne 1989), geomorphologists (Reneau and Harrington 1988) and geochemists (Clarke 1989; Watchman 1989). The age determinations were subsequently retracted (Dorn 1996).

6.2.2 Geology and geomorphological setting

In the Olary-Mannahill region rock varnish is found on fine-grained, low-grade regionally metamorphosed Adelaidean (Proterozoic) siltstones, dolomitic siltstones and tillites. Many exposures at the head of the pediment, along the break in slope, on low ridges and near watercourses in the region are coated by thin brown to black rock varnish. At a location known as Panaramitee South, approximately 2 km of discontinuous exposures of low platforms and sub-rounded protrusions (about 2.5 m high) on Umberatana Group metasediments (Forbes 1989) are covered by rock varnish. Varnishes are also typically found on the Enorma Shale metasediments along a low ridge at Karolta. Thin rock varnish is developed on three large exposures of varnished Pepuarta Tillite at the base of the steep slope near Pepuarta Bluff.

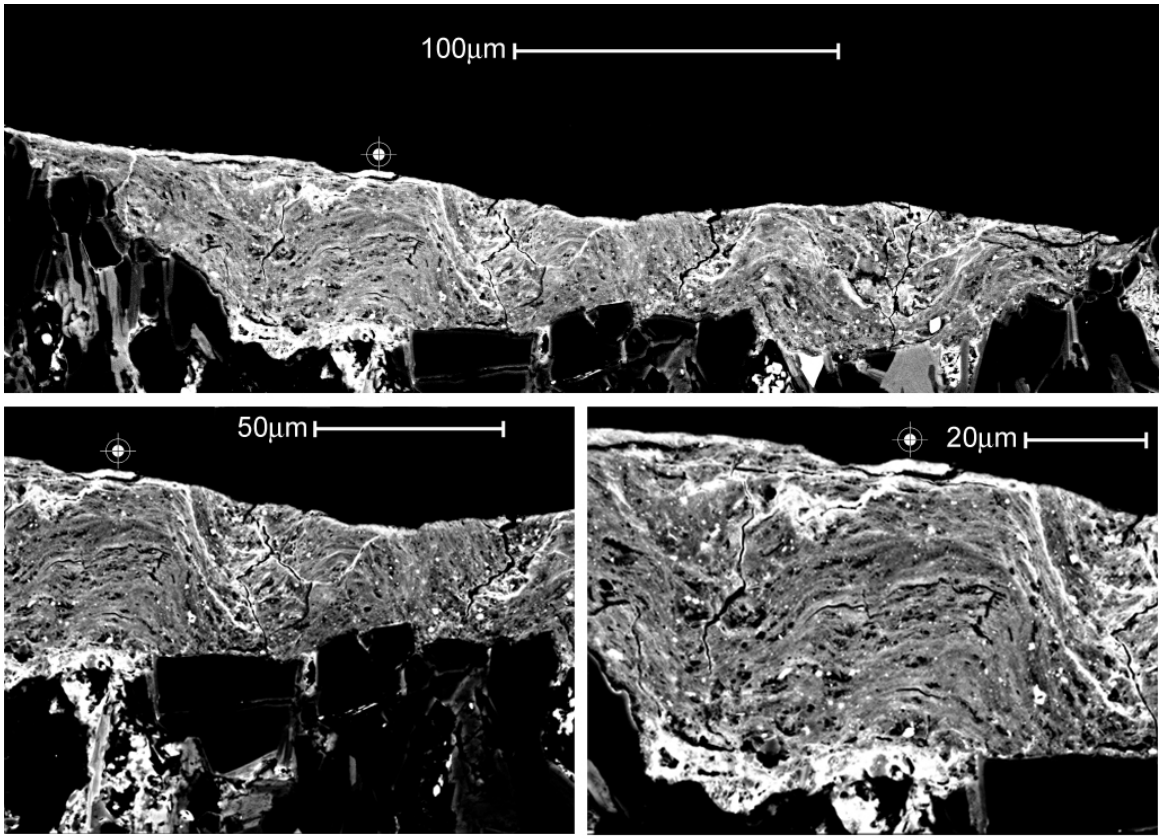

Figure 29. Backscattered electron microscope image of a polished cross section of rock varnish formed over sandstone at Karolta, South Australia, showing typical textural and compositional variability. Note the micro-stratigraphy and surface erosion.

Brown to grey varnish covers the tops and sides of many rock exposures in the region whereas the flat pavements and shallow depressions are coated with shiny black varnish up to 80 microns thick (fig. 29). Lichen and micro-colonial fungi are widely established across many varnished rocks. Thin veneers of calcrete are commonly formed at the interface between the rock and the surrounding soil (pH 8-8.5). Under the scanning electron microscope (SEM) (fig. 29), the undulating layers of the varnish appear to have formed on an eroded stable surface and do not follow the micro-topography of the rock substrate. Only the present surface of the varnish seems to be physically eroded.

6.3 Material and methods

Slabs of rock were collected from Karolta. Those slabs were covered with rock varnish and were not directly associated with petroglyphs. Under 30X magnification, the rock varnish coating was scraped away using a micro-drill equipped with tungsten carbide burrs. An area measuring approximately 5 cm x 5 cm was removed and the powder collected on aluminium foil. The underlying weathering rind as well as the unweathered heartrock was also collected using the same method. Milli-QTM water (> 18 MΩ cm), ultrapure acids and ultrapure salts were used during all chemical extractions and dissolutions.

6.3.1 Whole-sample analysis

A 200 mg aliquot of rock varnish, weathering rind and heartrock were separately dissolved with HF and HNO_3 in Teflon containers enclosed within steel jackets, and placed in a furnace (at 200°C) for 4 days. After successive additions of $HClO_4$ and evaporation to dryness, the residues were dissolved with concentrated 6N HCl solution, and again evaporated to dryness. Total rare-earth and other trace elements concentrations were determined on HCl solutions by inductively coupled plasma mass spectrometry (ICP-MS; VG Turbo Plasma Quad PQ^{2+} modified) at the Research School of Earth Sciences, Australian National University. Mn and Fe concentrations were measured on an ICP-AES at the Institut national de la recherche scientifique, Québec, Canada. A certified reference material (BHVO 2) was regularly submitted to the same digestion procedure as the soil samples. In, Re and Bi were used as an internal standards at a concentration of 10 ppb. Analytical precision was generally better than 3–5%.

6.3.2 Sequential extractions

To determine elemental speciation in the studied samples, a sequential extraction procedure has been carried out. Sequential extraction techniques have been initially developed for determining the mode of occurrence of trace metals in soils and sediments (Tessier 1979). The reactivity or mobility of heavy metals in soils and sediments, and thus their potential toxicity, depends upon the mineral phase in which the metals occur, their valence state and the chemical and physical processes that these phases are subjected to. The procedure used in this study was modified from Land *et al.* (1999). For instance, we used 0.05 g of sample instead of 1.0 g and all steps, including rinsing were done twice. Seven fractions were selected for extraction: (A) CH_3COONa-extractable (adsorbed/exchangeable/carbonate); (B) $Na_4P_2O_7$-extractable (labile organics); (C) 0.25 M $NH_2OH.HCl$-extractable (amorphous Fe-oxyhydroxides and Mn-oxides); (D) 1 M $NH_2OH.HCl$-extractable (crystalline Fe-oxides); (E) $KClO_3$/HCl-extractable (sulphides); (F) 4 M HNO_3-extractable (refractory organic) and (G) HNO_3/HF/$HClO_4$-extractable (residual silicates). After dilution of the extracts with Milli-QT water, elemental concentrations were determined by inductively coupled plasma mass spectrometry (ICP-MS; VG Turbo Plasma Quad PQ^{2+} modified) at the Research School of Earth Sciences, Australian National University. Mn and Fe concentrations were measured on an ICP-AES at the Institut national de la recherche scientifique, Québec, Canada.

6.3.3 Measurements of uranium and thorium isotopic ratios

6.3.3.1 Chemical separation of uranium and thorium

The separation of U and Th from the samples was achieved using Tru.spec extraction chromatography resin. All beakers and vials used in this study were made of PFA Teflon, and cleaned using hot Decon detergent, 20% HNO_3, 20% HCl and H_2O for 24-hours periods, refluxed with 2% HNO_3 + 0.1 M HF and rinsed with Milli-QTM water (> 18 MΩ cm). All acids used for sample dissolution and the separation chemistry were purified by sub-boiling distillation in quartz or PFA Teflon stills. The ion-exchange columns were made from PE and consist of a 1 ml solution reservoir, 0.25 ml of resin and 0.1 ml of pre-filter material.

The solutions from the sequential extraction procedure were evaporated to dryness, treated with H_2O_2 (to remove all traces of organics), dried again and diluted to 2 M HNO_3 for spiking. The samples were spiked with a mixed ^{229}Th-^{233}U, or "U-2" spike, which was calibrated against standard HU-1 uraninite solution in secular equilibrium. Finally, each solution was dried completely to equilibrate the sample with the spike and then re-dissolved in 2 M HNO_3 ready for the Tru.spec ion exchange column. A small amount of ascorbic acid was added to the sample prior to loading onto the column in order to reduce the Fe^{3+} in solution to Fe^{2+}.

The resin was cleaned by passing 0.05 M HC1 and a 0.1 M HC1 + 0.3 M HF mixture through the columns prior to use and then preconditioned with 1 M HNO_3. The ion exchange column chemistry is further outlined in table 3. After the sample solutions were loaded onto the resin bed as solutions in 1.5 M HNO_3, the columns were washed with 2 M HNO_3 and 0.1 M HCl + 0.1 M HF. Uranium and thorium were imperfectly separated from Tru.spec ion exchange medium, ~100% thorium and ~40% uranium in 0.1 M HCl + 0.1 M HF, and the remaining ~60% uranium in 0.1 M HC1 + 0.3 M HF evaporated and re-dissolved in 1 ml 2% HNO_3 (table. 3). An aliquot from the U fraction was added to the Th fraction, and diluted to 2 ml to yield a ~30 ppb uranium solution for thorium analysis. A separate aliquot from the uranium fraction was diluted to 2 ml to yield a ~30 ppb uranium solution for uranium analysis.

Tableau 3 : Chemical procedure for the separation of Th and U from rock varnish samples.

Step	Details	Column
Cleaning	Fill 0.05 M HCl (3X) Fill 0.1 M HCl/0.3 M HF (6X)	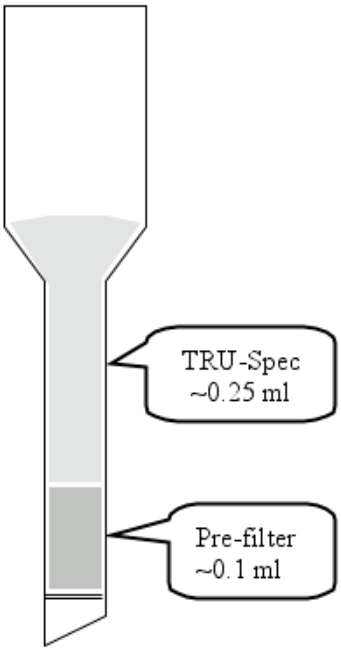
Conditioning	0.4 ml 1 M HNO3 (3X)	
Loading	Up to ~5 ml 2 M HNO3 (in 0.2 ml aliquots)	
Washing	Fill 2 M HNO3 ~0.75 ml 2 M HNO3 ~0.4 ml 2 M HNO3 ~0.3 ml 2 M HNO3 (2X) ~0.10 ml 0.1N HCl/0.1 M HF	
Collecting [Th]	~0.35 ml 0.1 M HCl/0.1 M HF (2X)	
Collecting [U]	~0.5 ml 0.1 M HCl/0.3 M HF ~1 ml 0.1 M HCl/0.3 M HF (6X)	

Uranium-series isotopic ratios were measured using a Finnigan Neptune double-focusing MC-ICP-MS equipped with electrostatic analyzer, secondary electron multiplier (SEM), and retarding potential quadrupole (RPQ) for high abundance sensitivity. The instrument has nine Faraday detectors: one fixed in the central position and four additional detectors on both the low-mass (L1-L4) and high-mass (H1-H4) sides. Samples were aspirated into the plasma through a conventional cyclonic glass spray chamber and a ISI Apex micro-concentric nebulizer and desolating system at an uptake rate of about 1.5 µl s^{-1} using a sample Ar gas flow.

6.3.3.2 Measurement of $^{229}Th/^{230}Th$ abundances

For thorium isotope measurements the isotopes ^{229}Th, ^{230}Th and ^{234}U and the baseline position $^{229.4}$Th are measured in 4 sequential steps in the ion counter. The isotopes ^{229}Th, ^{230}Th and ^{234}U are each measured concurrently with ^{238}U in a faraday cup (cups H3, H4 and H5) taking advantage of multi-collection measurements in reducing errors from the ion beam instabilities.

The measurement of ^{234}U is not however optimal in the thorium procedure as it relies on an externally measured gain with larger uncertainties introduced by the use of the RPQ. The RPQ is utilised in the thorium procedure as it results in a substantially improved abundance sensitivity of better than 0.2 ppm and hence tailing corrections are minimal for the thorium isotopes. With the RPQ, baselines are more than adequately accounted for by a single measurement at $^{229.4}Th$. This position was chosen to minimise the possibility of non integer interferences, particularly those that can occur in the mass region $^{230.5\text{-}231}Th$. Careful monitoring of blanks and possible spectral interferences are always essential in MC-ICP-MS and this is especially the case for measurement of the extremely low abundant ^{230}Th.

The abundance of ^{230}Th is directly proportional to the age of the sample, with the inherent precision being dictated by the sample size, together with the magnitude of systematic errors such as tailing, blank corrections, spectral interferences and the uncertainty in the correction of inherent ^{230}Th. Tails from uranium are reduced by chemical separation of thorium from uranium, but sufficient uranium (1-2 volts ^{238}U signal) must remain in the thorium fraction to enable the use of the $^{235}U/^{238}U$ ratio for mass bias corrections. The most effective means for reducing tails is the implementation of the RPQ energy filter, which effectively eliminates the need for tailing corrections to the thorium isotopes. The RPQ filter was therefore utilised for thorium measurements, but this has adverse consequences for the stability of the SEM/Faraday gain calibrations and therefore was not implemented for uranium isotope measurements where the SEM/Faraday gain must be precisely known.

6.3.3.3 Protocols for uranium isotopes measurements

Although $^{234}U/^{238}U$ ratios can be, in principle, directly measured using only the Faraday cup array this requires large ion beams for ^{238}U (300-500 volts), together with the use of relatively large amounts of tracer ^{233}U. This approach is not generally applicable (not enough uranium in the sample) and has the major disadvantage of introducing substantial uranium into the system and hence the possibility of compromising the measurement of low uranium samples. The preferred and more universally applicable approach adopted here is to measure ^{234}U on an ion counting system and to simultaneously measure ^{233}U, ^{235}U and ^{238}U on the Faraday array. Isotope ^{233}U is used for determining the uranium concentrations and $^{235}U/^{238}U$ for mass fractionation

corrections after subtracting the minor spike component from ^{233}U. This approach requires cross calibration of the gain of the SEM relative to the Faraday system.

6.3.3.4 SEM gain calibrations

Calibration procedures to determine the relative efficiency or gain of ion counting systems with respect to Faradays arrays can be categorized into two main types; internal or external. Internal calibrations are those undertaken by alternating a common isotope such as ^{235}U (or ^{233}U) between the ion counter and Faraday array as part of the overall measurement protocol. This is done during sample measurement, whereas an external (static) procedure refers to the standard/sample approach with the gain derived externally from measurement of ^{234}U in a separate standard solution. The internal or dynamic approach, described for example in TIMS measurements by Stirling et al (1995) and subsequently adapted for MC-ICP-MS by a number of workers, has the advantage of repeated, rapid measurements of the gain throughout the data acquisition sequence and can therefore account for short-term drifts in ion beam transmission and associated changes in mass bias that may effect the SEM gain. The disadvantage of this approach is that in order to have sufficient signal to measure accurately in both the Faraday cup and SEM, large (5-10 mv) signals, corresponding to high count rates ($>10^6$ cts/second) are generated in the ion counter. With such high count-rates, issues such as dead-time corrections, aging of the detector and the potential for non-linearity in the ion counter all become significant factors. It is noted that these limitations were minimal in the Stirling *et al.* TIMS procedure as that study utilised an older system with SEM operating in the analogue mode. The SEM analogue mode which can handle higher ion current (10^{-12} amps) can overcome the high count rate limitations of measuring internal gains, but is inherently less sensitive for measurement of extremely low count rate sample such as ^{230}Th in rock varnish. Analogue SEM systems are not currently available in most modern instruments.

The external approach is undertaken using standard/sample protocols which have been widely utilised in MC-ICP-MS systems for the measurement of naturally occurring mass bias in isotope systems such as Cu, Zn, Fe, etc. Gains are measured statically by measuring $^{234}U/^{235}U$ in SEM/Faraday system using the NBS 960 standard. We have adopted the use of NBS 960 as an external standard as it contains very minor quantities of ^{230}Th and thus effectively acts as a washout solution for the more intransigent thorium. The standard is measured at appropriate

intervals (every 1-2 hours) depending on instrumental drift and the ultimate stability required for the bracketing of the SEM gains. Relative gains derived from standard measurements are then interpolated to the unknowns. This external approach therefore requires not only a relatively constant gain but also that the drifts in signal intensity or mass bias that may differentially effect the SEM transmission, are minimal over time. This external approach has the major advantage of generating count rates for the standard and unknowns that are approximately similar, hence avoiding issues associated with high count rates, dead time corrections and ion counter non-linearity.

It is also essential to measure and correct uranium baselines directly. This is especially necessary for accurate, high-precision measurements of the low abundant ^{234}U isotope. For example, in measuring ^{234}U the effects of tailing from a 4-8 volt beam of ^{238}U are at the level of ~100 counts at mass 234 corresponding to a ~2.5% correction to the $^{234}U/^{238}U$ ratio. Thus, changes in the abundance sensitivity at the 10% or greater level can limit the ultimate precision of $^{234}U/^{238}U$ at the permil level. Although these errors are minimised by the use of standard/sample comparison where effects of tailing or abundance sensitivity should theoretically cancel out for similar uranium intensities. Direct measurements of the uranium baseline were therefore undertaken immediately adjacent to ^{234}U at masses 233.5 and 234.5; the isotope most sensitive to tailing correction from ^{238}U.

6.4 Results and Discussion

6.4.1 Mn and Fe speciation

It has long been recognised that a key to understanding varnish formation resides in explaining the large enrichment in Mn (e.g. von Humboldt 1812; Lucas 1905; Engel and Sharp 1958; Jones 1991). The speciation of manganese and iron determined from the sequential extractions from the varnish, and the weathered and unweathered bedrock from Karolta, reveal features that lead to a better understanding of the mechanisms responsible for the formation of these layers.

One of the most distinctive features is the enrichment of manganese in the weathered rock crust compared to the unweathered sandstone (factor of 13) and the further enrichment by a factor of 4 in the varnish compared to the crust resulting in a total manganese enrichment factor of 52 (fig. 30). At the same time, there is no significant iron enrichment in the varnish or crust over the sandstone.

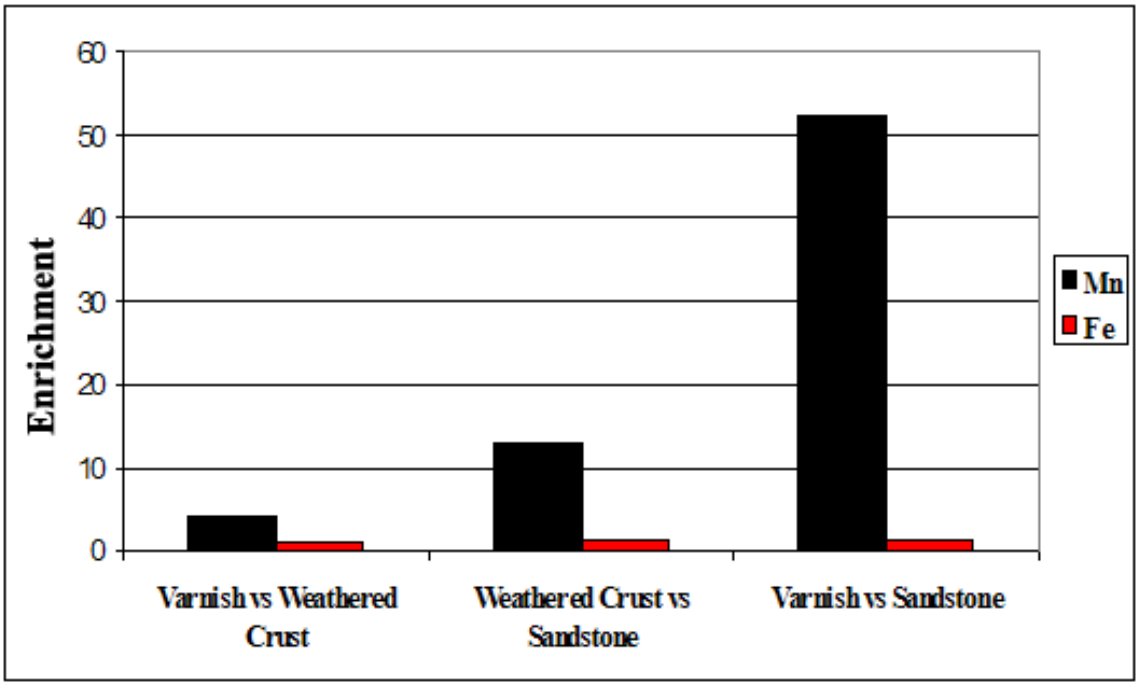

Figure 30. Total Mn and Fe enrichment factor in the varnish versus weathered rock, weathered rock versus unweathered rock and varnish versus unweathered rock.

In soil, manganese solubility is determined by two major variables; pH and redox potential. Under typical desert climatic conditions manganese is much more soluble than Fe (Engel and Sharp 1958). Therefore, the relative enrichment of Mn in the weathered crust can be explained by its release from unweathered rock which is in contact with meteoric water. This release could occur by diffusion processes as a result of a steep Mn (II) concentration gradient across the rock-water interface. Recycling at the redox boundary (i.e. oxic/anoxic transition) potentially creates a manganese enriched horizon.

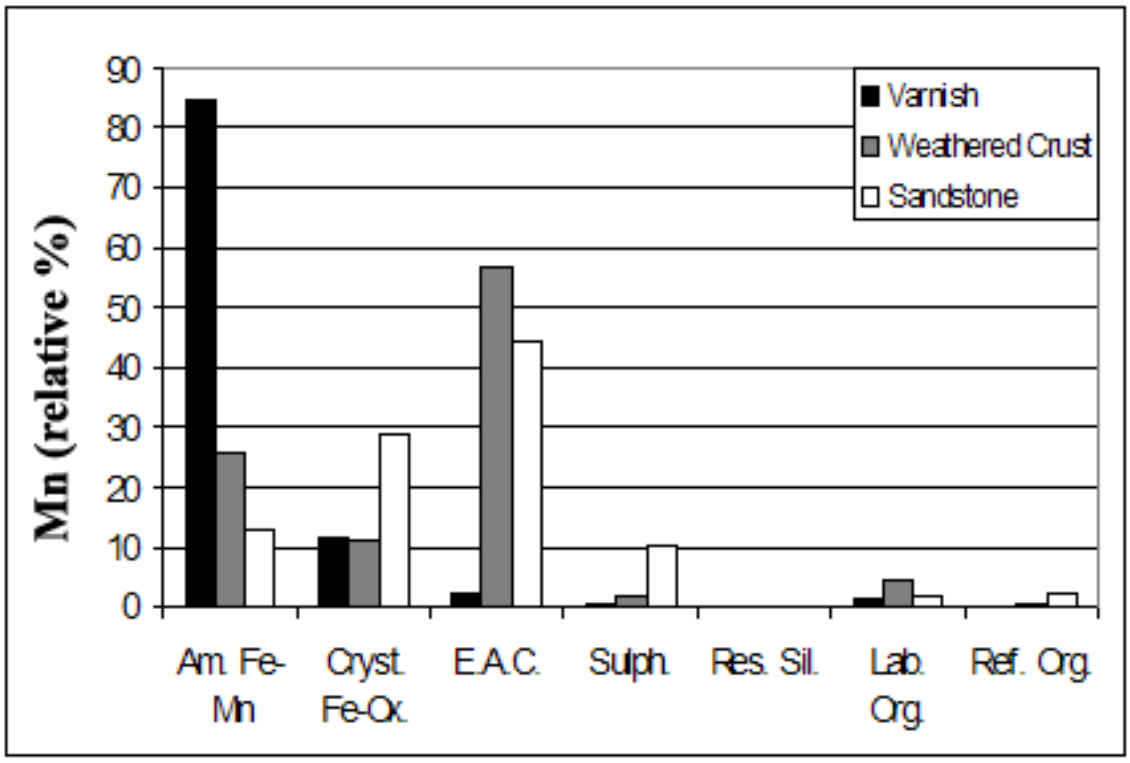

Figure 31. Speciation of Mn in the varnish, weathered and unweathered bedrock.

The manganese-enriched weathered crust is also subject to physical weathering resulting in Mn-enriched windblown particulates, being deposited in natural surface depressions. This observation is confirmed by high field strength element geochemistry (HFSE) presented below. In wet events, meteoric water accumulates in the same depressions and Mn is leached out of those particulates. In contact with the charged surfaces of particulates, it then forms manganese oxides, hydroxides and oxy-hydroxides through cation exchange reactions (Evans, 1989). This results in 85% of this manganese being concentrated in the amorphous Fe-oxyhydroxides and Mn-oxides phases of the varnish (fig. 31). In the presence of high Fe, concentrations of manganese can also be adsorbed to the Fe-hydroxides through ligand exchange reactions, but this phenomenon is not significant in the formation of the varnish studied here. (figs. 30 & 32).

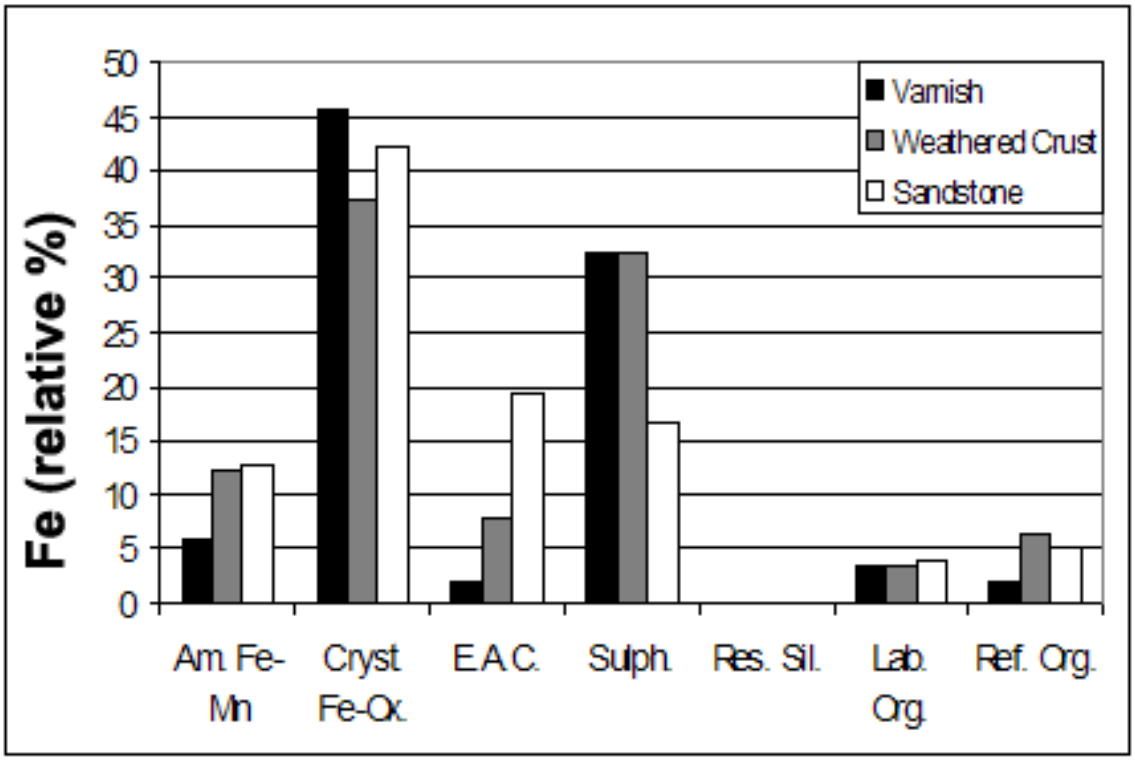

Figure 32. Speciation of Fe in the varnish, weathered and unweathered bedrock.

6.4.2 High field strength elements geochemistry (HFSE) (Nb, Ta, Zr, Hf)

These elements are highly insoluble even in the extreme case of acidic high-temperature hydrothermal fluid-rock interactions. Because of these chemical characteristics, HFSE are of interest to this study since they should reflect the provenance of the silicate fraction enclosed within the rock varnish layers. Furthermore, comparison of the behaviour and relative fractionation of the HFSE from the rare earth elements (REE) could be used to examine secondary enrichment processes of the REE since normally REE and HFSE are highly coupled in igneous, metamorphic and siliclastic sedimentary rocks.

Figure 33 shows bar charts of the absolute abundances of Zr, Hf, Nb and Ta in the rock varnish, the weathered crust and unweathered bedrock of the Karolta samples. Interestingly and unlike the REE, the HFSE display nearly similar abundances among the rock, weathered rock and varnish. At first glance, this may indicate the lack of secondary enrichment processes for these elements during the formation of the varnish.

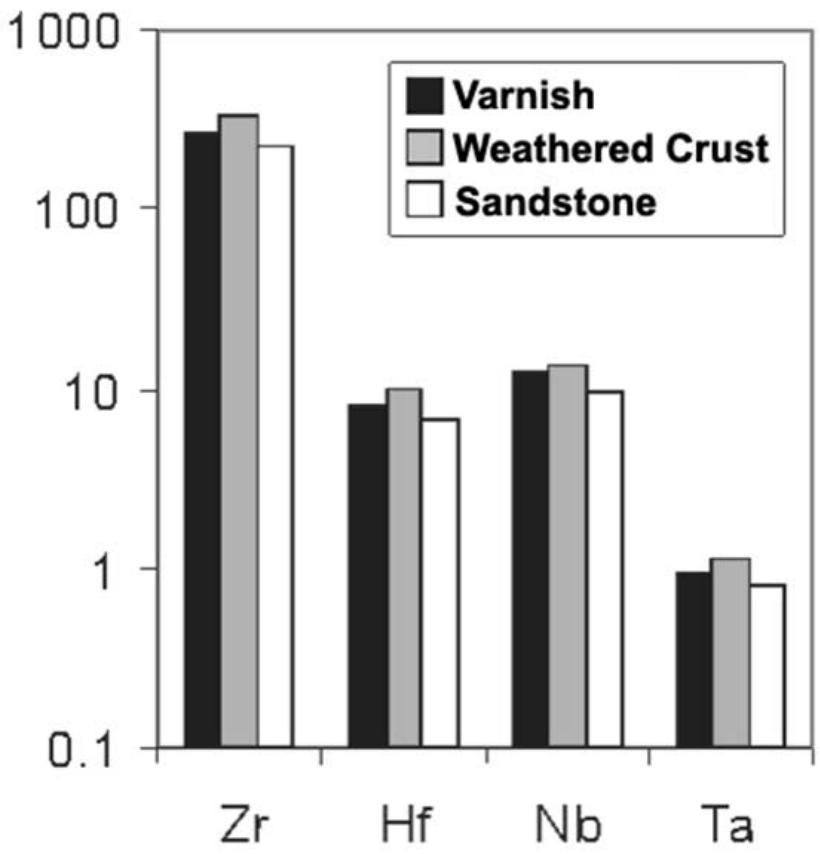

Figure 33. Zr, Hf, Nb and Ta abundances in the rock varnish, the weathered crust and the sandstone of the Karolta site.

In many geochemical studies, REE and HFSE are usually presented on multi-element spider diagrams in order of increasing magmatic incompatibility from the right to the left side of the diagram (fig. 34). On this diagram it is clear that the HFSE show limited variations when compared to the REE and other elements, such as the actinides (U and Th) and the alkaline earth elements (eg. Rb, Ba, Sr) and Pb.

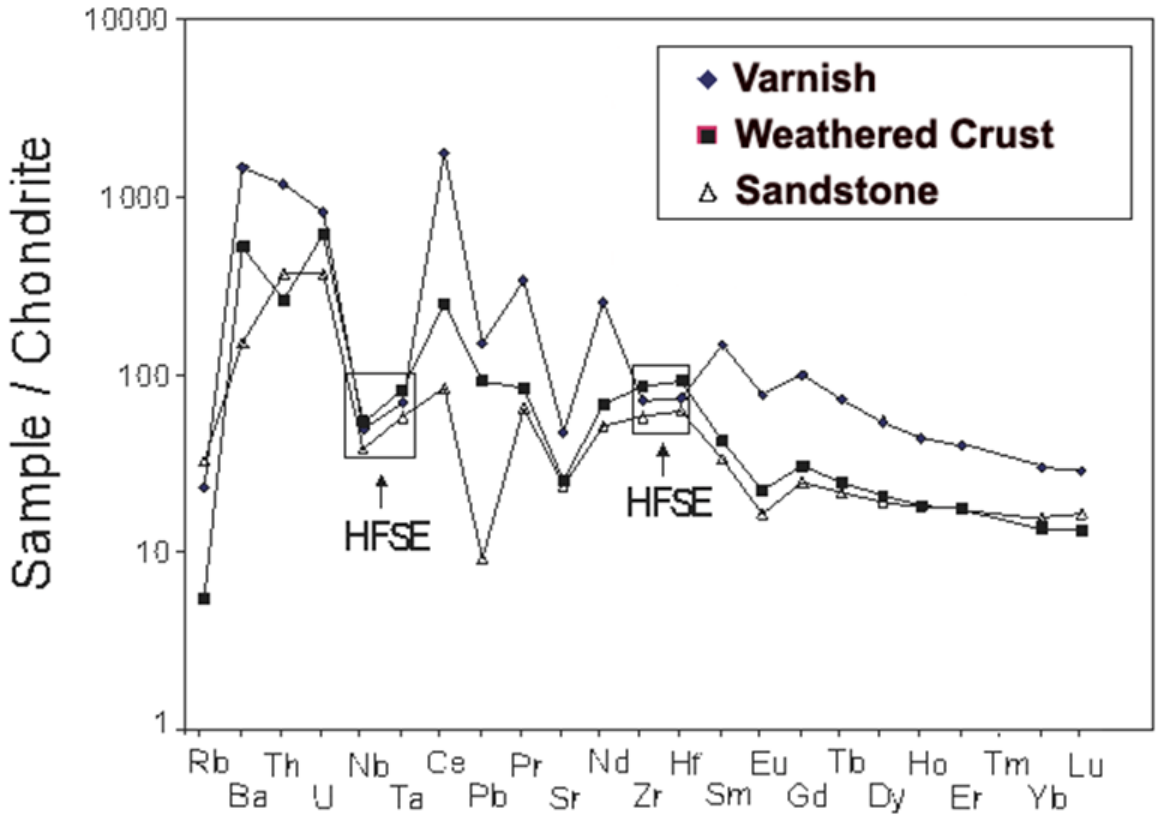

Figure 34. Multi-element spider diagram for the rock varnish, the weathered crust and the sandstone form the Karolta site.

Inter-element ratios show that there are no significant differences between the Zr/Hf, Zr/Nb, Nb/Ta and Hf/Ta among the sandstone, the weathered crust and the rock varnish (fig. 35). This indicates that the particulate rock component within the rock varnish is similar to the composition of the fresh and altered sandstone. The Zr/Hf and Nb/Ta ratios observed in the fresh and altered sandstone, and in the rock varnish are similar to the composition of upper crusted sediments. The relatively high Zr/Nb and Hf/Ta observed in the studied rocks may indicate some heavy accessory minerals accumulation by hydraulic sorting during sedimentation of the sandstone.

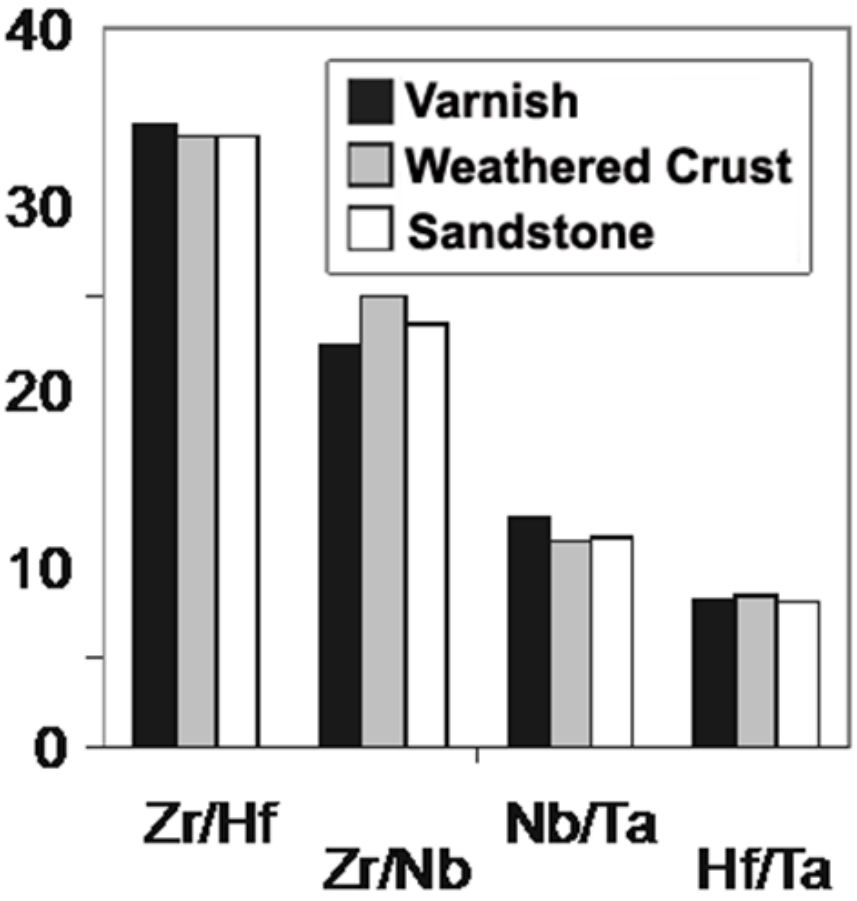

Figure 35. Zr/Hf, Zr/Nb, Nb/Ta and Hf/Ta of the sandstone, the weathered crust and the rock varnish.

6.4.3 REE geochemistry

Total dissolution Chondrite-normalized REE patterns of the sandstone bedrock and weathered crust display relatively flat REE patterns with LaN/LuN of 5-8 and small Eu negative anomalies ([Eu/Eu*]N: from 0.56 to 0.61) characteristic of siliclastic sediments derived from the upper crust. The weathered crust is, however, slightly enriched in the LREE when compared to the sandstone composition. A notable feature is a pronounced Ce positive anomaly ([Ce/Pr]N = 3.02) in the weathered crust and rock varnish when compared to the sandstone that lacks a significant Ce anomaly ([Ce/Pr]N = 1.29).

The REE pattern of the rock-varnish is nearly parallel, but systematically enriched relative to the pattern of the weathered crust (fig. 36). The Eu anomaly is identical in both layers ([Eu/Eu*]N = 0.61), but the rock-varnish displays a very strong Ce positive anomaly ([Ce/Pr]N = 5.2)

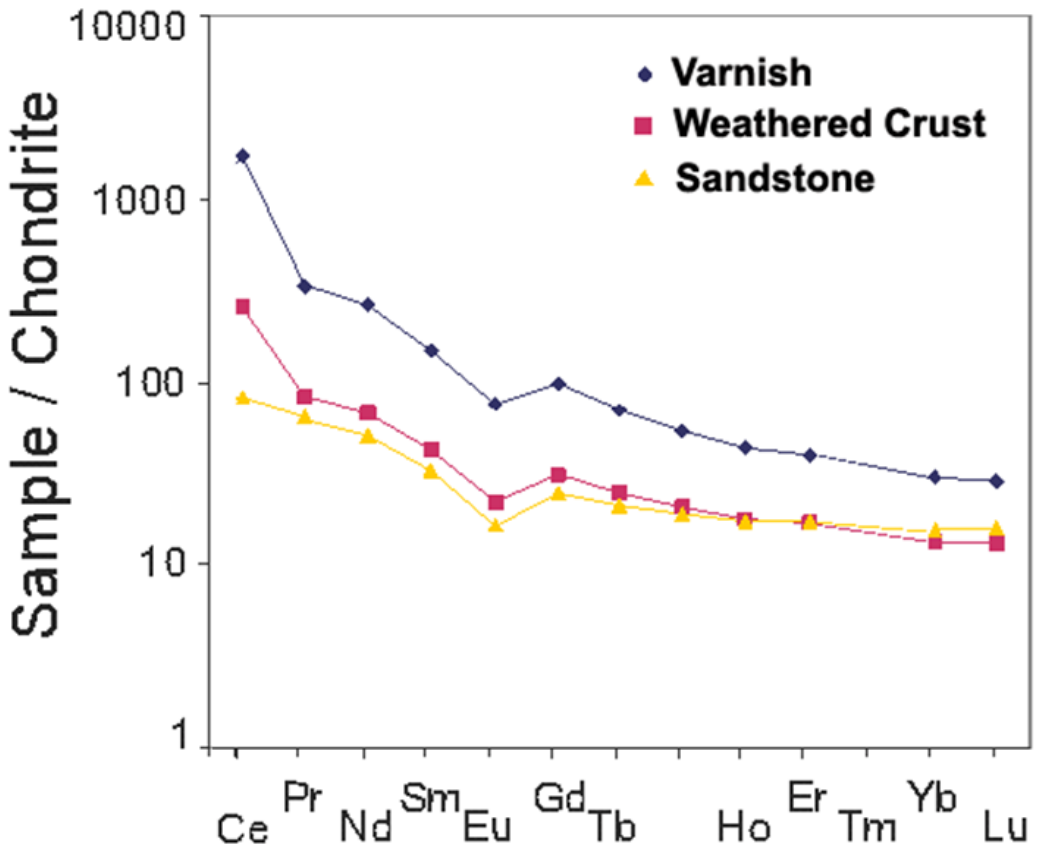

Figure 36. Chondrite-normalized REE patterns for the rock varnish, the weathered crust and the fresh sandstone. Note the systematic relative enrichment in Ce in the weathered crust and the rock-varnish.

When normalized to the composition of the unaltered sandstone, the differences and similarities between the weathered crust and the rock varnish are more evident. Firstly, with the exception of Ce, the weathered rock shows very limited enrichment in REE when compared to the composition of the sandstone. Contrast this with the fact that the rock varnish shows an enrichment of 2 times for the heavy rare earth elements (HREE) (Gd to Lu) and 5 times for the

light ones LREE (La to Sm). When compared to the sandstone composition, the Ce- normalized abundances of the weathered crust and the rock varnish are enriched from 3 to 20 times, respectively.

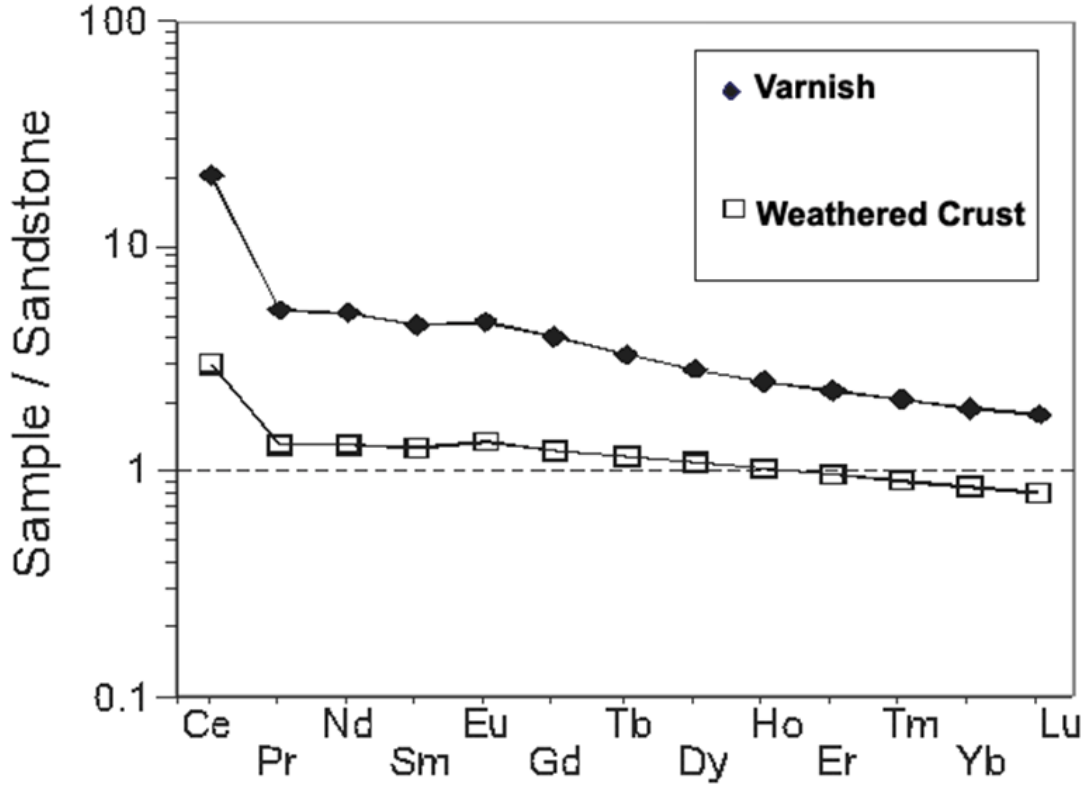

Figure 37. **Sandstone-normalized REE patterns for the rock varnish and the weathered crust.**

Figures 37 and 38 emphasise the important REE features of the different materials sampled on the Karolta site. With the exception of Ce, which is strongly enriched due to its higher ionic potential (+4 compare to +3 for the other LREE), the weathered crust and the rock varnish display similar LREE fractionation ([Pr/Sm]N ratios). On the other hand, the bulk REE concentration is much higher in the rock varnish than in the weathered crust (1294 vs 221 ppm) (fig. 38). This could indicate the involvement of an extremely efficient scavenging mechanism capable of producing a layer with REE content one order of magnitude higher than the host rocks (sandstone = 104 ppm). The enrichment factor in REE probably reflects the presence of Mn and

Fe oxides and hydroxides in the rock varnish. The results of the sequential chemical speciation explain the partitioning of these elements, as described below.

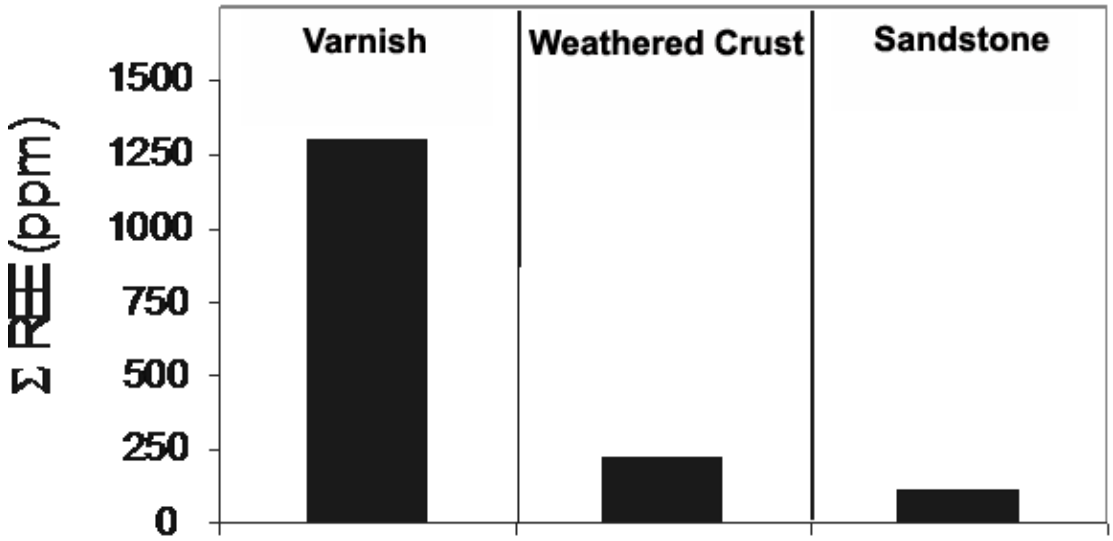

Figure 38. Total REE contents of the Karolta rock varnish, weathered crust and sandstone. Note the relative enrichment factor of the rock varnish when compared to the sandstone.

6.4.4 Rock-Varnish REE Speciation

The results from the sequential chemical speciation display wide variations in the host phases for REE among the rock, weathered rock and varnish (fig. 39). Interestingly, most of the REE in the varnish are partitioned in the amorphous Fe-oxyhydroxides/amorphous Mn-oxides and in the crystalline Fe-oxides (85%), and only 3% of the total REE are partitioned in the residual silicates. In the sandstone, 73% of the REE are in the EAC and sulphides fractions. Other phases, such as exchangeable, adsorbed, carbonates, sulphides, labile and refractory organics contain less than 12% of the total REE. In the weathered rock, 60% of the REE are partitioned in the Fe-oxyhydroxides/amorphous Mn-oxides and crystalline Fe-oxides indicating similar enrichment processes. In the unweathered bedrock, 75% of REE are partitioned in the exchangeable, adsorbed, carbonates and sulphides phases. Figure 39 also shows that 50% of the sandstone REE are partitioned in the sulphides phase. This seems unlikely. However, the total REE

concentration in the sandstone is very small compared to the weathered crust and varnish. Moreover, the sulphide fractions of the weathered crust and varnish have virtually the same REE concentration than the sulphide fraction of the sandstone.

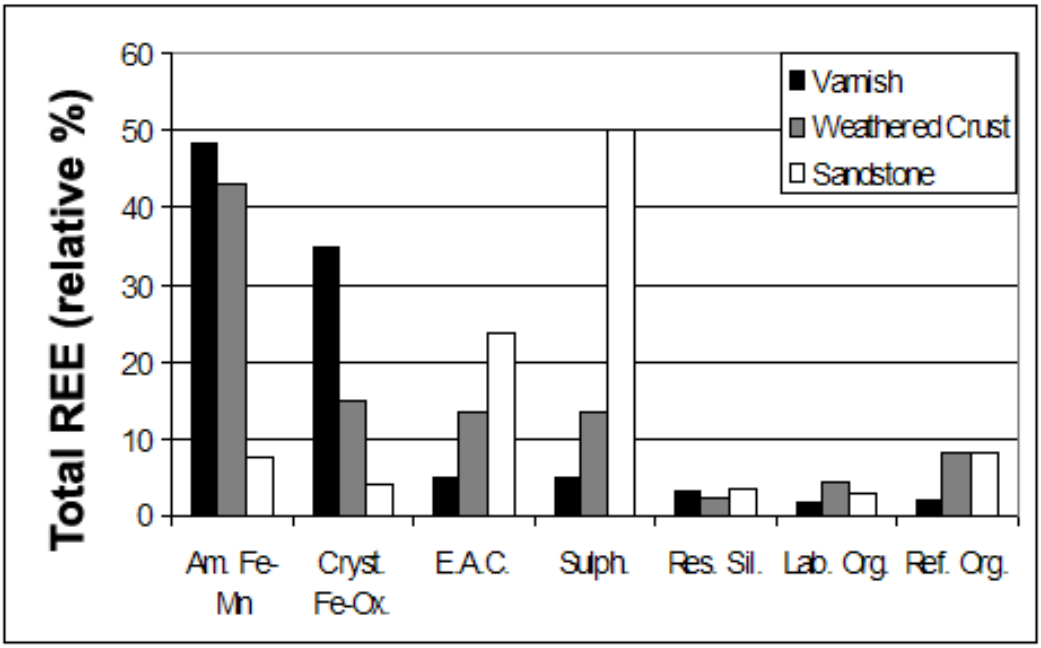

Figure 39 **Total REE content (relative %) in the different chemical fractions. Note that more than 85% of the REE in the varnish are partitioned in the Fe-oxyhydroxides/amorphous Mn-oxides and in the crystalline Fe-oxides.**

Figure 40 shows more details about the REE characteristics of the different chemical fractions. The speciation study reveals that the signatures of the Fe-oxyhydroxides/amorphous Mn-oxides and of the crystalline Fe-oxides are similar to the composition of the total rock varnish. This observation implies that these phases are mainly responsible for the REE signature of the rock varnish. These Fe-Mn phases also display the strongest Ce positive anomalies with [Ce/Pr]N ratios ranging from 5.5 to 6.7. On the other hand, it is noteworthy that the refractory organics and the residual silicates do not possess Ce anomalies. This confirms the preferential partitioning of Ce onto Fe–Mn oxyhydroxides because of its higher ionic potential.

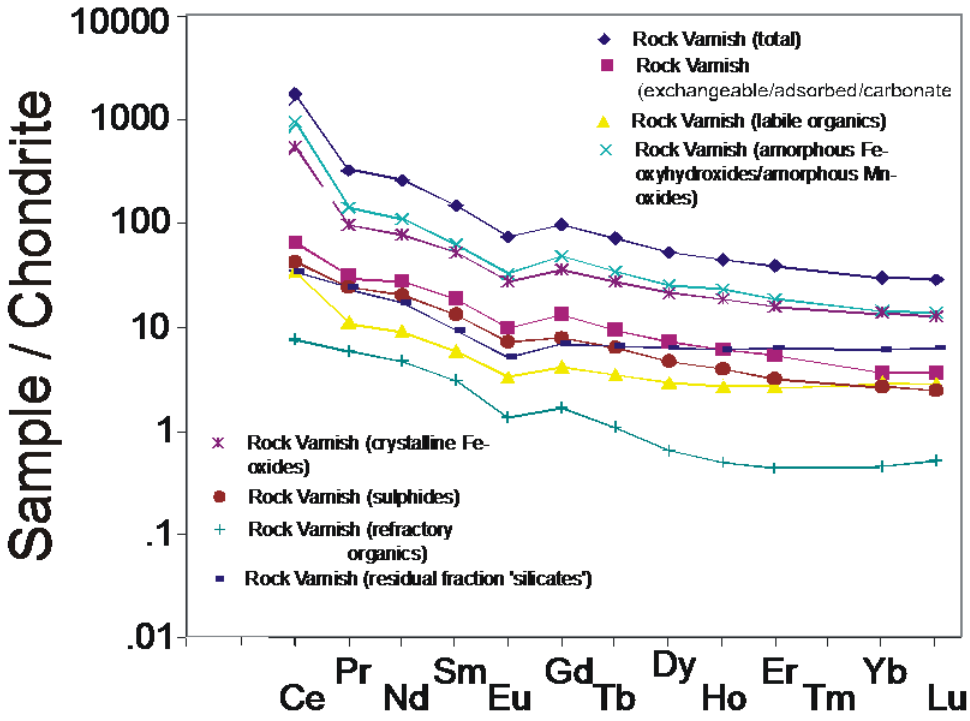

Figure 40. Chondrite-normalized REE patterns of the different chemical fractions from the sequential extraction procedure.

Figure 41 shows a summary of the speciation for each of the individual REE. As previously discussed, the Fe-oxyhydroxides/amorphous Mn-oxides and of the crystalline Fe-oxides contain most of the REE. This diagram also illustrates that the relative proportions of the residual silicate fraction increases from the LREE to the HREE. On the other hand, the REE, independent of their atomic number, are present to less than 10% in the exchangeable/adsorbed/carbonate fraction. This indicates that the REE in rock varnish are not present as weakly bonded elements.

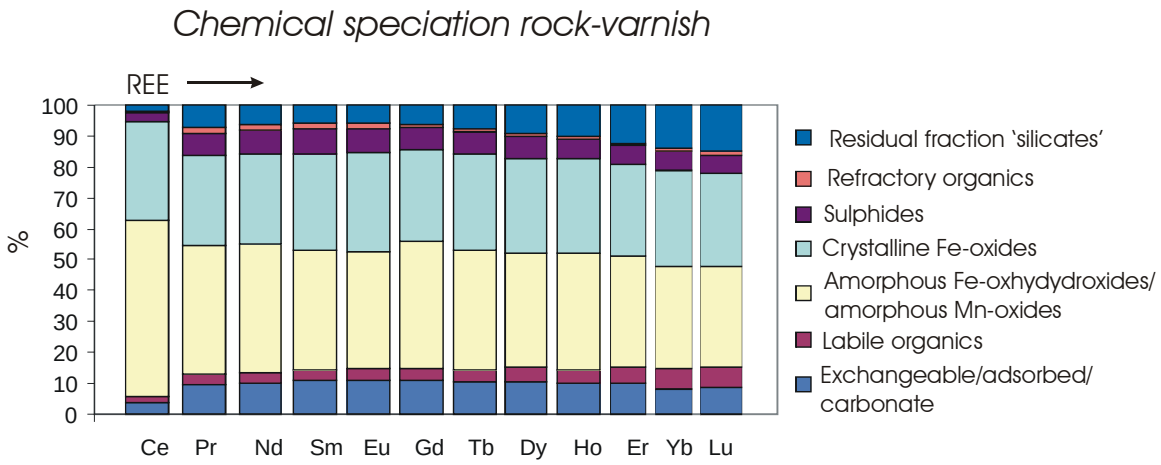

Figure 41. REE speciation expressed as relative proportions for the individuals REE. The REE are presented from left to right in increasing atomic number.

6.4.5 Uranium-series geochemistry

In 1980, Knauss and Ku suggested that uranium series isotopes could provide a means for determining the age of formation of rock varnish from the Colorado Plateau. They analysed the heartrock sandstone, altered rind and varnish and found that uranium concentration increases in that order while the thorium concentration decreases. They assumed that all of the ^{232}Th in the varnish came from clay and that the oxide phases in the varnish had low initial ^{230}Th and ^{231}Pa contents. Concordancy checks between ^{230}Th/^{234}U and ^{231}Pa/^{235}U measured by alpha-spectrometry indicated a closed system, for uranium-series dating. They recommended the use of acetic acid/hydroxylamine hydrochloride to leach the authigenic oxide phase in the varnish and to analyze the leached solution and residual fraction (for initial ^{230}Th and ^{231}Pa correction) to determine the age of the varnish.

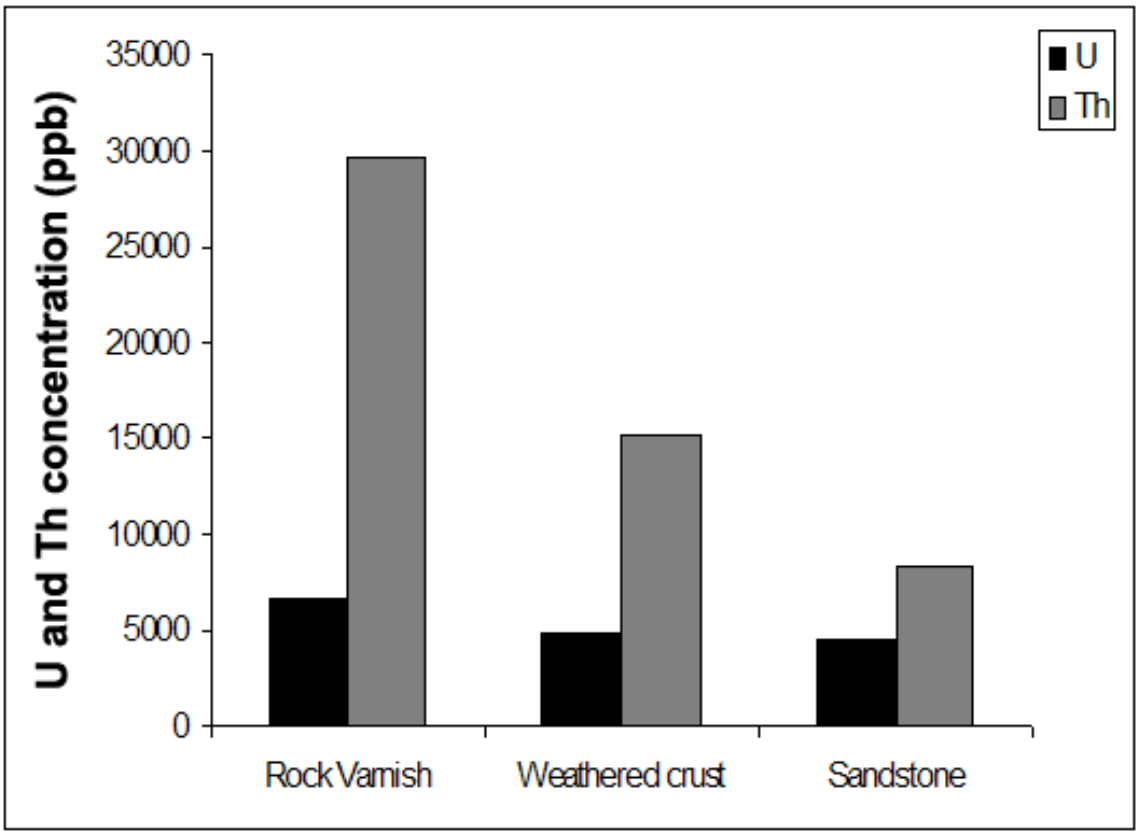

Figure 42. Concentration of uranium and thorium in the varnish, weathered crust and sandstone

The varnish from Karolta shows the exact opposite behaviour to that found by Knauss and Ku, where the thorium and uranium concentrations increased from the heart rock and weathered crust to the varnish (fig. 42). This indicates an allogenic source for most of the thorium in the varnish. The sequential extraction data shows that most of the uranium is partitioned in the residual silicate phase where its concentration decreases from the rock, weathered rock and varnish (fig.43). As previously shown, the HREE content of the residual silicates as well as the relatively high Zr/Nb and Hf/Ta ratios indicates the presence of HREE-rich accessory minerals. Those minerals are usually rich in uranium and are unlikely to be leached by low temperature natural processes. Another interesting feature is that a high proportion of uranium in the varnish is partitioned in the crystalline Fe-oxides, adsorbed/exchangeable/carbonate and suphides phases indicating an increase in the proportion of authigenic uranium. Interestingly, the phase of amorphous Fe-oxyhydroxides and Mn-oxides is the lowest uranium-bearing phase (fig. 43).

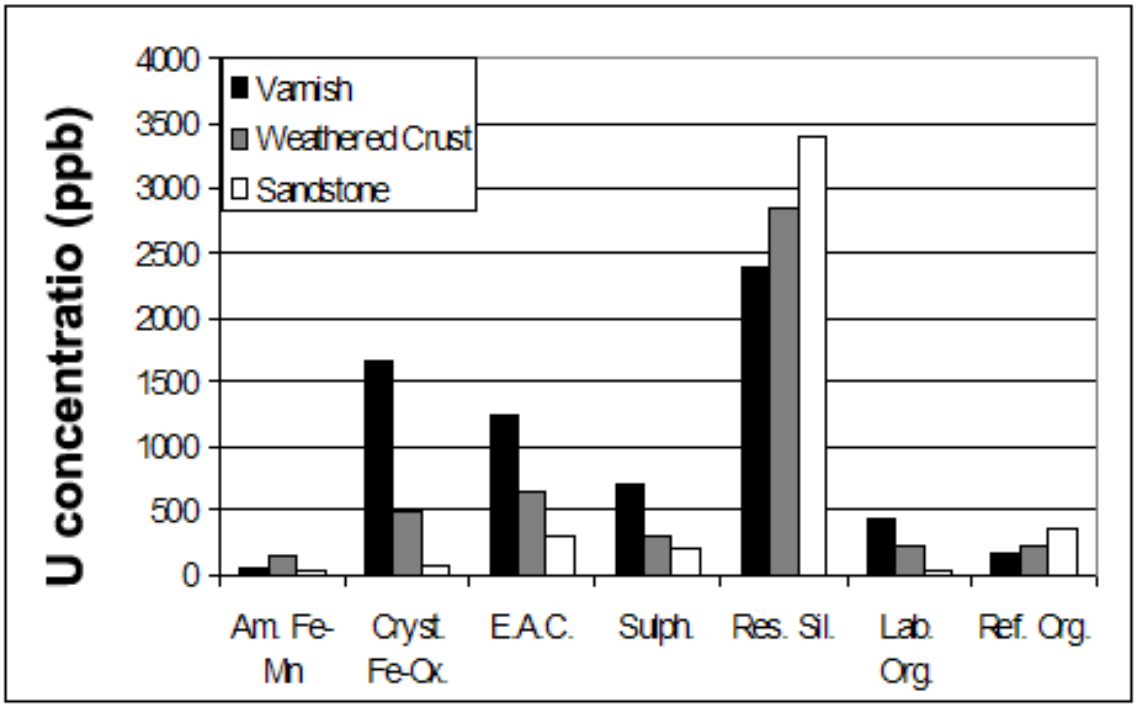

Figure 43. Speciation of uranium in the varnish, weathered crust and sandstone.

As mentioned by Knauss and Ku (1980), authigenic iron oxy/hydroxides have a high affinity towards dissolved uranyl complexes and they should form a closed system for uranium-series isotopes. If corrections could be made for the initial $^{230}Th/^{232}Th$, it might be possible to determine the age of the varnish on the basis of the insolubility of Th in aqueous solution and the growth of radiogenic ^{230}Th towards secular equilibrium.

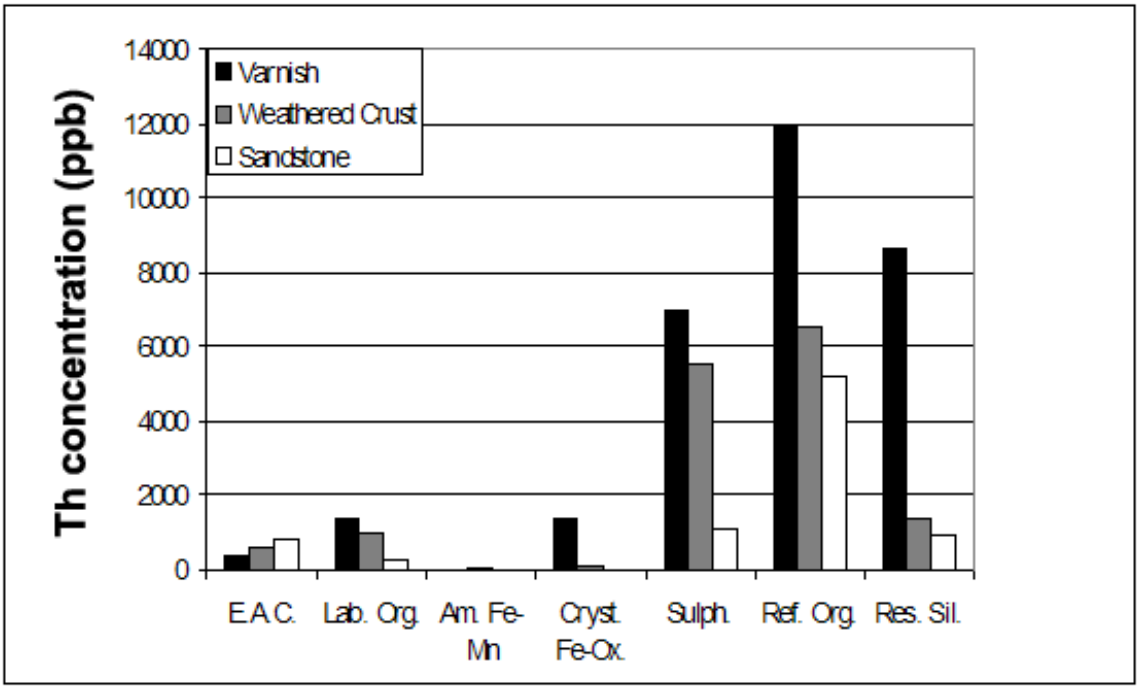

Figure 44. Speciation of thorium in the varnish, weathered crust and sandstone in extraction order. Note the accumulation of Th.

The sequential extraction process used in this study was modified from Land *et al.* (1999) and was initially developed in order to study the mobility and the natural fractionation of rare earths in soils and sediments. This protocol was selected because the actinides and the rare earth elements have similar chemical behaviours. However, it appears that the chosen method was inefficient in sequentially extracting thorium from each mineral phase. As shown in figure 44, there is a net increase of Th relative to the order of extraction. This is confirmed by the high $^{230}Th/^{234}U$ activity ratio in the refractory organics phase (the last extracted phase) with a ratio of 8.65 (table 4). It seems that during the previous extraction steps, thorium was either briefly in solution or was simply not leached at all. It is therefore impossible to study the partitioning of thorium and consequently date the formation of the varnish using this particular method.

Tableau 4. Summary of the results of U-series analyses following chemical sequential extraction of rock varnishes from Karolta, Australia. The enormously high $^{230}Th/^{234}U$ ratio in the refractory organics phase (with a ratio of 8.65) suggests readsorbtion and/or accumulation of thorium in the last extracted phase (the refractory organics).

	Activity Ratios		
Mineral Phase in extracted order	**$^{230}Th/^{232}Th$**	**$^{234}U/^{238}U$**	**$^{230}Th/^{234}U$**
1. exchangeable/adsorbed/carbonate	0.9	4.0573	0.0205
2. labile organics	0.9	3.8731	0.2669
3. amorphous Fe-oxyhydroxides/Mn-oxides	0.8	3.0167	0.0382
4. crystalline Fe-oxides	1.0	3.5057	0.0216
5. sulphides	0.8	3.0813	0.9226
6. refractory organics	0.8	2.153	**8.6554**
7. residual fraction (silicates) (quartz grains and other silicates)	0.8	2.7868	0.4917

6.5 Conclusion and Perspective

It appears that the formation of manganese-rich rock varnish layers at Karolta, South Australia, is a two step process starting with manganese enrichment in the weathered bedrock surface (compared to the unweathered sandstone). The mechanical weathering of this enriched crust and its redeposition as windblown particulates form the key ingredients of the varnish. In the presence of water accumulating periodically at the surface of the outcrop, manganese is dissolved from those windblown particulates and eventually forms Mn oxides, hydroxides and oxy-hydroxides cementing the leached residual particulates and other accumulating debris forming undulating layers. This process also concentrates the mobile rare earth elements and occurs with or without the presence of micro-organisms affecting the redox potential of the solution.

While most of the uranium is partitioned in the residual silicate fraction, there is an important contribution from allogenic uranium. However, the strong accumulation of detrital thorium, coupled with the inability of the chemical procedure to extract thorium sequentially, hampers the uranium-series dating of the varnish.

If thorium is briefly in solution during the chemical extractions it may be possible to collect it in a separate plating deposition step before it reattaches to the refractory organics. Additionally, new developments in microprobe technology may enable the direct dating of authigenic oxides *in situ* within rock sections.

7 HIGH RESOLUTION ANALYSIS OF URANIUM AND THORIUM CONCENTRATION AS WELL AS U-SERIES ISOTOPE DISTRIBUTIONS IN A NEANDERTHAL TOOTH FROM PAYRE USING LASER ABLATION ICP-MS

Rainer Grün[1], Maxime Aubert[1,2], & Marie-Hélène Moncel[3]

[1] Research School of Earth Sciences, Australian National University, Canberra, Australian Capital Territory 0200, Australia

[2] Eau, Terre & Environnement, Institut National de la Recherche Scientifique, G1K 9A9, Québec, Canada

[3] Département de Préhistoire, Muséum National d'Histoire Naturelle, 1 Rue René Panhard, 75013 Paris, France

Abstract

We have mapped U (^{238}U) and Th (^{232}Th) elemental concentrations as well as U-series isotope distributions in a Neanderthal tooth from the Middle Palaeolithic site of Payre using laser ablation ICP-MS. The U concentrations in an enamel section varied between 1 and 1500 ppb. The U concentration maps show that U-migration through the external enamel surface is minute, the bulk of the uranium having migrated internally via the dentine into the enamel. The uranium migration and uptake is critically dependent on the mineralogical structure of the enamel. Increased U concentrations are observed along lineaments, some of which are associated with cracks, and others may be related to intra-prismatic zones or cracks reaching from the dentine into the enamel. The uranium concentrations in the dentine vary between about 25,000 and 45,000 ppb. Our systematic

mapping of U-concentration and U-series isotopes provides insight into the time domain of U-accumulation. Most of the uranium was accumulated in an early stage of burial, with some much later overprints. None of the uranium concentration and U-series profiles across the root of the tooth complied with a single stage diffusion-adsorption (D-A) model that is used for quality control in U-series dating of bones and teeth. Nevertheless, in the domains that yielded the oldest apparent U-series age estimates, U-leaching could be excluded. This means that the oldest apparent U-series ages of around 200 ka represent a minimum age for this Neanderthal specimen. This is in good agreement with independent age assessments (200 to 230 ka) for the archaeological layer in which it was found.

The Th elemental concentrations in the dental tissues were generally low (between about 1 to 20 ppb), and show little relationship with the nature of the tissue.

7.1 Introduction

In recent years, micro-analytical techniques have greatly advanced through the development of *in situ* laser ablation sampling combined with inductively coupled plasma mass spectrometry analysis (LA-ICP-MS; Eggins *et al.* 1998a,b). This technique is highly sensitive to uranium, allowing the analysis of sub-ppb concentrations with a spatial resolution of in the range of 100 by 10 μm.

The direct dating of human remains, that are older than 50 to 60 ka (the present uppermost limit for radiocarbon dating of bones: Higham *et al.* 2006, Jacobi *et al.* 2006), is confined to U-series and ESR (Grün 2006). Both methods are seriously compromised by the fact that bones and teeth accumulate large amounts of uranium following their deposition in sediments. Over the past 30 years, a range of models have been developed to account for this uranium uptake and provide a basis for open system dating. The diffusion-adsorption (D-A) model, developed by Millard (1993) and Millard and Hedges (1996), refined by Pike (2000) and Pike *et al.* (2002) is the most sophisticated of these. It is based on a continuous diffusion of uranium from the outside of a bone or tooth towards the interior, and on the assumptions that the partitioning between the bone and solution (groundwater) and the U-concentration in the solution are constant. The bone or tooth is

treated as a homogeneous medium. Under constant conditions, the cross sections of bones that conform with the D-A diffusion model are expected to have both ∪-shaped U-concentration and apparent U-series age profiles, with the apparent ages at the surface being closest to the correct age of the sample. Deviations from the ideal profiles can be explained either by leaching or changes in the U-concentration in the solution. In the first applications of the D-A model, U-concentration profiles and U-series measurements were based on a few mechanically drilled samples, chemical separation of U and Th isotopes and their measurement either with an ICP or thermal ionisation mass spectrometer (e.g. Pike 2000). Laser ablation ICP-MS provided a breakthrough in micro-scale U and U-series analyses and has subsequently been used to measure these isotopes continuously along profiles (Eggins *et al.* 2003, 2005).

Numerous faunal teeth from the Middle Palaeolithic site of Payre have been analysed for a range of isotopic techniques. We selected a Neanderthal tooth to evaluate and advance *in situ* analyses, including U-series, Sr, Ca and O isotopes. Preliminary results on oxygen isotope analysis using SHRIMP (with spot sizes of 35 μm diameter, about 2 μm deep, allowing a potential weekly to bi-weekly resolution for human molars) and Sr elemental distributions on this tooth using laser ablation were further reported by Grün *et al.* (2006b), maps of Sr isotopes by Aubert *et al.* (2007). In this paper we present the first high resolution U (^{238}U) and Th (^{232}Th) elemental concentration and U-series isotope maps on a human fossil and discuss their implications for future dating studies.

The site of Payre is located 60 m above the Payre river, a small tributary of the Rhône river, on a cliff opening towards the southeast. Regular excavations have taken place since 1990 (Combier, 1967; Moncel, 2003). The site belongs to the Jurassic and Cretaceous complexes, which cover a large part of the right edge of the middle Rhône Valley (Debard, 1988). It yielded a sequence with different archaeological layers, numerous artifacts, and fauna remains (Debard, 1988; Moncel *et al.*, 2002; Moncel, 2004). The human remains, consisting of 14 teeth and a fragment of parietal, were discovered in the different archaeological levels (Moncel and Condemi, 1996, 1997).

The sedimentary sequence was about 5m thick and composed of five main levels (from top to bottom: A-B, C-D, E, F, and G) each of them including sub-layers. 25 to 60 m² have been excavated down to the substratum. Layers A and B were formed of karstic sediments and do not

contain any archaeological remains. Layers C and D consisted of brown clay and stony sediments, and Layer E of large blocks of limestone indicating the collapse of the cave's roof. Layer F contained seven cyclic deposits of grey sediments and beds of rubble and clay. This layer contained four separate human occupation layers, which alternated with those indicating cave bear occupation. Layer G consisted of orange clays containing pebbles and blocks. It yielded two distinguishable phases of human occupation. This clastic sequence was underlain by a stalagmitic floor, which was subdivided into six separate units (H2 to H7). An additional stalagmitic unit (H1) was difficult to associate with the other sedimentary layers.

Most of the human remains were found in the oldest level G, which yielded nine teeth and one fragment of parietal. These human remains were found close to each other. Four teeth belong to the oldest human settlement (sub-level Gb) and the others, including the fragment of parietal, to sub-level Ga. Level F yielded three teeth, the Level E one, and the upper level D one (Moncel and Condemi, 1996, 1997; Moncel *et al.*, 2002).

The human behaviour was the same in all archaeological levels. Seasonal occupations (evidence of hunting of cervids, associated to equids and bovids) were observed associated with a discoid debitage on flint, which came from local and semi-local outcrops. Other stones were also used, such as quartz, quartzite, basalt and limestone for a secondary flaking, hammers and pebble tools. The lithic assemblage belongs to Early Middle Palaeolithic, typical of Middle Rhône Valley and South France (Moncel 2003). It is different from Orgnac 3, dated of MIS 9 and 8, where Levallois flaking was observed (Moncel *et al.* 2005).

The dating studies involving a range of methods has recently been summarised by Valladas *et al.* (2008). Layers D and E yielded ESR/U-series age estimates on faunal materials as well as thermoluminescence results on burnt flint in the vicinity of 150,000 years, while those on layers F and G were in the range of 200,000 to 300,000 years without being distinguishable between these two layers. The underlying stalagmitic floor yielded a TIMS U-series ages in the range of 230 to 290 ka.

The Neanderthal tooth (# 1) was found in Level G, Layer D, Square N8, at a depth of 400 cm below datum. Considering the recent dating results, its age can be expected to fall within a range

of 200,000 to 230,000 years (the older age bracket provided by the more reliable TIMS dating results on the underlying speleothems).

7.2 Experimental

The tooth was cut into halves with a thin (100 µm) diamond saw (fig. 45) along the buccallingual (cheek to tongue) axis. The enamel section analysed covers the lingual half (facing the mouth) of the tooth (for details on tooth histology see Hillson 1986). One half was imbedded in a removable resin, which is required for SHRIMP oxygen isotope analysis. The imbedded sample was then mounted in a sample holder so that the sectioned surface lies in the focal plane of the laser. After analysis, the two halves can be glued back together with little visible damage. The greatest material loss derives from the cutting width.

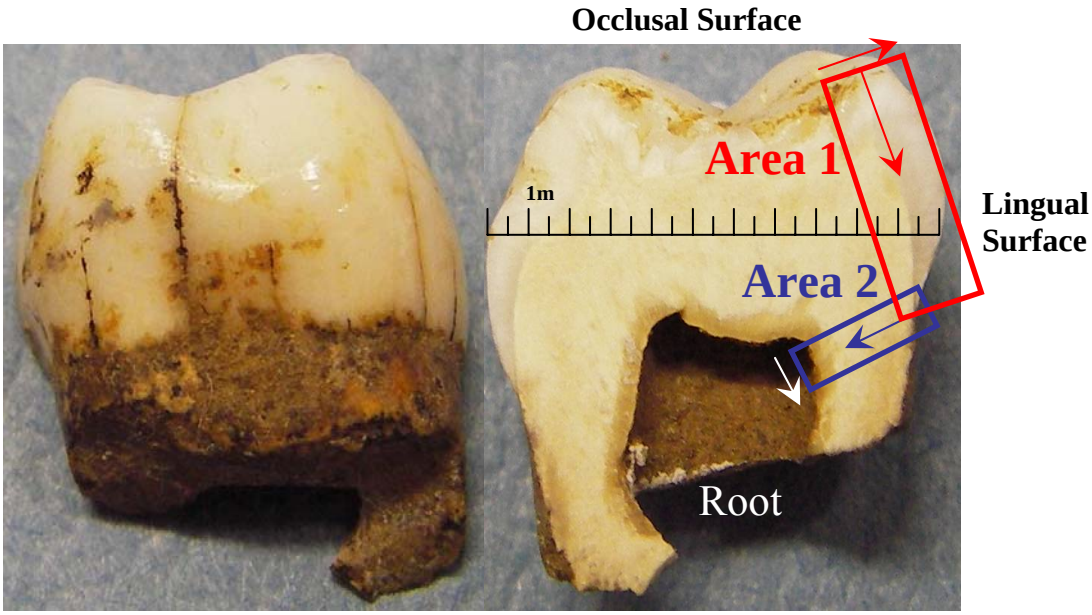

Figure 45 **Photos of the Neanderthal tooth from Payre. Area 1 was scanned for U (238U) and Th (232Th) elemental concentrations, Area 2 for U and Th elemental concentrations and Useries isotopes. The arrows indicate the directions of the laser tracks.**

The analyses were carried out using a custom-built laser sampling system interfaced between an ArF Excimer laser (193 nm; Lambda Physik LPX120i) and an ICP mass-spectrometer. Elemental U and Th distributions were measured on a Quadrupole Varian-820, U and Th isotopic distributions on a multi-collector Finnegan Neptune. Details of this system and its capabilities have been described previously (Eggins *et al.* 1998a, b). In brief, it employs a single long-working distance lens to project and demagnifying (by a factor of 20) the image of a laser-illuminated aperture onto the sample surface, which enables a range of geometries to be ablated within bounding dimensions of between 1 μm and 400 μm. In this study, laser pulse rates of 10 Hz were employed with a fluence of 10 J/cm2 (power density 0.3 GW/cm2), the latter resulting in removal of a uniformly thick layer (~200 μm) from the targeted sample site with each laser pulse. The in-house developed laser ablation cell produces very fast response times, which permits high spatial resolution analysis. Data reduction followed established laser ablation ICP-MS protocols (after Longerich *et al.* 1996), using the international glass reference materials NIST SRM610 glass and a rhinoceros tooth (where the U-series ratios were established by repeated TIMS analysis) for external calibration, tailing correction and elemental fractionation. Mean background count rates measured with the 'laser off' were subtracted from all measured isotope intensities. All measured atomic ratios were converted into activity ratios, unless indicated otherwise.

7.3 Results and discussion

Prior to interpreting the results it should first be noted that the scans showed in various places small spots of anomalously high Th and/or U-concentrations (some are clearly visible in the resin, see e.g. Figure 47: lower left area). These may either be due to small sample fragments dislocated by the laser pulsing, air bubbles in the resin and other voids that have been filled with some sample material during polishing.

In a first exploration of the U-distribution, 21 parallel scans were measured, covering a cross section of occlusal and lingual enamel and the adjacent dentine (for the approximate position of Area 1 see fig. 45). The laser tracks had a width of 85 μm, with a spacing of 100 μm (centre to centre). The measurements covered an area with a width of about 2085 μm and a length of about 5500 μm. Each scan consisted of 1100 individual measurements. These were smoothed using a

sliding 20 point average. The data were then interpolated for a three dimensional presentation using the commercial SigmaPlot (Ver. 10) software. There is a very large contrast between the U-concentrations in the dentine and enamel, uranium concentrations vary overall between about 1 to 40,000 ppb. A linear scale enhances the details in the U-distribution of the dentine while the U-concentrations in the enamel are indistinguishable from background (fig. 46A). In contrast, a logarithmic scale enhances the details in the enamel (fig. 46B). The U-concentration contrast between enamel and dentine is sharp, dropping from about 25,000 ppb in dentine to a few 100 ppb in enamel, by a factor of around 100. Much of the apparent width of this concentration slope is due to the spot size of the laser. A sharp concentration contrast (e.g. a step function in U-concentration) is widened (i) over the laser spot size of 85 μm, which corresponds to approximately 17 measurement cycles, and (ii) by the averaging process, which widens the U-concentration transition by another 20 cycles. The observed U-decrease at the dentine-enamel junction (DEJ) takes place within 25 and 40 cycles, which is an indication that the U-concentrations drop instantly at the DEJ and demonstrates the extremely fast response of the RSES laser ablation system. Similar large concentration contrasts (~ 100) in the U-concentrations between dentine and enamel have previously been observed in a range of faunal teeth (Eggins *et al.* 2003).

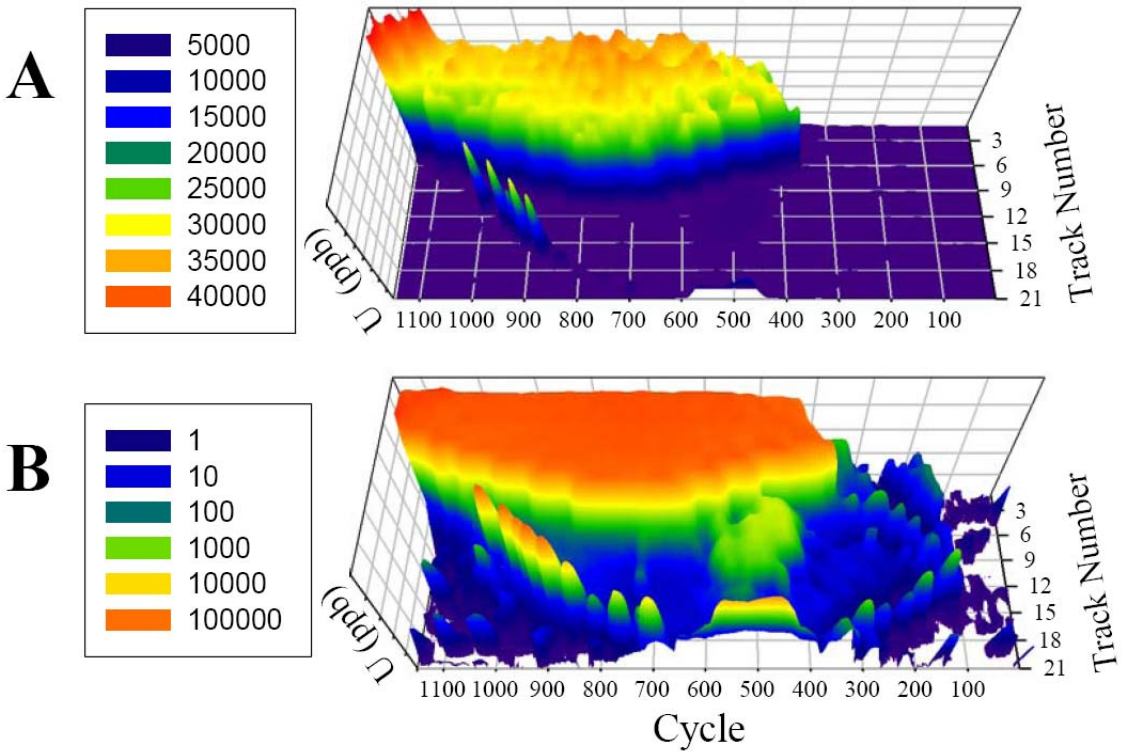

Figure 46. Uranium concentration distributions in Area 1. A: linear scale; B: logarithmic scale.

Figure 47 shows maps of the U and Th elemental distributions in the enamel. Th is predominantly enriched right at the surface of the enamel (fig. 47C) and is there associated with detrital coatings (see fig. 45). In the three dimensional presentation, this thin veneer occurs as separate isolated cones, which is the result of rastering caused by the track width and interpolation strategies of the software. The Th concentrations on the occlusal surface are lower than on the lingual surface. This is partly due to the angle between the surface and the laser track. The ablation tracks passed the occlusal surface at approximately right angles, so that less volume of the thin surface layer was measured here than at the lingual surface, where the tracks passed the surface at shallow angles and partly ran along the surface (see Track 21 between Cycles 400 and 600 in fig. 47C).

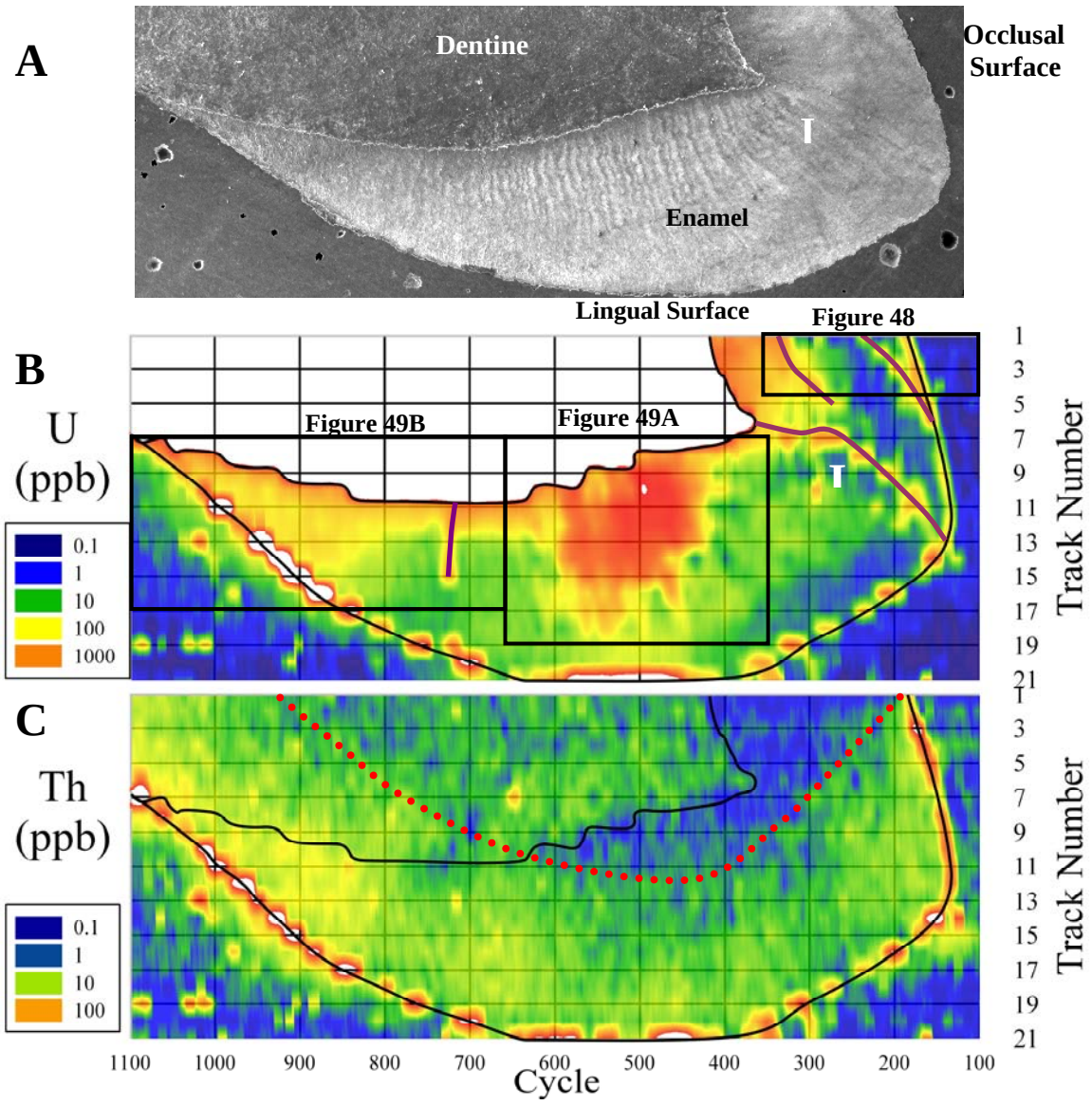

Figure 47. SEM image of Area 1.

B. U-distribution. The solid lines indicate the enamel boundaries and lineaments of increased U-concentration. The squares indicate enhancements in Figures 48 and 49.
C. Th-distribution. The dotted line limits and area of higher Th concentration, which is unrelated to the dentine-enamel junction (DEJ).

There is an approximately 1 mm wide rim on the outside of the tooth (between the surface and the dotted line in fig. 47C) with enriched Th concentrations in the range of 10 to 20 ppb, irrespective of the nature of the dental tissue. Only near the occlusal surface of the tooth, is a minor contrast observable between the Th concentrations in the dentine (around 1 to 6 ppb) and

enamel (around 0.3 to 1 ppb; see DEJ below Cycle 600). Relatively high Th concentration in enamel occur above Cycle 800, a region which also contains elevated U (fig. 50) and Sr concentrations (Grün *et al.* 2006b, Aubert *et al.* 2007). Nevertheless, there does not seem to be any evidence for Th diffusion paths into the tooth, although it is clear that this tooth contains significantly higher Th concentrations than observed on modern humans, which average Th concentrations in bones in the sub-ppb range, as we have measured on modern teeth.

Uranium diffusion into the enamel did not follow a simple D-A model with constant conditions, which would have produced ∪-shaped U distributions. In general it is expected that uranium migrates from the dentine side into the enamel, the surface being more or less impenetrable to U-diffusion as long as the outer non-prismatic layer is intact (e.g., Eggins *et al.* 2003). Starting from the DEJ, we have observed in many samples a more or less steady U-concentration decrease across the enamel layer, with increased U-concentrations right at the outer surface. The enamel of the Payre Neanderthal has on its outside a thin veneer of high U-concentrations, particularly at the base where up to 25,000 ppb is observed. Similar to the Th distribution, near the occlusal surface the U veneer is less pronounced with U-concentrations in the range of only 500 ppb. This may simply indicate variable amounts of detrital residue on the surface (see fig. 45).

Within the enamel, the U-distribution varies by several orders of magnitude. The lowest concentrations are found near the occlusal surface where U-concentrations drop to less than 10 ppb, indicating little or no U-uptake. Elsewhere uranium has migrated into the enamel in a variety of modes. Firstly, U is concentrated along visible cracks. There is a clearly visible crack starting from the cusp of the dentine reaching to the surface (just above "I" in fig. 47A and B). Uranium is also enriched along other linear features, as shown in fig. 48. At least three different lineaments with enriched U-concentration are visible, all running at shallow angles to the surface and the DEJ. It becomes obvious that U-mapping is essential to understanding the mode of U-migration. If Track 4 was taken in isolation, significant U-diffusion normal to the surface could be postulated (fig. 48C). Instead, U migrated within the enamel along a lineament, which forms a shallow angle to the surface. Given the observed concentration gradient, it seems that U migrated from the outer surface into the enamel. Whether this particular feature or the other lineaments are associated with cracks or interprismatic zones has yet to be confirmed. There is

also a lineament of increased U-concentration in the lingual enamel, perpendicular to the DEJ (Tracks 11 to 15, around Cycle 725, see figs. 47B and 50).

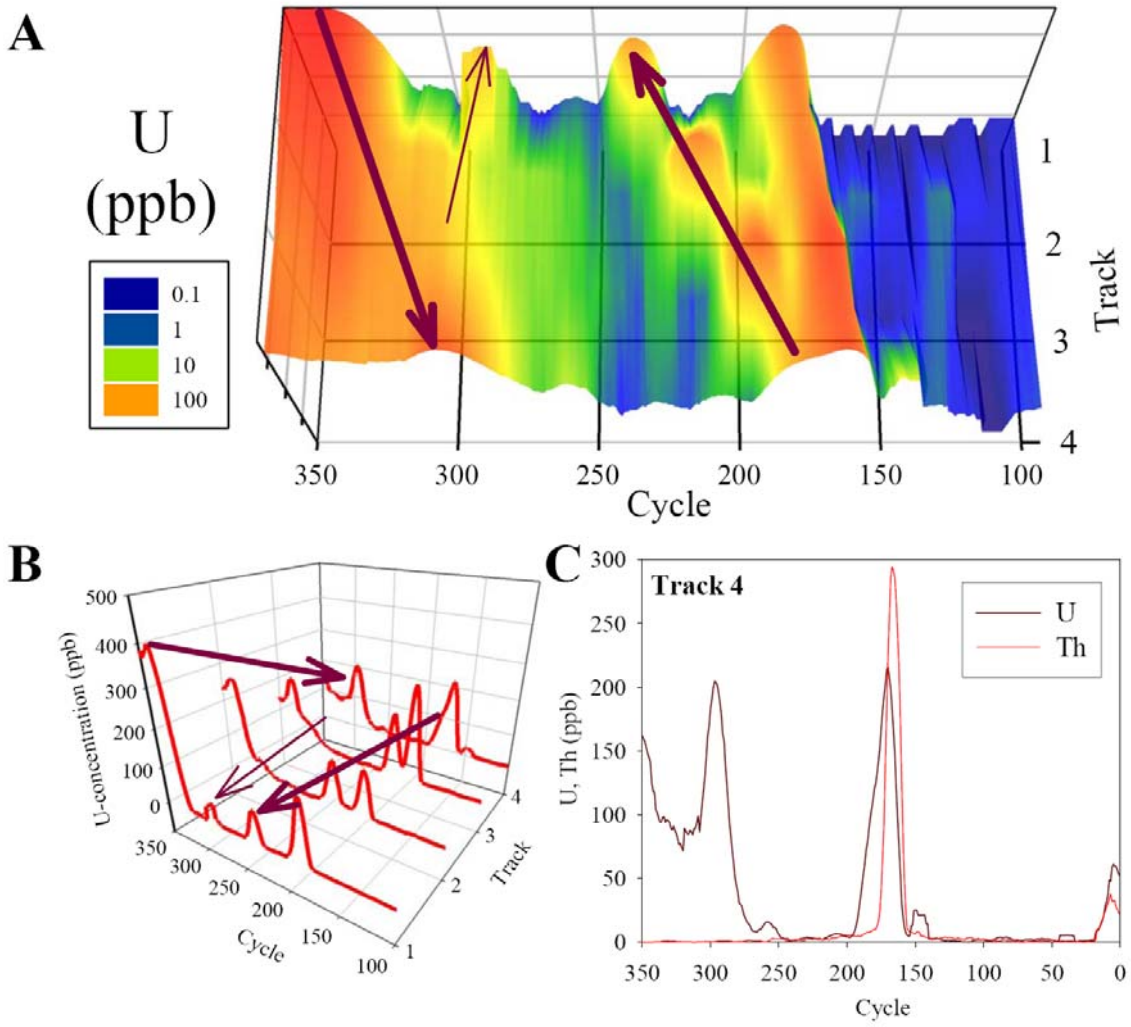

Figure 48. Details of increased U-concentrations along linearments

A. enhancement of Figure 47A
B. individual tracks (reversed to A)
C. U and Th concentrations along Track 4. As a stand alone measurement the wide U-peak between Cycles 150 to 200 would indicate a significant U-migration perpendicular from the surface of the tooth.

The most obvious feature in the enamel is a relatively large domain of greatly increased U-concentrations of up to 1500 ppb (around Cycle 500 in Tracks 9 to 14, fig. 47B, enhanced in fig. 49A). Uranium migrated from the dentine into the enamel along two pathways leading to more or less constant enrichment in an area which reaches about 600 μm into the enamel and has a width of about 800 μm. From this area there is a series of smaller linear diffusion paths further into the enamel. This domain of high U can obviously not be explained by monotonic diffusion into a homogeneous layer, but more likely is due to a mineralogical change in this area or its subsurface. The SEM (fig. 47A) indicates that this area is dominated by relatively large prismatic bundles, which perhaps allow preferential U-migration along wider intra-prismatic zones. Unfortunately, we cannot further investigate the mineralogical structure in this area, because the sample has been polished several times for subsequent analyses and due to the complexity of the three dimensional structure of enamel (e.g. Macho *et al.* 2003). It is interesting to note that the enamel has also experienced a significant uptake of Sr. However, we do not find a similar distinct accumulation of Sr in this particular area (Aubert *et al.* 2007).

Near the base of the lingual enamel, U-concentrations drop from about 300 ppb close to the dentine to about 100 ppb close to the surface, implying that U-diffusion had penetrated the enamel over its whole thickness (fig. 49B).

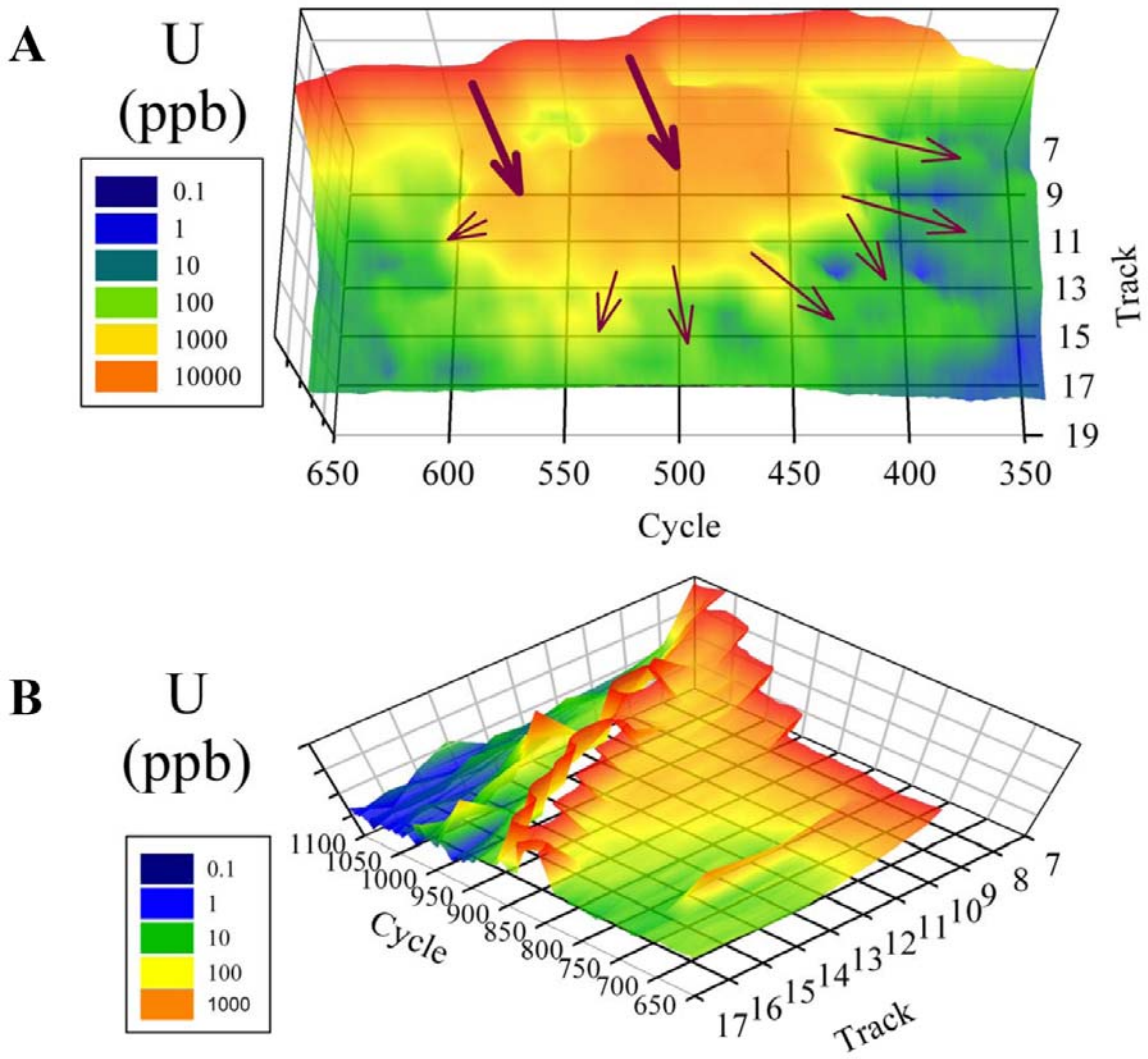

Figure 49A. Details of increased U-concentration in the central part of the lingual enamel.

B. Details of increased U-concentration at the base of the lingual enamel.

One can use the position of the Th peak to fix the boundary between detrital surface contamination and the enamel, on the assumption that there is no Th diffusion into the enamel. The comparison of the Th with the associated U peak allows the assessment of any U diffusion from the surface into the enamel. Figure 50 shows one of the largest effects of U migrating perpendicular from the surface into the enamel (Track 16). At the occlusal side of the enamel, the potential U-diffusion may be on a length scale of up to 30 µm and perhaps 60 µm at the lingual

side. Correcting for the incident angle between laser track and enamel surface, and excluding the effect of lineaments reaching the surface (see Figure 48C), we observe an average diffusion of uranium of about 5 µm (1 cycle) into the enamel at the occlusal surface (Tracks 1 to 15; between Cycles 130 and 190), and about 20 µm at the upper part of the lingual enamel (Tracks 16-20, Cycles 170 to 350) and 15 µm at the lower end (Tracks 9 to 20, Cycles 680 to 1100).

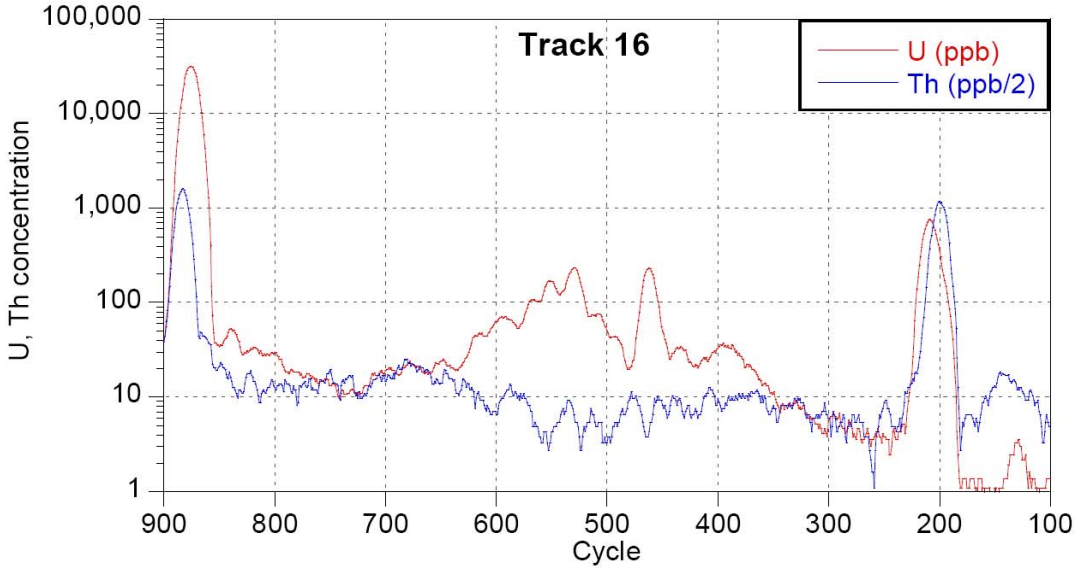

Figure 50. U and Th measurements along Track 16.

The uranium concentrations in dentine ranged from about 25,000 ppb to 45,000 ppb (fig. 51A). The higher concentrations are observed in the region that is not covered by enamel (see Track 1, Cycles 1050 to 1100 in figs. 46A and 51). There is a general gradient from the centre of the dentine (Cycles 500-800, Tracks 1 to 5) towards the enamel. It is unclear whether this is the result of diffusion, or whether this is due to different adsorption capacity in different domains in the dentine. The increased U-concentration at the lower end of the dentine (Track 1, between Cycles 1050-1100) is due to diffusion into the dentine not covered with enamel (see fig. 53, below). As mentioned above, the Th distribution in the dentine was not associated with the U distribution, nor with the DEJ. The elemental U/Th ratio was in most areas well above 10,000,

the lowest values in the range of 2,600. This implies that any U-series age calculations on dentine are not affected by detrital Th contamination.

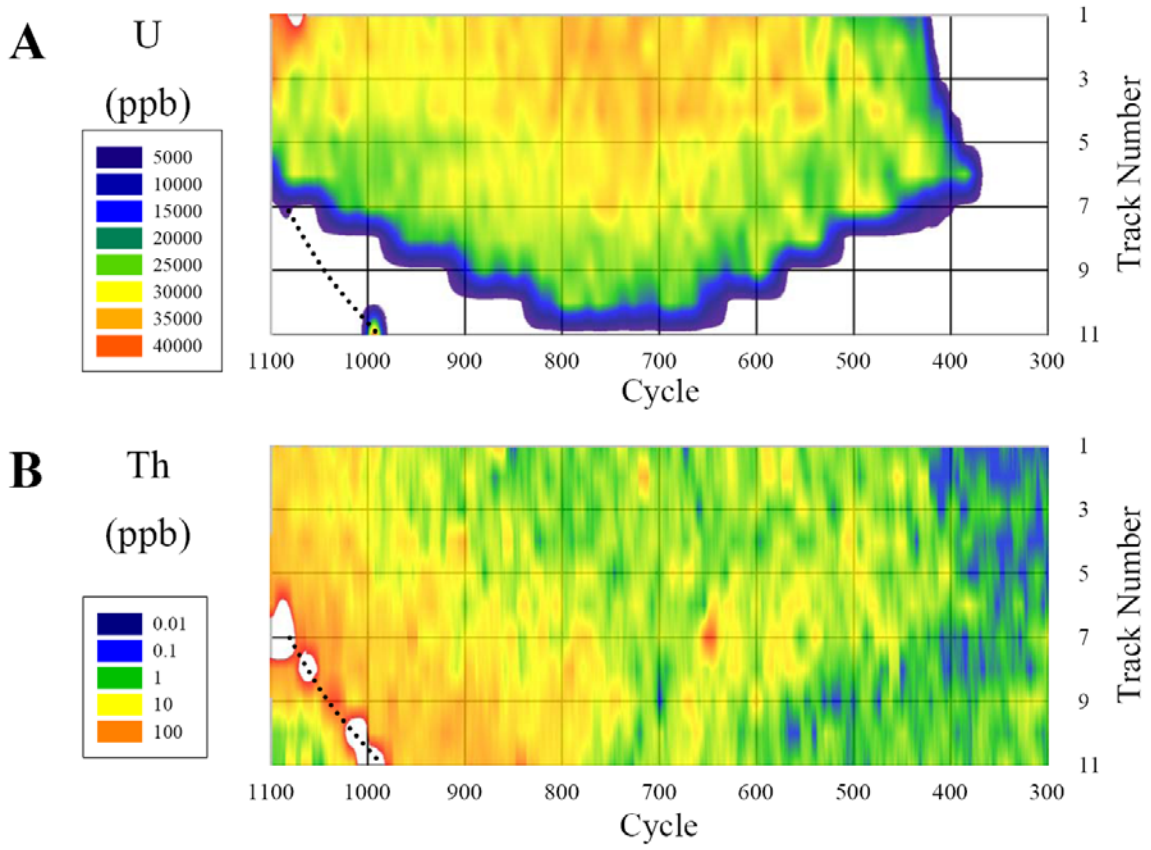

Figure 51 **Details of U (Figure A) and Th (Figure B) distributions in dentine. The outer enamel boundary is indicated by the dotted lines.**

The U-concentrations in the enamel were too low to obtain meaningful U-series data using laser ablation. For the scanning of U-series isotopes, we therefore decided to investigate a cross section of the root, most closely assembling a bone cross section (see fig. 45 for the approximate position of Area 2). Area 2 includes the part of the dentine where the uranium increased significantly in Area 1.

^{238}U, ^{234}U and ^{230}Th were measured on the Neptune sector ICP-MS. The laser track width was 178 μm and track spacing 150 μm, during each measurement cycle the track advanced by 10 μm. The total area analysed was about 900 μm wide and 3000 μm long. Figure 52 shows the effect of data reduction, after applying a 20 cycle sliding average, and calculating the mean value and error of the mean.

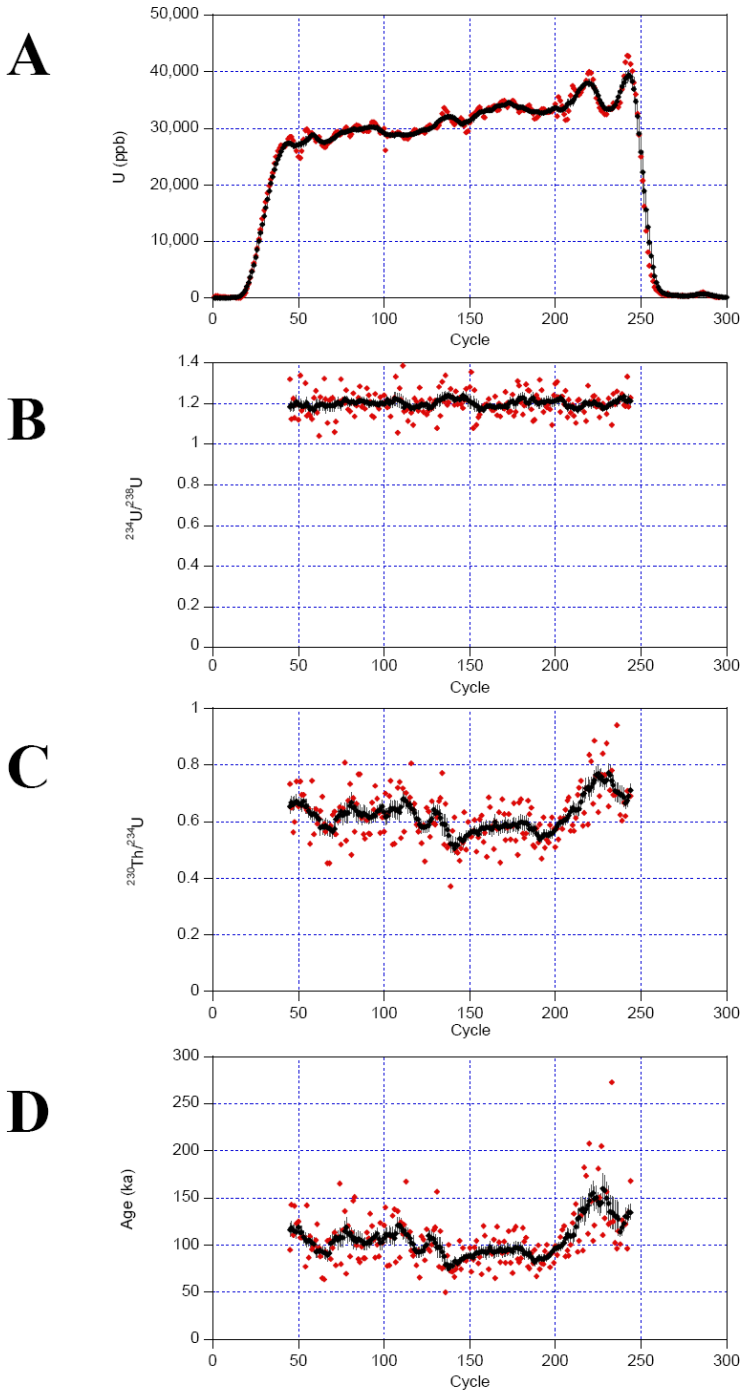

Figure 52. Effect of data reduction for the measurements in Area 2. Errors of the means are indicated by the error bars.

A. U-concentration
B. $^{234}U/^{238}U$ activity ratio
C. $^{230}Th/^{234}U$ activity ratio
D. U-series age

Figure 53A shows an SEM photograph of the approximate dentine region of Area 2. This SEM was recorded some time after the U-series isotopes and subsequent analyses were carried out and shows an area that lies about 50 μm below the original tracks. Figure 53B shows the ^{232}Th distribution in Area 2. Th was adsorbed at the outside of the dentine and shows no sign of diffusion into the dental tissue. Inside the dentine, the elemental U/Th ratios were well above 10,000. U-series ratios and age estimates were calculated from the U maxima at the surfaces of the dentine (figs. 53C to E). At the outside surface, elemental U/Th concentrations ratios were as low as 350, at the inside surface well in excess of 1000. This again implies that none of the U-series age calculations were affected by the presence of detrital ^{230}Th, particularly those of Track 6 (see below).

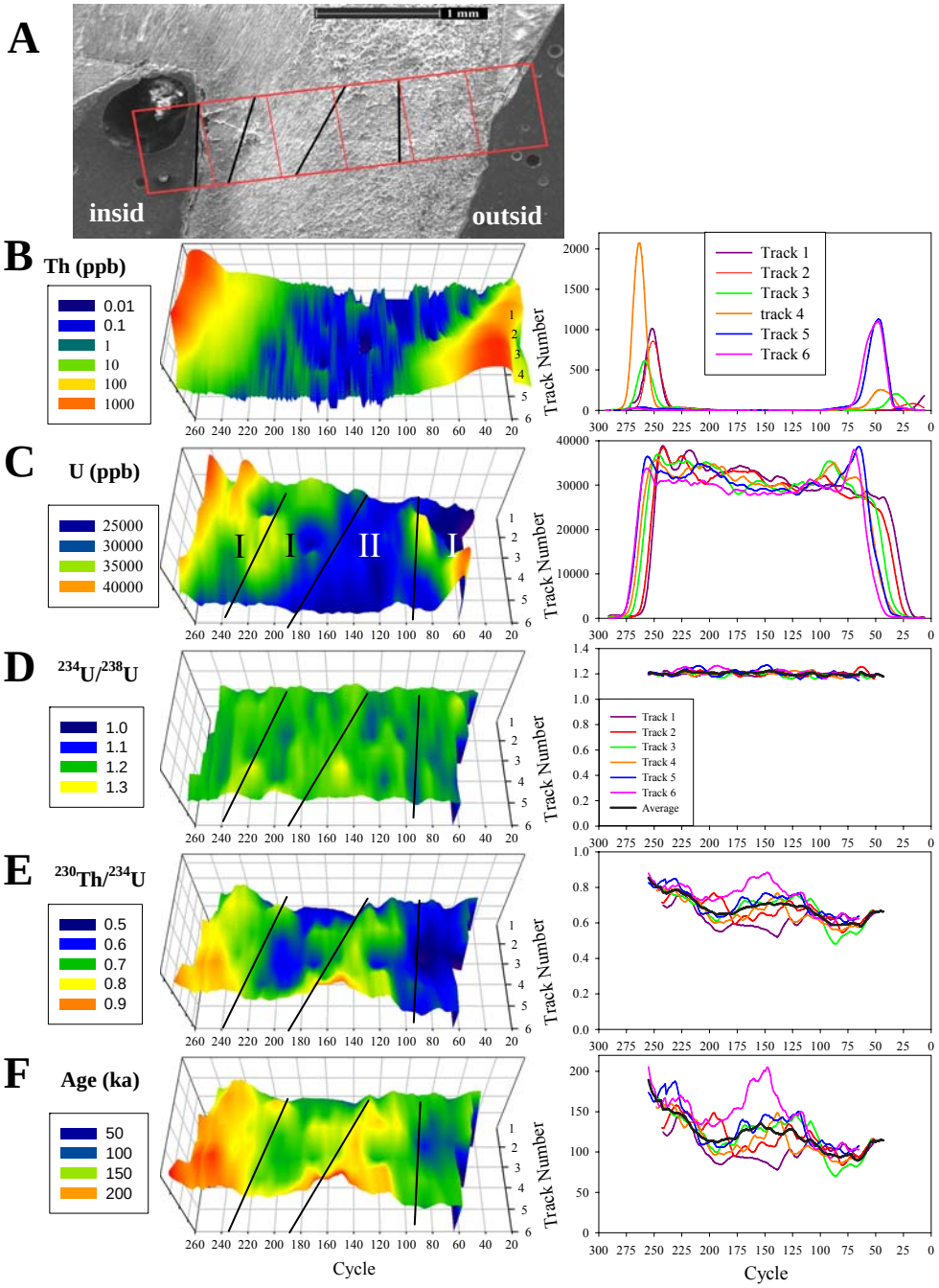

Figure 53. Elemental, isotopic and age distributions in Area 2.

A. SEM of the dentine in Area 1, but about 50 ìm below in depth. The large red square is for orientation subdivided into 50 cycle sections. Black lines indicate the boundaries of Regions I to IV (see fig. C)

B. Th distribution

C. U distribution, Regions I to IV indicate areas of different relationships between U concentrations and U-series age calculations

D. $^{234}U/^{238}U$ ratios

E. $^{230}Th/^{234}U$ ratios

F. U-series age estimates

The uranium concentrations in Area 2 ranged from about 27,000 ppb to 39,000 ppb, similar to the concentrations in Area 1. It can also be seen that the higher U-concentrations in the dentine of Area 1 (Track 1, Cycles 1050 to 1100 in figs. 46A and 51A) seems to have originated from a volume in the dentine that was not covered by enamel (see Tracks 3 to 6, Cycles 60 to 85 in 53C). The structure of U-distribution, however, is much more complex than in Area 1.

The U-concentrations show distinct peaks at the outside surface of the dentine, where it was not covered by enamel (Tracks 5 and 6, cycle 60 to 75, fig. 53C). Tracks 1 and 2 show the gradual increase of the U-concentration from the DEJ, as observed for most of the dentine in Area 1. In Tracks 3 and 4, the U maximum was located somewhat further to the inside, about 400 μm from the dentine outer surface. At the inside surface of the dentine, all tracks had their U-maximum at or near the surface. Tracks 1 to 5 had a second maximum further to the inside. U-series isotope ratios and ages were only calculated in the region between the U-concentration maxima on the outside and inside surfaces. This avoided any potential problems with detrital Th contamination.

The $^{234}U/^{238}U$ ratios (fig. 53D) varied within a small band width, the average value being 1.202±0.023 (1-σ standard deviation of all calculated values). The $^{230}Th/^{234}U$ ratios (fig. 53E), on the other hand, varied greatly along and between the tracks. The same applies, of course, to the calculated apparent U-series age estimates (fig. 53F). It can be seen, however, that there are some systematic patterns in the apparent U-series age estimates. Depending on the relationships between U-concentration and apparent U-series ages, we can distinguish four regions (I-IV, marked in fig. 53C). In Region I, at and near the inner surface of the dentine, the highest U-concentrations are associated with the higher apparent U-series ages. This is generally expected from the predictions of the D-A model. The oldest ages occur at the inner surface (Cycles 240 to 260) and are steadily increasing from Track 1 to Track 6. Region II shows some distinct U maxima and minima, and these are inversely associated with U-series ages, i.e. in areas of relative high U-concentration, the ages are lower than in areas with relatively low U-concentration. In the central Region III, the U-concentrations are lowest, but the apparent U-series ages are significantly higher then in the surrounding Regions II and IV. Region IV shows a similar pattern as Region II. The apparent U-series ages near the outer surface (Cycles 40 to 80, Region IV) are significantly lower than on the opposite side (Region I). When transferring these regions of distinctive U-concentration and U-series patterns onto the SEM

image (fig. 53A), it can be seen that Region I closely correlates to the darker rim around the pulp cavity (see fig. 45), which consists of secondary dentine and/or weathered primary dentine. Region II seems to be dominated by tubules, while Regions III and IV are undistinguishable in the SEM characteristics with a non-directional patterns, perhaps caused by an overprint of secondary dentine or other secondary minerals.

To investigate whether there is a systematic relationship between U-concentration and apparent U-series age estimate, these two parameters were plotted on top of each other in figs. 54 A to F. In Region I, high U-concentrations are associated with high U-series ages (see Tracks 3 to 6). This is expected from the D-A model for the volumes at and near the surface. In most of the other areas, relatively high U-concentrations are associated with relatively low U-series ages and vice versa. Closer to the outer surface, U-series ages generally increase and are not immediately affected by the high concentrations at the outside (see Tracks 5 and 6, Cycles 60 to 70). However, the U-concentration peaks slightly further to the inside in Tracks 3 and 4, around Cycles 80 to 90, are clearly associated with significantly younger U-series ages, indicating that these peaks are the result of a relatively recent accumulation of U. The older apparent ages in the central part of the dentine (Region III in fig. 53, Tracks 2 to 6, between Cycles 100 and 160) are clearly not associated with distinct minima in U-concentration.

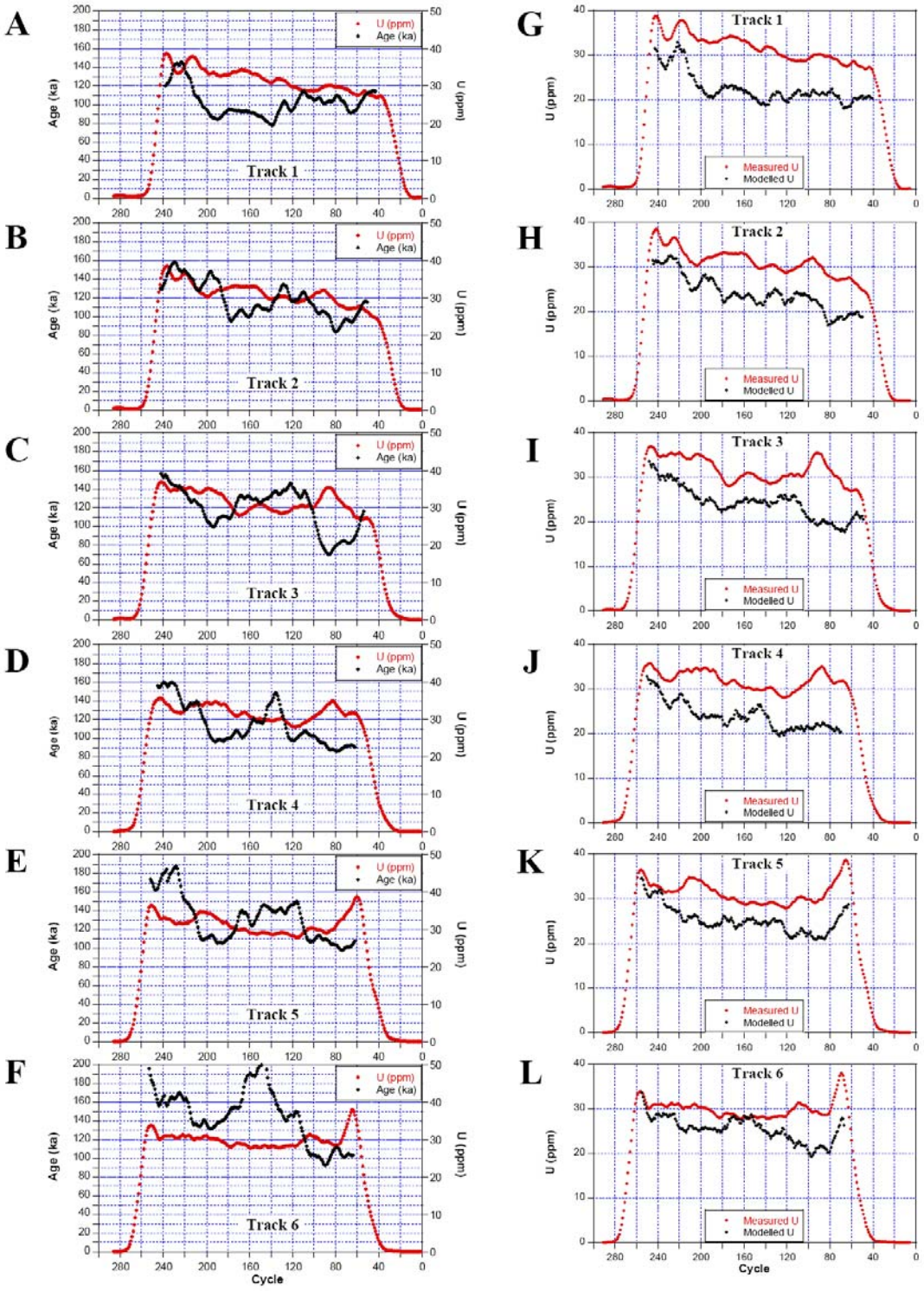

Figure 54A-F. Age and U-concentration along the individual Tracks 1 to 6.

G to L. Calculation of a two phase model of U-uptake. The early one at 200 ka ago, the latter recently. The modelled U concentrations are derived from the difference of the measured $^{230}Th/^{234}U$ ratio and that of 200 ka. The amount of late U-accumulation is the difference between the modelled and measured concentrations.

None of the profiles show distributions in U-concentration and/or apparent U-series age estimates predicted from a single stage D-A model. The distributions of U-concentration and U-series ages in Regions II and IV point to at least two distinct phases of U-uptake. Nonetheless, if the age of the specimen is indeed somewhere in the 200 to 230 ka region, the age estimates near the inside surface and in some central parts come close to this expected age range, implying some early U-accumulation in these domains.

In order to gain some insight about the U-uptake history, it was assumed that the age of the tooth was 200 ka. This corresponds to a $^{230}Th/^{234}U$ ratio of about 0.875 for a $^{234}U/^{238}U$ ratio of 1.2. Using a simple two stage model of U-uptake, namely that the first stage of U-uptake was rapid around 200 ka ago and a second stage followed in recent times, the U-concentration distribution of the first stage of U-uptake can be calculated from the measured $^{230}Th/^{234}U$ ratios. For example, a data point with a $^{230}Th/^{234}U$ ratio of 0.5 would have acquired about 57% of its present day U-concentration 200 ka ago (this fraction has a $^{230}Th/^{234}U$ ratio of 0.875) and 43% most recently (with $^{230}Th/^{234}U = 0$; figs. 54G to L). All profiles of these calculated initial U-concentrations show a more of less monotonic decrease from the inner to the outer surface, from about 30 to 20 ppm, respectively. This continuous concentration drop may well be associated with changes in the mineralogical composition of the dentine or size of its internal surface for U-adsorption. Only Tracks 5 and 6 have a distinct U-concentration peak at the outer surface, most probably in the cement layer. On the whole, these calculated U-concentration profiles are closer to those expected from a single stage D-A model, than the measured ones. The second phase of U accumulation is particularly strong in the outer volume (about Cycles 60 to 100) and around Cycles 180 to 220. It cannot entirely be excluded that the high ages of Region III and the low ages in the surrounding regions are the result of relatively recent U-leaching from Region III and re-deposition in Regions II and IV. However, this would require U-migration against the U-concentration gradient. One has to remember that U-redistribution must not necessarily only take place in the measured plane. U-injection may have originated in a volume above or below.

7.4 Implications for dating

The U-concentration and U-series profiles measured in Area 2 of the dentine do not concur with a single stage D-A model. As such, this sample should be disregarded for dating (Pike 2000, Pike *et al.* 2002). Nevertheless, some domains in the dentine yielded U-series results that are close to the expected age of the sample. In view that laser ablation provides insight into detailed U migration, it is possible to investigate U-leaching and Th contamination. U-leaching would be expressed by a drop of U-concentration near the outside with an associated increase in the U-series age. This would generally look similar to the pattern shown in Track 3 between Cycles 40 to 80 (Figure 54C), except that here the mapping indicates a secondary overprint. Near the inner surface, there is no sign of U-leaching, so that the apparent U-series ages in Region I, around 200 ka, can be regarded as minimum age estimates for the tooth. The same restrictions (i.e. that the U-series results are only minimum age estimates) also apply to bones that concur the D-A model under constant conditions (see Grün 2006).

Data from laser ablation tracks are also used for assessing U-concentrations and U-series isotope ratios on dentine and enamel for ESR dating analysis (e.g. Grün 2006, Grün *et al.* 2006a, Smith *et al.* 2007). For any open system modelling, bulk data are required, because ESR measurements do not allow for spatial resolution (at least for the spin concentrations usually found in fossil human teeth, see Oka *et al.* 1997). It is clear from the U-distribution in the enamel that for this sample, any single laser ablation track would yield U-concentrations that may be completely unrelated to the bulk U-concentration that is required for ESR dating. Similarly, the U-concentration distribution in the dentine is not homogeneous, and the critical $^{230}Th/^{234}U$ ratios vary greatly. When laser tracks show such inhomogeneities, it seems necessary to carry out bulk analyses on the dental tissues that were used for ESR dating.

7.5 Conclusion

The detailed mapping of U-concentration data in dentine and enamel give insight into the U-migration patterns in these tissues. However, it is necessary to measure U-series isotope ratios to understand aspects of the time domain of these U-migration patterns. The U-uptake into the enamel does not follow any model that has been proposed so far. While some regions in the dentine may concur with a single stage D-A model, most regions do not. Laser ablation mapping allows the investigation of U-leaching and if this process can be excluded, the derived apparent U-series data provide a minimum age estimate for the specimen. Single tracks are critically dependent on the mineralogical structure of the measured tissue. The U-series results and their interpretation may vary greatly, depending on where the track was measured.

The areas measured here are still to small to obtain a clear picture how uranium behaved in this particular tooth. We shall attempt to provide a complete map of the whole cross section. Even here, U-concentrations and isotopes will still be affected from the volumes below and above the measured cross section. Although it is desirable to obtain three dimensional distributions, this is clearly not feasible in view of the exceptional value of human fossils. Furthermore, it is also a question whether the detailed insights obtained from one tooth are applicable for any other teeth from the same site. Nevertheless, a complete map will only require a couple of days of measuring time, which is very short when comparing this to mechanical drilling, isotope separation and subsequent TIMS measurements that used to be carried out for obtaining D-A data. The latter could only provide a few coarsely spaced measurements. It also seems necessary to find out where the uranium is located, i.e. whether it all accumulated on crystal surfaces or whether some of it was incorporated into the hydroxyapatite structure, for example replacing Ca ions.

U-concentration and U-series data derived from single laser ablation tracks may be a poor proxy for bulk data. When solution analysis is not an option, for example when analysing human fossils (Grün 2006), laser ablation mapping should be carried out.

8 CONCLUSION GÉNÉRALE

Depuis quelques années, l'introduction de techniques microanalytiques comme les systèmes à ablation laser et l'ICP-MS à multicollecteurs a révolutionné la géochimie. La plupart de ces progrès analytiques et techniques ont été élaborés dans les départements de Sciences de la Terre et sont la conséquence directe de questions axées sur la géologie/géochimie. En plus d'avoir une connaissance approfondie sur les systèmes géochimiques, les chercheurs de pointe en Sciences de la Terre ont la possibilité d'améliorer les techniques et les instruments mis à la leur disposition.

Cependant, plusieurs années sont généralement nécessaires pour que ces innovations soient appliquées en archéologie. Une des raisons de ce retard pourrait s'expliquer par le manque de collaboration réciproque entre les archéologues et les chercheurs en Sciences de la Terre. Cette recherche doctorale porte sur le développement de techniques analytiques modernes directement applicables en archéologie et tente de renforcer les liens entre l'archéologie et les Sciences de la Terre. À propos, plusieurs premières ont été réalisées comme la datation de peintures rupestres naturellement recouvertes de dépôts de carbonate et les premières cartes de distribution isotopique permettant de dater les fossiles humains.

L'objectif principal de ce travail était d'évaluer le potentiel de la datation par les séries de l'uranium en archéologie à travers une application de la méthode sur des échantillons provenant de sites rupestres et paléoanthropologiques.

Différents types de dépôts minéraux, principalement des carbonates et des enduits minéraux de type 'rock varnish' riches en manganèse ont été observés sur plusieurs sites rupestres de la planète. La datation de ces concrétions offre le potentiel d'évaluer l'ancienneté relative des sites rupestres lorsque le substrat rocheux a été recouvert par différentes couches de dépôt avant et après la création de peintures, de dessins et de gravures. Dans cette recherche, la datation par les séries de l'uranium a été utilisée afin de démontrer la possibilité de dater d'infimes dépôts de carbonate directement associés aux œuvres rupestres. Cette percée majeure connaîtra sans doute d'autres applications où des dépôts de carbonate sont présents en contexte rupestre.

Les enduits minéraux de type ‘rock varnish’ posent quant à eux un problème de taille car leur mode de formation n’est pas totalement connu. De plus, comme ces dépôts ne sont pas purs, le thorium et l’uranium peuvent également être présents dans les minéraux accessoires comme les particules d’argile et autres phases minérales. Afin d'éliminer ces contaminants potentiels et d’étudier leur mode de formation, on a développé un protocole de microextraction chimique séquentielle. Cette technique chimique a permis de séparer les phases organiques, carbonatées, les oxydes de fer et de manganèse, les phosphates et les sulfures pouvant contenir des quantités importantes d'uranium et de thorium. On a pu ainsi démontrer le mode de formation du vernis étudié. Par contre, cette technique s’est avérée inefficace à extraire séquentiellement le thorium limitant ainsi la possibilité de dater le vernis par la méthode choisie.

Dans le cas de la datation de fossiles humains, leur datation par les séries de l’uranium se présente comme problématique car les os et les dents fossiles constituent des systèmes ouverts pour l’uranium. Cette technique a néanmoins connu un récent stimulus avec le raffinement du modèle de diffusion-adsorption de l’uranium (Pike *et al.* 2004). L’utilisation de ce modèle exigeait plusieurs mois de travail afin d’obtenir un seul profil de distribution isotopique en microéchantillonnant le spécimen à l’aide d’une microforeuse et en préparant les échantillonnages pour des analyses par spectrométrie de masse à thermo-ionisation (TIMS). Dans cette recherche doctorale, un système à ablation laser a été utilisé afin de profiler les isotopes d’uranium. Après avoir obtenu un profil de distribution, il est apparu nécessaire d'en produire plusieurs afin d’obtenir des cartes détaillées. On a pu ainsi constater que les fossiles humains peuvent avoir des concentrations et des distributions en isotopes d’uranium très complexes. Par exemple, les zones de fractures diagénétiques dans les tissus dentaires constituent des zones préférentielles de diffusion des radio-éléments. De telles analyses permettent également de réaliser des acquisitions rapides quasi non destructives. Cette technique révolutionnera sans doute la paléoanthropologie où l’âge des fossiles humains est essentiel à toutes discussions.

Les résultats présentés dans cette thèse de doctorat montrent qu’il est possible de dater l’art rupestre et les fossiles humains par les séries de l’uranium. Cependant, il apparaît également évident que cette méthode est difficilement applicable en routine, car l’équipement nécessaire n’est pas facilement disponible et l’établissement d’une carte de distribution isotopique sur une

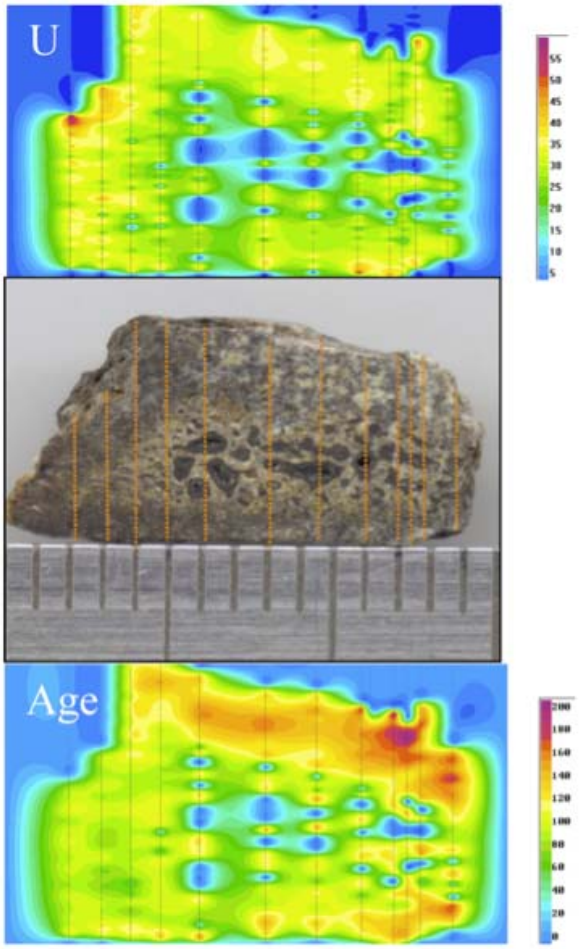

dent ou un os fossile coûte plusieurs dizaines de milliers de dollars à produire.

La Research School of Earth Sciences/Australian National University m'a proposé de continuer mes recherches et j'ai récemment produit des cartes de distribution isotopique d'uranium provenant de plusieurs fossiles humains. J'ai pu ainsi dater le plus vieux Homo sapiens sapiens, Omo Kibish 1, âgé de deux cent mille ans (Fig.55) confirmant les âges obtenus par datation Ar/Ar des cendres volcaniques laminant les ossements (McDougall *et al.* 2005). De plus, je viens d'échantillonner des peintures rupestres recouvertes de carbonate dans le Sud-Ouest de la Chine et je dois prochainement visiter aussi plusieurs sites australiens et étudier d'autres types de dépôts comme les pellicules de silice amorphe.

Figure 55. Cartes d'âge U-series et de concentration en uranium d'un os fossile de deux cent mille ans, Homo Kibish 1.

RÉFÉRENCES

Allegre, C. J., Manhes, G., & Gopel, C., 1995. The age of the Earth. *Geochim. Cosmochim. Acta.* 59; 1445–56.

Anati, E., 2001. L'art rupestre : Archives de notre histoire primordiale. *Revue du patrimoine Mondial*. Unesco, numéro 19.

Aubert, M., O'Connor, S., McCulloch M.T., Mortimer, G., & Richer-LaFlèche, M., 2007. Uranium-series dating rock art in East Timor, *Journal of Archaeological Sciences*, 34; 991-996.

Aubert M., Grün R., Eggins S. and Moncel, M.H., 2007. High resolution elemental and isotopic distribution in fossil teeth: Implications for diet and migration. XVII INQUA Congress, 28 July - 3 August 2007, Cairns, Australia, Abstract 0880, *Quaternary International* 167-168, 17-18.

Augustinus, P.C., 1999. Dating the Late Cenozoic glacial sequence, Pieman River basin, western Tasmania, Australia. *Quaternary Science Reviews*. 18; 1335-1350.

Augustinus, P.C., Short, S.A., Heijnis, H., 1997. Uranium/thorium dating of ferricretes From mid to late Pleistocene glacial sediments, western Tasmania, Australia. *Journal of quaternary science.* 12 (4) 295–308.

Ballard, C., 1992. Painted Rock Art Sites in Eastern Melanesia: Locational Evidence for an 'Austronesian' Tradition. In *State of the Art Regional Rock Art Studies in Australia and Melanesia*, edited by J. McDonald and I. Haskovec, pp. 94-106. *Occasional AURA publication* No. 6. Melbourne: Australian Rock Art Research Association.

Barnes, J.W., Lang, E.J., Potratz, H.A., 1956. Ratio of ionium to uranium in coral limestone. *Science*. 124; 175-176.

Bar-Yosef, O., Callander, J., 1999. The woman from Tabun: Garrod's doubts in historical perspective. *Journal of Human Evolution*, 37; 879-885.

Beaumont, P.B., 1980. On the age of Border Cave hominids 1-5. *Palaeontologia Africana* 23; 21-33.

Beck, W., Donahue, D.J., Jull, A.J.T., Burr, G., Broecker, W.S., Bonani, G., Hajdas, I. and Malotki, E., 1998. Ambiguities in direct dating of rock surfaces using radiocarbon measurements. *Science* 280 5732, pp. 2132–2139.

Becquerel, H., 1896a. Sur les radiations invisibles émises par les corps phosphorescents. *Compte Rendus*. 122, 501.

Becquerel, H., 1896b. Sur les radiations invisibles émises par les sels d'uranium. *Compte Compte Rendus*. 122, 689.

Bednarik, R.G., 1998. The first stirrings of creation, *UNESCO Courier*, 51(4):4.

Bellwood, P., 1997. *Prehistory of the Indo-Malaysian Archipelago*. Honolulu: University of Hawaii Press.

Bird, M.I., Ayliffe, J.K., Fifield, L.K., Turney, C.S.M., Cresswell, R.G., Barrows, T.T., David, B., 1999. Radiocarbon dating of "old" charcoal using a wet oxidation, stepped-combustion procedure. *Radiocarbon* 41; 1-14.

Birdsell, J. B., 1977. The recalibration of a paradigm for the first peopling of Greater Australia, in J. Allen, J. Golson & R. Jones (ed.), Sunda and Sahul: Prehistoric Studies in Southeast Asia, Melanesia and Australia: 113-167. Academic Press: Londres.

Bischoff, J. L., Fitzpatrick, J. A., 1991. U -series dating of impure carbonates: An isochron technique using total-sample dissolution. *Geochimica Cosmochimica Acta*. 55; 543-554.

Blanco Rodríguez, P., Vera Tomé. F. and Lozano, J. C., 2001. Concerning the low uranium and thorium yields in the electrodeposition process of soil and sediment analyses *Applied Radiation and Isotopes*. 54(1):29-33

Boltwood, B.B., 1907. Note on a new radioactive element, *Amer J Sci*, 24: 370-372.

Bourdon, B., Henderson, G.M., Lundstrom, C.C., Turner, S.P., (Eds.) 2003. Uranium-series geochemistry. *Reviews in Mineralogy and Geochemistry*. 52.

Chaloupka, G., 1993. Journey in Time: The world's longest continuing art tradition, Reed Books, Australia.

Chazine, J.-M., 2003. Rock art and ceramics in east Borneo: logical discovery or new cornerstone? In C. Sand (ed.), *Pacific Archaeology: assessments and prospects. Proceedings of the International Conference for the 50th anniversary of the first Lapita excavation (July 1952), Koné-Nouméa 2002*, pp. 43-52, Nouméa: Le Cahiers de l'Archéologie en Nouvelle-Calédonie 15.

Chen, T.M. & Yuan, S., 1988. Uranium-series dating of bones and teeth from Chinese palaeolithic sites. A*rchaeometry* 30; 59-76.

Cheng, H., Edwards, R.L., Hoff, J., Gallup, C.D., Richards, D.A., Asmerom, Y., 2000. The half-lives of uranium-234 and thorium-230. *Chemical Geology*. 169; 17-33.

Chen, J.H., Edwards, R.L., Wasserburg, G.J., 1986. ^{238}U, ^{234}U and ^{232}Th in seawater. *Earth and Planetary Science Letters,* 80; 241-251.

Cherdyntsev, V.V., Kazachevskiy, I.V., Kuz'mina, Y.A., 1965. Dating of Pleistocene carbonate formations by the thorium and uranium isotopes. *Geokhimiya*. 1965(9), 1085-1092.

Cherdyntsev, V.V., Kazachevskii, I.V., Kuz'mina, E.A., 1963. Isotopic composition of uranium and thorium in the supergene zone. *Geokhimiya*. 1963(3), 254-265.

Clarke, J., 1977. *Rock patination and the age of aboriginal engravings at Dampier, W.A.*, Department of Aboriginal Sites, Perth

Clarke, J., 1989. Further comments on Nobbs and Dorn 1988. *Rock Art Res.* 6, pp. 63–65.

Clottes, J., Chauvet, J.-M., Brunel-Deschamps, E., Hillaire, C., Daugas, J.-P., Arnold, H., Cachier, H., Evin, J., Fortin, P., Oberlin, C., Tisnerat, N., 7 Valladas, H., 1995. Les peintures paléolithiques de la Grotte Chauvet-Pont-d'Arc, à Vallon-Pont-d'Arc (Ardèche, France) : datations directes et indirectes par la méthode au radiocarbone. Comptes-rendus de l'Académie des Sciences. Paris, série 11a, tome 320, 11; 1133-1140.

Clottes, J., 2000. Le musée des roches. Seuil, 118 pages.

Clottes, J., 2001. L'Art Rupestre : Une étude thématique et critères d'évaluation, International Council on Monuments and Sites (ICOMOS). http://www.icomos.org/studies/rupestre.htm.

Cole, N., Watchman, A., & Morwood, M.J., 1995. Chronology of Laura rock art. In M.J. Morwood and D.R. Hobbs (eds), Quinkan prehistory: the archaeology of Aboriginal art in S.E. Cape York Peninsula, Australia, pp. 146-60. Tempus 3, Queensland University Anthropology Museum, Brisbane.

Combier J., 1967. *Le Paléolithique de l'Ardèche dans son cadre paléoclimatique*. Mémoire 4, Delmas, Bordeaux.

Cowan, G.A., Adler, H.H., 1976. The variability of the natural abundance of ^{235}U. *Geochimica et Cosmochimica Acta*. 40; 1487-1490.

Curie, M., 1898. Rays emitted by compounds of uranium and thorium. Comptes Rendus de séances de l'académie des Sciences 126: 1101-1103.

Curie, P., Curie, M., 1898. Sur une nouvelle substance radioactive, contenue dans la pechblende, Comptes Rendus de séances de l'académie des Sciences 127: 175-178-

Curie, P., Curie, M., Bemont, G., 1898. Sur une nouvelle substance fortement radioactive, contenue dans la pechblende, Comptes Rendus de séances de l'académie des Sciences 127: 1215-1217.

Debard E., 1988. Le Quaternaire du Bas-Vivarais d'après l'étude des remplissages d'avens, de porches de grottes et d'abris sous roche. Dynamique sédimentaire, paléoclimatologie et chronologie, Document des laboratoires de géologie, Université de Lyon 13.

DiGregorio, B. E., 2002. "Rock varnish as a habitat for extant life on Mars," in *Instruments, Methods, and Missions for Astrobiology IV*, R. B. Hoover, G. V. Levin, R. R. Paepe, and A. Y. Rozanov, eds. (SPIE, Bellingham Washington, 2002), pp. 120-130.

Dorn, R.I., 1991. Rock varnish. *American Scientist*. 79; 542-553.

Dorn, R.I. 1994. Surface exposure dating with rock varnish. In C. Beck (ed), *Dating in Exposed and Surface Context*, pp. 77-113. University of New Mexico Press, Albuquerque.

Dorn, R.I. 1998. *Rock Coatings*. Developments in Earth Surface Processes 6, Elsevier, Amsterdam.

Dorn, R.I., 1996., A change of perception. *La Pintura* 23 (2); 10-11.

Dorn, R.I. et T.M. Oberlander., 1982. Rock Varnish. *Progress In Physical Geography*.6, 317-367.

Dorn, R.I. 1983. Cation-ratio dating : a new rock varnish age determination technique. *Quaternary Research* 20; 49-73.

Dorn, R.I., Nobbs, M.F., Cahill, T.A., 1988. Cation-ratio dating of rock engravings from the Olary Province of arid South Australia. *Antiquity*. 62; 681–689.

Dorn, R.I., Clarkson, P. B., Nobbs, M. F., Loendorf, L. L., and Whitley, D. S., 1992a. New approach to the radiocarbon dating of rock varnish, with examples from drylands. *Annals of the Association of American Geographers* 82, pp. 136–151.

Dorn, R.I., Jull, A.J.T., Donahue, D.J., Linick, T.W., Toolin, L.J., Moore, R.B., Rubin, M., Gill, T.E., and Cahill, T.A., 1992b. Rock Varnish on Hualalai and Mauna Kea, Volcanoes, Hawaii. *Pacific Science* 46: 11-34.

Dragovich, D., 1986. Minimum age of some desert varnish near Broken Hill, NewSouthWales, *Search*, 17: 149-151.

Dragovich, D., 1988 A preliminary electron probe study of microchemical variations in desert varnish in western New South Wales, Australia. *Earth Surface Processes and Landforms* 13, pp. 259–270.

Edwards, R.L., Cheng, H., Murrell, M.T., Goldstein, S.J., 1997. Protactinium-231 dating of carbonates by thermal ionization mass spectrometry: implications for Quaternary climate change. *Science*. 276; 782-786.

Edwards, R.L., Chen, J.H., Wasserburg, G.J., 1987a. ^{238}U-^{234}U-^{230}Th-^{232}Th systematics and the precise measurement of time over the past 500,000 years. *Earth and Planetary Science Letters*. 81; 175-192.

Edwards, R.L., Chen, J.H., Ku, T.L., Wasserburg, G.J., 1987b. Precise timing of the last interglacial period from mass spectrometric determination of thorium-230 in corals. *Science*. 236; 1547-1553.

Eggins S.M., Grün R., McCulloch M.T., Pike A.W.G., Chappell J., Kinsley L., Shelley M., Murray-Wallace C.V., Spötl C. and Taylor L., 2005. *In situ* U-series dating by laserablation multi-collector ICPMS: new prospects for Quaternary geochronology. *Quaternary Science Reviews* 24, 2523-2538.

Eggins, S., Grün, R., Pike, A., Shelley, A., Taylor, L., 2003. 238 U, 232 Th profiling and U-series isotope analysis of fossil teeth by laser ablation-ICPMS. *Quaternary Science Reviews*. 22, 1373-1382.

Eggins, S., Rudnick, R.L., & McDonough, W.F., 1998a. The composition of peridotites and their minerals, a laser-ablation ICPMS study. *Earth Planet Sci. Lett.*, 154; 53-71.

Eggins, S., Kinsley, L.K., & Shelley, J.M.G., 1998b. Deposition and element fractionation processes occurring during atmospheric pressure laser sampling for analysis by ICPMS. *Applied Surface Science*. 127-129; 278-286.

Edwards, R.L., Chen, J.H., Wasserburg, G.J., 1987a. ^{238}U-^{234}U-^{230}Th-^{232}Th systematics and the precise measurement of time over the past 500,000 years. *Earth and Planetary Science Letters*. 81; 175-192.

Edwards, R.L., Chen, J.H., Ku, T.L., Wasserburg, G.J., 1987b. Precise timing of the last interglacial period from mass spectrometric determination of thorium-230 in corals. *Science*. 236; 1547-1553.

Fajans. K., 1913. Radioactive transformations and the periodic system of the elements, *Berichte der Dautschen Chemischen Gesellschaft*, 46: 422-439.

Flannery, T.F., 1994. *The future eaters*. Reed Books, Melbourne.

Field, J. & Boles, W., 1998. *Genyornis newtoni* and *Dromaius novaehollandiae* at 30,000 b.p. from Cuddie Springs, southeastern Australia. *Alcheringa* 22; 177-188.

Field, J. & Dodson, G., 1999. Late Pleistocene megafauna and archaeology from Cuddie Springs, south-eastern Australia. *Proc. Prehist. Soc.* 65; 275-301.

Field, J. & Fullagar, R., 2001. Archaeology and Australian megafauna. *Science* 294; 7a.

Field, J & Wroe, S., 2001. Mystery of megafaunal extinction remains. *Australasian Science*; 21-25.

Field, J., H., R. Fullagar and G. Lord, 2001. A large area archaeological excavation at Cuddie Springs. *Antiquity* ; 696-702.

Fleisher, M., Liu, T., Broecker, W.S., 1999. A clue regarding the origin of rock varnish. *Geophysical Research Letters*. 26; 103-106.

Francis, W. D., 1921. The origin of black coatings of iron and manganese oxides on rocks. Proceedings of the Royal Society of Queensland 32: 110-116.

Francis, J.E., Loendorf, L.L. and Dorn, R.I., 1993. AMS radiocarbon and cation-ratio dating of rock art in the Bighorn Basin of Wyoming and Montana. *Am. Ant.* 58 4, pp. 711–737

Goldstein, S.J., Stirling, C.H., 2003. Techniques for measuring uranium-series nuclides: 1992-2002. *Reviews in Mineralogy and Geochemistry*. 52; 23-57.

Gould, S.J., 1996. Up against a wall, *Natural History*, 105(7)16.

Grün R., Aubert M., Eggins S., Williams I. and Moncel M.H., 2006. High-resolution *in situ* analysis of O and Sr isotopes in fossil human teeth. Poster at 150 years of Neanderthal discoveries. Early Europeans - continuity & discontinuity. 21-26 July 2006, Bonn, Germany. Abstract, *Terra Nostra* 2006/2: 115.

Grün R., 2006. Direct dating of human remains. *Yearbook of Physical Anthropology* 49, 2-48.

Grün, R., Brink, J.S., Spooner, N.A., Taylor, L., Stringer, C.B., Franciscus, R.G., Murray, A.S., 1996. Direct Dating of Florisbad Hominid. *Nature* 382; 500-501.

Grün, R. & Stringer, C.B., 2000. ESR and U-series analyses of dental material from Tabun C1. *J. hum. Evol.* 39; 601-612.

Grün, R. & Beaumont, P., 2001. Border Cave revisited: A revised ESR chronology. *J. hum. Evol.* 40; 467-482.

Hedges, S.B., 2000. A start for population genomics. *Nature* 408; 652-653.

Henshilwood, C.S., D'errico, F., Yates, R., Jacobs, Z., Tribolo, C., Duller, G.A.T.,

Mercier, N., Sealy, C., Valladas, H. Watts, I. & Wintle, A.G., 2002. Emergence of Modern Human Behaviour: Middle Stone Age engravings from South Africa, *Science* 295; 1278-1280.

Higham T.F.G., Jacobi R.M. and Bronk Ramsey C., 2006. AMS radiocarbon dating of bone from the European Palaeolithic using ultrafiltration. *Radiocarbon* 48, 179-195.

Hillson, S., 1986. *Teeth*. Cambridge Manuals in Archaeology. Cambridge University Press, Cambridge.

Horton, D.R. 1994. Panaramitee Style. In D. Horton (ed), *The Encyclopaedia of Aboriginal Australia*, Vol. 2. Aboriginal Studies Press, Canberra.

Ingman, M., Kaessmann, H., Pääbo, S., Gyllensten, U., 2000. Mitochondrial genome variation and the origin of modern humans. *Nature* 408; 708-713.

Ivanovich, M., Harmon, R.S., 1992. *Uranium series disequilibrium: Applications to Earth, Marine, and Environmental Sciences*. Clarendon Press, Oxford.

Israel, E.J., Arvidson, R.E., Wang, A., Pasteris, J.D. & Jolliff, B.L., 1997. *Laser Raman spectroscopy of varnished basalt and implications for in situ measurements of Martian rocks* J. Geophys. Res. Vol. 102 , No. E12 , p. 28, 705.

Jacobi R.M., Higham T.F.G. and Bronk Ramsey C., 2006. AMS radiocarbon dating of Middle and Upper Palaeolithic bone in the British Isles: Improved reliability using ultrafiltration. *Journal of Quaternary Science* 21, 557-573.

Jaffey, A.H., Flynn, K.F., Glendenin, L.E., Bentley, W.C., Essling, A.M., 1971. Precision measurement of half-lives and specific activities of ^{235}U and ^{238}U. *Physical Review*. 4, 1889-1906.

Johnson, B. J., Miller, G. H., Fogel, M. L., Magee, J. W., Gagan, M. K., Chivas, A. R. 1999. 65,000 years of vegetation change in Central Australia and the Australian summer monsoon. *Science* 284; 1150-1152.

Kaufman A., 1993. An evaluation of several methods for determining ^{230}Th/U ages in impure carbonates. *Geochimica et Cosmochimica Acta*. 57; 2303-2317.

Kaufman, A., Broecker, W.S., Ku, T.L., Thurber, D.L., 1971. The status of U-series methods of mollusk dating. *Geochimica Cosmochimica Acta*. 35; 1155-1189.

Kendall, A.C., & Broughton, P.L., 1978. Origin of fabrics in speleothems composed of columnar calcite crystals. *J. Sediment. Petrol.* 48; 519-538.

Klein, R.G., 1989. The human career: human biological and cultural origins. University of Chicago Press, Chicago.

Knauss, K.G., Ku, T.-L., 1980. Desert varnish: potential for age dating via uranium-series isotopes. *J. Geol.* 88; 95–100.

Kosasih, E. A., 1991. Rock art in Indonesia. In *Rock Art and Prehistory*, edited by P. Bahn and A. Rosenfeld, pp. 65-77. Oxbow Monograph 10. Short Run Press, Exeter.

Krinsley, D., 1998. Models of rock varnish formation constrained by high resolution transmission electron microscopy. *Sedimentology*. 45; 711-725.

Krinsley, D. and Anderson, S., 1989. Desert varnish: a new look at chemical and textural variations. *Geol. Soc. Am. Abstr. Prog.* 21 5, p. 103

Ku, T.L., 1968. Protactinium 231 method of dating coral from Barbados island. *Journal of Geophysical Research*. 73; 2271-2276.

Ku, T.L., 2000. Uranium-series methods. In: Noller, J.S., Sowers, J.M., Lettis, W.R. (eds) *Quaternary Geochronology Methods and* Applications. American Geophysical Union, Washington DC, pp 101-114.

Ku, T.L., Liang, Z.C., 1984. The dating of impure carbonates with decay-series isotopes. *Nuclear Instruments and Methods in Physics Research*. 223; 563-571.

Land, M., Öhlander, B., Thunberg, J., 1999. Solid speciation and fractionation of rare earth elements in a spodosol profile from northern Sweden as revealed by sequential extraction. *Chemical Geology*. 160; 121-138.

Latham, A.G., 2001. *Uranium-series dating*. In: Pollard, M., Brothwell, D. (eds) Introduction to Archaeological Sciences. Wiley, London, 63-72.

Leitner-Wild, E. & Steffan, I., 1993. Uranium-series dating of fossil bones from Alpine caves. *Archaeometry* 35; 137-146.

Liu, T., 1994. Visual microlaminations in rock varnish : a new paleoenvironmental and geomorphic tool in drylands. PhD thesis, Arizona State University, Tempe.

Liu, T., Broecker, W.S., 2000, How fast does rock varnish grow? *Geology*. 28, 183-186.

Llosas, M.I.H., Watchman, A., Southon, J., 1999. Pigment analysis and absolute dating of rock paintings, Jujuy, Argentina. In: Bahn, P. (Ed.), Dating and the Most Ancient Rock Art, Oxbow Monographs, Oxford, pp. 67–74.

Longerich, H.P., Jackson, S.J., Gunther, D., 1996. Laser ablation inductively coupled mass-spectrometric transient signal data acquisition and analyte concentration calculation. *Journal of Analytical and Atomic Spectrometr.y* 11; 899–904.

Ludwig, K.R., & Titterington, D.M.,. 1994, Calculation of 230Th/U isochrons, ages, and errors: *Geochimica et Cosmochimica Acta*, 58; 5031–5042.

Ludwig, K.R., & Paces, J.B., 2001. Uranium-series dating by TIMS of pedogenic silica and carbonate: an example from Crater Flat, Nevada. *Geochimica et Cosmochimica Acta*, 66; 487-506.

Ludwig, K.R., 2003. Mathematical-statistical treatment of data and errors for 230 Th/U geochronology. *Reviews in Mineralogy and Geochemistry*. 52 ; 631-656.

Luo, X., Rehkämper, M., Lee, D.-C., Halliday, A.N., 1997. High precision $^{230}Th/^{232}Th$ and $^{234}U/^{238}U$ measurements using energyfiltered ICP magnetic sector multiple collector mass spectrometry. *International Journal of Mass Spectrometry and Ion Processes* 171; 105-117.

Luo, S. et T. L. Ku , 1991. U-series isochron dating: A generalized method employingtotal-sample dissolution. *Geochimica et Cosmochimica Acta*. 55; 555-564.

Macho G.A., Jiang Y. and Spears I.R., 2003. Enamel micro structure - a truly three-dimensional structure. *Journal of Human Evolution* 45, 81-90.

McDougall, I., Brown, F. H. & Fleagle, J. G., 2005. Stratigraphic placement and age of modern humans from Kibish, Ethiopia. *Nature*. 433:733-736.

McDonald, J., Officer, K., Jull, T., Donahue, D., Head, J. and Ford, B., 1990. Investigating ^{14}C AMS: dating prehistoric rock art in the Sydney Sandstone Basin, Australia. *Rock Art Res.* **7**, pp. 83–92.

McKeown, D.A. and J.E. Post 2001. Characterization of manganese oxide mineralogy in

rockvarnish and dendrites using X-ray absorption spectroscopy. *American Mineralogist* 86; 701–713.

McDermott, F., Stringer, C., Grün, R., Williams, C.T., Din, V.K., Hawkesworth, C.J.,1996. New Late-Pleistocene Uranium-Thorium and ESR dates for the Singa hominid (Sudan). *J. hum. Evol.* 31; 507-516.

Mercier, N., Valladas, H., Bar-Yosef, O., Vandermeersch, B., Stringer, C., Joron, J.-L.,1993. Thermoluminescence Date for the Mousterian Burial Site of Es-Skhul, Mt.Carmel. *J. Arch. Sci.* 20; 169-174.

Millard, A.R. & Hedges, R.E.M., 1996. A diffusion-adsorption model of uranium uptake by archaeological bone. *Geochim. Cosmochim. Acta* 60; 2139-2152.

Miller, G.H., Magee, J.W., Johnson, B.J., Fogel, M., Spooner, N.A., McCulloch, M.T., Ayliffe, L.K. 1999. Pleistocene extinction of *Genyornis nemtoni*: human impact on Australian megafauna. *Science* 283; 205-208.

Millard A.R., 1993. Diagenesis of archaeological bone: the case of uranium uptake. D.Phil. Thesis, University of Oxford.

Moncel M.H., 2004. Continuité et variabilité des occupations humaines à la fin du Pléistocène moyen et au début du Pléistocène supérieur (stades isotopiques 9 à 3). L'exemple de la moyenne vallée du Rhône (France), In *Settlement Dynamics of the Middle Palaeolithic and Middle Stone Age II* (ed. N.J. Conard) Kerns Verlag, Tübingen, pp. 295-317.

Moncel M.H. and Condemi S., 1996. Découverte de dents humaines dans le site Paléolithique moyen de Payre (Ardèche, France), *Comptes Rendus de l'Academie des Sciences Serie II Fascicule A-sciences de la Terre et des Planetes* 322, 251-257.

Moncel M.H. and Condemi S., 1997. Des restes humains dans le site Paléolithique moyen ancien de Payre (Ardèche): dents et pariétal. Nouvelles découvertes de 1996. *Bulletin de la Société Préhistorique Française* 94/2, 168-171.

Moncel M.H, Debard E., Desclaux E., Dubois J.M., Lamarque F., Patou-Mathis M. and Vilette P., 2002. Le cadre de vie des hommes du Paléolithique moyen (stades isotopiques 6 et 5) dans le site de Payre (Rompon, Ardèche): d'une grotte à un abri-sous-roche effondré. *Bulletin de la Société Préhistorique Française* 99/2, 249-275.

Moncel M.H., Moigne A.M. and Combier J., 2005. Pre-Neandertal behaviour during isotopic stage 9 and the beginning of stage 8. New data concerning fauna and lithics in the different occupation levels of orgnac 3 (Ardeche, South-East France): occupation types. *Journal of Archaeological Science* 32, 1283-1301.

Morwood, M.J., Soejono, R.P., Roberts, R.G., Sutikna, T., Turney, C.S.M., Westaway, K.E., Rink, W.J., Zhao, J.-X., van den Bergh, G.D., Due, R.A., Hobbs, D.R., Moore, M.W., Bird, M.I. & Fifield, L.K., 2004. Archaeology and age of a new hominin from Flores in Eastern Indonesia. *Nature* 431;1087-91.

Nagy, B. 1991, Rock varnish in the Sonoran Desert: microbiologically mediated accumulation of manganiferous sediments. *Sedimentology*. 38; 1153-1171.

Nakai, S., Fukuda, S., Nakada, S., 2001. Thorium isotopic measurements on silicate rock samples with a multicollector inductively coupled plasma mass spectrometer. Analyst 126; 1707e1710.

Nier, A.O., 1939. The isotopic constitution of uranium and the half-lives of the uranium isotopes. *I. Physical Review*. 55; 150-153.

Nobbs, M. and R.I Dorn 1993. New surface exposure ages for petroglyphs from the Olary Province, South Australia. *Archaeology in Oceania* 28; 18-39.

O'Connor, S., 2003. Report of nine new painted rock art sites in East Timor inthe context of the western Pacific region. Asian Perspect 42 (1); 96e128.

O'Connor, S., Oliveira, N.V., 2007. Inter and intra regional variation in theAustronesian painting tradition: a view from East Timor. Asian Perspect 46 (2).

O'Connor, S., Veth, P., 2005. Early Holocene Trochus shell fish-hooks fromEast Timor. Antiquity 79; 8.

O'Connor, S., Spriggs, M., Veth, P., 2002. Excavation at Lene Hara establishesoccupation in East Timor at least 30,000e35,000 years ago: results of recent fieldwork. Antiquity 76; 45e50.

O'Connor, S., Aplin, K., Szabo` , K., Pasveer, J., Veth, P., Spriggs, M., 2005.Liang Lemdubu, a Pleistocene cave site in the Aru Islands. In: O'Connor, S., Spriggs, M., Veth, P. (Eds.). The

Archaeology of the Aru Islands, Eastern Indonesia. Terra Australis 23. Pandanus Press, Canberra, pp. 171e204.

Oka T., Grün R., Tani A., Yamanaka C., Ikeya, M. and Huang H.P., 1997. ESR microscopy of fossil teeth. *Radiation Measurements* **27**: 331-337.

Palmer, F.E., Staley, J.T., Murray, R.G.E., Counsell, T., Adams, J.B., 1986. Identification of Manganese-Oxidizing Bacteria from Desert Varnish. *Geomicrobiology Journal*. 4; 343-360.

Pickett, D.A., Murrell, M.T. & WILLIAMS, R.W. 1994. Determination of Femtogram Quantities of Protactinium in Geologic Samples by Thermal Ionization Mass Spectrometry. *Anal. Chem*. 66; 1044–1049.

Pike, A.W.G., Pettitt, P.B., 2003. U-series dating and human evolution. *Reviews in Mineralogy and Geochemistry*. 52; 607-630.

Pike A.W.G., Hedges R.E.M. and Van Calsteren P., 2002. U-series dating of bone using the diffusion-adsorption model. *Geochimica et Cosmochimica Acta* 66, 4273-4286.

Pike, A.W.G., 2000. U-series dating of archaeological bone by thermal ionisation mass spectrometry. DPhil. Thesis, University of Oxford, Oxford.

Plagnes, V., Causse, C., Fontugnew, M., Valladas, H., Chazine, J.-M. & Fage, L.-H., 1993. Cross dating (Th/U-14C) of calcite covering prehistoric paintings in Borneo. *Quaternary Research* 60; 172-179.

Przybylowicz, W., Schwarcz, H.P., Latham, A.G., 1991. Dirty calcites 2. Uranium-series dating of artificial calcite-detritus mixtures. *Chemical Geology (Isotope Geoscience Section)*. 86; 161-178.

Reneau, S.L. and R. Raymond 1991. Cation-ratio dating of rock varnish : why does it work? Geology 19 (9); 937-940.

Reneau, S.L., Raymond, R. and C. Harrington 1992. Elemental relationships in rock varnish stratigraphic layers, Cima volcanic field, California : implications for rock varnish development and the interpretation of varnish chemistry. *American Journal of Science* 292; 684-723.

Richards, D.A., Bottrell, S.H., Cliff, R.A., Ströhle, K., Rowe, P.J., 1998. U-Pb dating of a speleothem of Quaternary age. *Geochimica Cosmochimica Acta*. 62; 3683-3688.

Robert, J., Miranda, C.F., Muxart, R., 1969. Mesure de la période du protactinium 231 par microcalorimétrie. *Radiochimica Acta*. 11; 104-108.

Roberts, R.G., Jones, R., Smith, M.A., 1994a. Beyond the radiocarbon barrier in Australian prehistory. *Antiquity* 68; 611-616.

Roberts R.G., Jones, R., Spooner, N.A., Head, M.J., Murray, A.S., Smith, M.A., 1994b. The human colonisation of Australia: optical dates of 53,000 and 60,000 years bracket human arrival at Deaf Adder Gorge, Northern Territory. *Quaternary Science Reviews*. 13; 575-586.

Roberts, R.G., Walsh, A., Murray, A.S., Olley, J., Jones, R., Morwood, M., Tuniz, C., Lawson, E., Mscphail, M., Bowdery, D. & Naumann, I., 1997. Luminescence dating of rock art and past environments using mud-wasp nests in northern Australia. *Nature*, 387; 696-9.

Roberts, R., Flannery, T., Ayliffe, L., Yoshida, H., Olley, J. Prideaux, G., Laslett, G., Baynes, A., Smith, M., Jones, R., and Smith, B., 2001a. New ages for the last Australian megafauna: continental-wide extinction about 46,000 years ago. *Science* 292; 1888-1892.

Roberts, R., Flannery, T., Ayliffe, L., Yoshida, H., Olley, J. Prideaux, G., Laslett, G., Baynes, A., Smith, M., Jones, R., and Smith, B., 2001b. Response to Field & Fullagar. *Science* 294; 7a.

Roberts, R., Flannery, T., Ayliffe, L., Yoshida, H., Olley, J. Prideaux, G., Laslett, G., Baynes, A., Smith, M., Jones, R., and Smith, B., 2001c. The last Australian megafauna. *Australasian Science* 22; 40-41

Romer, L.R., 2001. Isotopically heterogeneous initial Pb and continuous ^{222}Rn loss in fossils: The U-Pb systematics of Brachiosaurus brancai, *Geochimica et Cosmochimica Acta,* Vol. 65, No. 22, pp. 4201–4213.

Rosholt, J.N., Antal, P.S., 1962. Evaluation of the Pa 231 /U-Th 230 /U method for dating Pleistocene carbonate rocks. *Geological Survey Research Professional Papers*. 450E, E108-E111.

Russell, R.D., Farquhar, R.M., 1960. *Lead isotopes in geology*. Interscience, New York.

Rutherford, E., 1899. Uranium Radiation and the Electrical Conduction Produced by It, *Philos Mag*, 47:109-163.

Rutherford, E., 1900. A Radioactive Substance emitted from Thorium Compounds, *Philos Mag, 49: 1-14.*

Rutherford, E., 1903. Radioactive Change, *Philos Mag, 5: 576-591.*

Rutherford, E., 1904. The Succession of Changes in Radioactive Bodies*Phil Trans of the Roy Soc*, **204:**169-219.

Sackett, W.M., 1958. *Ionium-uranium ratios in marine deposited calcium carbonates and related materials*. PhD Thesis, Washington University, Saint Louis, Missouri.

Schwarcz, H.P., Latham, A.G., 1989. Dirty calcites 1. Uranium-series of contaminated calcite using leachates alone. *Chemical Geology*. 80; 35-43.

Schwarcz, H.P., 1993. Uranium series dating and the origin of modern man. In: Aitken, M.J., Stringer, C.B., Mellars, P.A. (eds) The origins of modern humans and the impact of chronometric dating.

Simpson, J.J. & Grün, R., 1998. Non-destructive gamma spectrometric U-series dating. *Quat. Sci. Rev.* 17 ; 1009-1022.

Staley, J. T., Jackson, M. J., Palmer, F. E., Adams, J. C., Borns, D.J., Curtiss, B. & Taylor-George, S., 1983. Desert varnish coatings and microcolonial fungi on rocks of the Gibson and Great Victoria Desert, Australia. *BMR Journal of Australian Geology and Geophysics*, 8: 83-87.

Stringer, C.B., Grün, R., Schwarcz, H.P., Goldberg, P., 1989. ESR dates for the hominid burial site of Es Skhul in Israel. *Nature* 338; 756-758.

Stirling, C.H., Lee, D.-C., Christensen, J.N., Halliday, A.N., 2000. High-precision in situ ^{238}U-^{234}U-^{230}Th isotopic analysis using laser ablation multiple-collector ICPMS. *Geochimica et Cosmochimica*. 64; 3737-3750.

Schwarcz H.P., 1997. *Uranium series dating*. In: Taylor RE, Aitken MJ (eds) Chronometric dating in Archaeology. Plenum, New York, pp 159-182.

Schulmeister, J., Short S. A., Price, D. M., Murray A. S., 1993. Pedogenic uranium/thorium chronologies and evolutionary Agency, Harwell, Laboratory Report, AERE-R 12558. history of a coastal dunefield, Groote, Eylandt, Northern Australia.

Smith, C. & Rosenfeld, A., 1997. The uses of radiometric and stylistic approaches to rock art dating. *Antiquity* 72 (272); 405-11.

Soddy, F., 1910. *Radioactivity*. In Annual Reports on the Progress of Chemistry, 7: 257-286.

Soddy, F., 1913. The Radio-elements and the Periodic Law *Chemical News,* 107: 97-99.

Taçon, P., Aung, D.Y.Y., & Thorne, A., 2004. Myanmar prehistory: rare rock markings revealed. Archaeology in Oceania, 39(3); 138.

Tessier, A., Campbell, P.G.C., Bisson, M., 1979. Sequential extraction procedure for the speciation of particulate trace metals. *Anal. Chem*. 51; 844–851.

Thorne, A., Grün, R., Mortimer, G., Simpson, J. J., McCulloch, M., Taylor, L., Curnoe, D., 1999. Australia's oldest human remains: age of the Lake Mungo 3 skeleton. *Journal of Human Evolution*, 36; 591-692.

Tuniz, C. & Watchman, A.L., 1994. The ANTARES AMS spectrometer. Accelerators and lasers for dating rock art in Australia. *Rock Art Research* 11(1), 71-73.

Wang, X., Auler, A.S., Edwards, R.L., Cheng, H., Cristalli, P.S., Smart, P.L., Richards, D.A. Shen, C.-C., 2004. Wet periods in northeastern Brazil over the past 210 kyr linked to distant climate anomalies. *Nature*. 432; 741-742.

Ward, I., Watchman, A.L., Cole, N. & Morwood, M., 2001. Identification of Minerals in Pigments from Aboriginal Rock Art in the Laura and Kimberley Regions, Australia. *Rock Art Research* 18(1), 15-23.

Watchman, A., 1992a. WATCHMAN, A. 1992. Investigating the cation-ratio calibration curve: evidence from South Australia. *Rock Art Research* 9(2):106-110.

Watchman, A., 1992b. Composition, formation and age of some Australian silica skins. *Australian Aboriginal Studies* 1, 61-66.

Watchman, A., 1992c. Doubtful dates for Karolta engravings. *Australian Aboriginal Studies* 1; 51-55.

Watchman, A.L., 1993. Evidence of a 25,000-year-old pictograph in northern Australia. *Geoarchaeology* 8(6), 465-473.

Watchman, A.L., 1994. Radiocarbon dating fatty acids in Holocene siliceous rock surface accretions. *Australian Journal of Earth Sciences.* 41; 179-180.

Watchman, A.L., 2000a. A Review of the history of rock varnish dating. *Earth Science Reviews.* 49; 261-277.

Watchman, A.L., 2000b. Micro-excavation and laser extraction methods for dating carbon in silica skins and oxalate crusts. In G.K. Ward and C. Tuniz (eds*), Advances in dating Australian rock-markings,* pp. 35-39. Occasional AURA Publication 10.

Watchman, A.L. & Cole, N., 1992. Accelerator radiocarbon dating of plant-fibre binders in rock paintings from northeastern Australia. *Antiquity* 67; 355-358.

Watchman, A.L., Lessard, R.A., Jull, A.J.T., Toolin, L.J. & Blake Jnr, W., 1993. ^{14}C dating of laser-oxidized organics. *Radiocarbon* 35(2); 331-333.

Watchman, A., David, B. McNiven, I., & Flood, J., 2000a. Micro-archaeology of engraved and painted rock surface crusts at Yiwaralarlay (The Lightning Brothers site), Northern Territory, Australia. *Journal of Archaeological Science*, 27; 315-325.

Watchman, A., Taçon, P., Fullagar, R., & Head, L., 2000b. Minimum ages for pecked rock markings from Jinmium, northwestern Australia. *Archaeology in Oceania*, 35: 1-10.

Wright, J.S., 2000. Tufa accumulations in ephemeral streams: observations from the Kimberley, north-west Australia. *Australian Geographer* 31; 333-347.

Wilson, M., M. Spriggs & E. Lawson., 2001. Dating the rock art of Vanuatu: AMS radiocarbon determinations from abandoned mud-wasp nests and charcoal pigment found in superimposition. *Rock Art Research* 18; 24-32.

Yokoyama, Y., Nguyen, H.V., 1980. Direct and non-destructive dating of marine sediments, manganese nodules, and corals by high resolution Gamma Ray Spectrometry. *Isotope Marine Chemistry*. 1980; 259-289.

ANNEXE 1

PROTOCOLES

500 ML SOLUTIONS FOR SEQUENTIAL EXTRACTION (ROCK)

Fraction A) (exchangeable/adsorbed/carbonate) **1.0M CH_3COONa (pH 5)/500 ml**

- 41.015 g of ultra pure CH_3COONa

- 14.25 ml of conc. ultra pure CH_3COOH (adjust to pH 5)

Fraction B) (labile organics) **0.1M $Na_4P_2O_7$/500 ml**

- 22.3 g of ultra pure $Na_4P_2O_7$

Fraction C) (amorphous Fe-oxyhydroxides/Mn-oxides) **0.25 M $NH_2OH.HCl$ in 0.1M HCl/500 ml**

- 8.686 g of ultra pure $NH_2OH.HCl$

- 4.17 ml conc. ultra pure HCL (0.1 M/500 ml)

Fraction D) (crystalline Fe-oxides) **1.0 M $NH_2OH.HCl$ in 25% CH_3COOH/500 ml**

- 34.75 g of ultra pure $NH_2OH.HCl$

- 125 ml of conc. ultra pure CH_3COOH/500 ml

- 25% of ultra pure CH_3COOH (12.5 ml/50 ml)

SEQUENTIAL EXTRACTION (ROCK)

Protocol for 0.05g

Fraction A) (exchangeable/adsorbed/carbonate)

- 1) place 0.05 g of sample (powder) in a centrifuge tube
- 2) add 0.5 ml of ultra pure 1.0M CH_3COONa (pH 5)
- 3) shake for 6 hrs
- 4) centrifuge for 15 minutes at 7000 rpm
- 5) transfer supernatant into a test tube
- 6) add 0.5 ml of ultra pure 1.0M CH_3COONa (pH5) to the residue and shake for 6 hrs
- 7) centrifuge for 15 minutes at 7000 rpm
- 8) transfer supernatant into the test tube used in step 5)
- 9) rinse the residue with 0.25 ml milliQ H_2O
- 10) centrifuge for 15 minutes at 7000 rpm and transfer supernatant into the test tube used in step 5)
- 11) rinse the residue with 0.25 ml milliQ H_2O and centrifuge for 15 minutes at 7000 rpm and transfer supernatant into the test tube used in step 5)

Fraction B) (labile organics)

- 12) to the residue in step 11) add 2.5 ml of ultra pure 0.1M $Na_4P_2O_7$
- 13) shake for 1 hr and centrifuge for 15 minutes at 7000 rpm
- 14) transfer supernatant into a new test tube
- 15) add 2.5 ml of ultra pure 0.1M $Na_4P_2O_7$ to the residue
- 16) centrifuge for 15 minutes at 7000 rpm and transfer supernatant into the test tube used in step 14)
- 17) rinse the residue with 0.25 ml milliQ H_2O
- 18) centrifuge for 15 minutes at 7000 rpm and transfer supernatant into the test tube used in step 14)
- 19) rinse the residue with 0.25 ml milliQ H_2O and centrifuge for 15 minutes at 7000 rpm and transfer supernatant into the test tube used in step 14)

Fraction C) (amorphous Fe-oxyhydroxides/Mn-oxides)

- 20) to the residue in step 19) add 0.5 ml of ultra pure 0.25 M $NH_2OH.HCl$ in 0.1M HCl
- 21) place the centrifuge tubes in a water bath at 60^oC for 2 hrs
- 22) centrifuge for 15 minutes at 7000 rpm
- 23) transfer supernatant into a new test tube
- 24) add 0.5 ml of ultra pure 0.25 M $NH_2OH.HCl$ in 0.1M HCl to the residue
- 25) place the centrifuge tubes in a water bath at 60^oC for 2 hrs

- 26) centrifuge for 15 minutes at 7000 rpm
- 27) transfer supernatant into the test tube used in step 23)
- 28) rinse the residue with 0.25 ml milliQ H_2O
- 29) centrifuge for 15 minutes at 7000 rpm and transfer supernatant into the test tube used in step 23)
- 30) rinse the residue with 0.25 ml milliQ H_2O and centrifuge for 15 minutes at 7000 rpm and transfer supernatant into the test tube used in step 23)

Fraction D) (crystalline Fe-oxides)

- 31) to the residue in step 30) add 0.75 ml of ultra pure 1.0 M $NH_2OH.HCl$ in 25% CH_3COOH
- 32) place the centrifuge tubes in a water bath at 90^oC for 3 hrs
- 33) centrifuge for 15 minutes at 7000 rpm
- 34) transfer supernatant into a new test tube
- 35) add 0.75 ml of ultra pure 1.0 M $NH_2OH.HCl$ in 25% CH_3COOH to the residue
- 36) place the centrifuge tubes in a water bath at 90^oC for 1.5 hr
- 37) centrifuge for 15 minutes at 7000 rpm
- 38) transfer supernatant into the test tube used in step 34)
- 39) rinse the residue with ultra pure 0.25 ml of 25% CH_3COOH
- 40) centrifuge for 15 minutes at 7000 rpm and transfer supernatant into the test tube used in step 30)
- 41) rinse the residue with 0.25 ml of ultra pure 25% CH_3COOH and centrifuge and transfer supernatant into the test tube used in step 34)

Fraction E) (organics and sulphides)

- 42) to the residue in step 41)add 37.5 mg of ultra pure $KCLO_3$ and 0.25 ml of ultra pure 12M HCl
- 43) shake (vortex) and add 0.5 ml of ultra pure 12M HCl and wait 30 minutes.
- 43) add 0.75 ml of milliQ H_2O and centrifuge for 15 minutes at 7000 rpm
- 44) transfer supernatant into a new test tube
- 45) add 0.5 ml of ultra pure 4M HNO_3 to the residue
- 46) place the centrifuge tubes in a water bath at 90^oC for 20 minutes.
- 47) centrifuge for 15 minutes at 7000 rpm
- 48) transfer supernatant into a new test tube
- 49) rinse the residue with 0.25 ml milliQ H_2O
- 50) centrifuge for 15 minutes at 7000 rpm and transfer supernatant into the test tube used in step 48)
- 51) rinse the residue with 0.25 ml milliQ H_2O and centrifuge for 15 minutes at 7000 rpm and transfer supernatant into the test tube used in step 48)

- Always keep the residues in the fridge (4^oC)

Modify from :

Land *et al.*, 1999. Solid speciation and fractionation of rare earth elements in a spodosol profile from northern Sweden as revealed by sequential extraction. Chemical geology, 160, 121-138.

TOTAL DISSOLUTION (ROCK)

Protocol for 0.05g

- 1) place 0.05g of sample (powder) in high pressure bomb
- 2) add 0.4 ml of milliQ H_2O
- 3) add 1 ml of conc. ultra pure HNO_3
- 4) add 0.5 ml of conc. ultra pure HCL
- 5) add 0.25 ml of conc. ultra pure HF
- 6) keep it open for 15-30 minutes
- 7) close the bomb and place in the oven at 150^oC for 4 days
- 8) put the residue from step 7) in low pressure Teflon Savilex bomb
- 9) rinse the high pressure bomb with milliQ H_2O
- 10) add 0.05 ml of conc. ultra pure $HCLO_4$
- 11) evaporate to dryness on a hot plate at 170^oC

ANNEXE 2

RÉSULTATS ANALYTIQUES

ICP-MS ANU/RSES	**Karolta rock** exchangeable/ adsorbed/ carbonate	**Karolta weathered rock** exchangeable/ adsorbed/ carbonate	**Karolta varnish** exchangeable/ adsorbed/ carbonate	**matrix blank** exchangeable/ adsorbed/ carbonate
Isotope	**PPB**	**PPB**	**PPB**	**PPB**
Mn 55	478123.2836	1750074.759	1687780.82	1.364758129
Rb 85	22616.02205	5703.102845	1703.247948	0.006871735
Sr 88	141503.8839	37996.91218	91220.8821	0.440978217
Zr 90	259.1012615	685.6444761	371.9809574	-0.000999126
Nb 93	1.379495653	0.167261172	-1.657107194	0.000253606
Ba 135	41099.56816	172408.9781	240970.1973	0.12066639
Ba 137	41058.29725	173613.0212	242819.1198	0.118300664
Ba 138	40788.46283	172952.2775	240384.1231	0.113789117
Ce 140	13087.43693	35557.19594	39934.45267	0.026313839
Pr 141	1532.178516	2194.672363	3086.58108	0.000995267
Nd 143	5649.340847	8936.760979	12902.97253	0.00389672
Nd 146	5707.25581	8971.316049	13043.60863	0.003789039
Sm 147	1099.685096	1915.710308	2830.921855	0.000744253
Sm 149	1095.904882	1906.050347	2795.61173	0.000655098
Eu 151	214.5882979	387.1945681	582.3882271	0.000179315
Eu 153	212.8777737	385.0665974	576.7042606	0.000113912
Gd 157	1207.153921	1886.080042	2703.283965	0.000682027
Tb 159	190.9211626	251.2799955	356.7889661	9.42968E-05
Dy 163	1136.936922	1329.315019	1883.604863	0.000374879
Ho 165	227.9167972	253.6128388	354.3700268	0.000113812
Er 167	650.2491207	661.8020703	911.9416266	0.000312543
Tm 169	17.14444207	14.81552599	19.81304128	2.11265E-05
Yb 173	652.0323118	481.925699	622.3952487	0.000448042
Lu 175	103.310868	73.69434637	95.67012779	7.21865E-05
Hf 178	7.372783214	24.1646067	18.445402	1.38436E-05
Ta 181	0.37634439	0.377751742	0.414970901	-4.50079E-06
Pb 208	10359.14996	3868.716666	624.8393413	-0.013386912
Th 232	820.1111647	574.5225013	348.647377	-0.001684357
U 238	305.7766842	649.6707022	1229.117243	0.000434711

ICP-MS RSES/ANU	**Karolta rock** labile organics	**Karolta weathered rock** labile organics	**Karolta varnish** labile organics	**matrix blank** labile organics
Isotope	**PPB**	**PPB**	**PPB**	**PPB**
Mn 55	20020.6298	454707.3156	1046208.234	0.755642756
Rb 85	9034.941962	3455.666436	1438.533896	0.049457558
Sr 88	3382.318466	4114.435081	5917.062205	0.182073578
Zr 90	1987.895852	6101.74309	7082.522576	0.044676749
Nb 93	23.51945493	34.56778548	35.86039462	0.007511917
Ba 135	10030.84648	24864.07808	42791.7598	0.300532354
Ba 137	10065.20241	24742.55088	42957.11719	0.298956934
Ba 138	9556.674045	23473.39988	38612.59823	0.267682188
Ce 140	1926.006816	11013.54754	15831.4092	0.015210532
Pr 141	196.0745234	717.5692071	932.9390017	0.00129318
Nd 143	758.0212368	2699.506497	3728.972661	0.049575083
Nd 146	730.0808115	2714.046788	3721.054822	0.005308455
Sm 147	129.4697222	595.4445357	836.4850759	0.001016049
Sm 149	133.3577219	586.429139	842.4004844	0.001116677
Eu 151	20.14025988	120.1816618	172.1754735	0.000150125
Eu 153	20.10368628	117.0410658	173.0384439	0.000168931
Gd 157	98.7457948	551.5368703	766.0778883	0.000756118
Tb 159	11.43223349	83.9512982	122.0952954	0.000108896
Dy 163	54.91722646	470.8724422	677.7623782	0.000346454
Ho 165	9.902336255	91.73933013	143.6400579	5.81122E-05
Er 167	26.76930422	265.2113341	404.9282305	0.000188155
Tm 169	0.741780112	7.770899966	12.82268272	9.09687E-06
Yb 173	27.08813969	278.8787492	465.9512727	0.0007284
Lu 175	3.91620128	41.55561349	68.12510912	3.93701E-05
Hf 178	59.65487283	197.016642	281.6182436	0.000873361
Ta 181	10.51085642	8.895530066	7.942886641	0.010951827
Pb 208	893.5971518	5341.003037	4170.459444	0.001662867
Th 232	292.6794633	969.845684	1368.612905	0.003878799
U 238	36.67103479	214.2577103	449.6263579	0.000591035

ICP-MS RSES/ANU	**Karolta rock** amorphous Fe-oxyhydroxides/ amorphous Mn-oxides	**Karolta weathered rock** amorphous Fe-oxyhydroxides/ amorphous Mn-oxides	**Karolta varnish** amorphous Fe-oxyhydroxides/ amorphous Mn-oxides	**matrix blank** amorphous Fe-oxyhydroxides/ amorphous Mn-oxides
Isotope	**PPB**	**PPB**	**PPB**	**PPB**
Mn 55	61445.40113	Overrange	Overrange	-0.644796905
Rb 85	9768.639318	4985.443818	2627.26988	0.002493549
Sr 88	11417.07586	28273.19188	131868.0282	0.05021531
Zr 90	26.39107932	59.81147712	6.712525489	0.003744652
Nb 93	5.96074877	2.464700545	0.247476987	0.000787144
Ba 135	16404.34712	639932.5244	2871346.922	0.042703679
Ba 137	16482.72127	645465.8092	2885247.346	0.042519323
Ba 138	14673.27521	588810.0451	2650096.215	0.036713446
Ce 140	2717.901343	147792.7324	600592.7207	0.011690726
Pr 141	397.5058026	4335.246769	14481.57881	0.000731863
Nd 143	1922.942573	17307.06443	56338.77938	0.002378729
Nd 146	1907.493851	17331.34348	56108.51389	0.002613021
Sm 147	557.3251822	3593.976577	10147.13579	0.000466108
Sm 149	555.8890892	3619.951314	10182.63228	0.000483598
Eu 151	98.19488592	736.0169367	1998.554369	8.53101E-05
Eu 153	96.540539	738.4465345	2016.310533	9.72568E-05
Gd 157	741.4774904	3739.129465	10424.7582	0.000558651
Tb 159	120.0377971	542.2282438	1308.53847	8.16902E-05
Dy 163	658.3787071	2841.788771	6516.727499	0.000238442
Ho 165	129.5329234	576.7577778	1318.506661	7.07385E-05
Er 167	294.6800298	1409.564291	3167.692269	0.00014867
Tm 169	6.655485089	36.15347516	80.09076475	3.49E-06
Yb 173	188.1679124	1156.381677	2473.373679	0.000260377
Lu 175	24.39510426	164.4310633	351.0025722	3.09411E-05
Hf 178	1.19987731	3.66520802	1.779629087	0.000167004
Ta 181	1.077817065	0.773650942	0.297786634	4.24397E-05
Pb 208	4506.559681	85998.64359	69530.27975	0.012901351
Th 232	10.05344641	31.29860483	6.273568087	0.000706627
U 238	38.79497359	148.0746257	57.17906991	0.000153041

ICP-MS RSES/ANU	**Karolta rock** sulphides	**Karolta weathered rock** sulphides	**Karolta varnish** sulphides	**matrix blank** sulphides
Isotope	**PPB**	**PPB**	**PPB**	**PPB**
Mn 55	5327.79714	41811.41496	111313.1888	-1.58678307
Rb 85	6180.737043	6568.147277	5206.048158	4.738918157
Sr 88	625.4535114	2990.598391	2042.102725	-0.009720558
Zr 90	1081.483039	3889.209185	2546.548759	0.019355382
Nb 93	9.276089826	18.40535261	18.92601496	0.000783935
Ba 135	1455.012958	10499.01184	14433.13694	-0.005372566
Ba 137	1474.264991	10513.4252	14500.53698	0.003464455
Ba 138	1461.01829	9652.895773	13230.71693	-0.002464354
Ce 140	30769.16696	26846.0277	37468.84147	0.079303853
Pr 141	3697.221459	3402.99552	3006.505956	0.00054421
Nd 143	13952.24687	13160.2414	12388.54593	0.001023961
Nd 146	14005.41782	13100.94907	12453.07774	0.0012098
Sm 147	2172.712535	2268.280084	2701.042139	-1.03228E-06
Sm 149	2190.518963	2275.650495	2714.328798	0.000254395
Eu 151	242.4922715	350.3630723	542.7750169	8.76138E-05
Eu 153	243.4412637	348.8616321	542.9397666	7.15611E-05
Gd 157	1195.808226	1534.745901	2132.367818	0.000388142
Tb 159	89.65230643	178.0306751	320.6699648	3.98574E-05
Dy 163	243.5352732	788.9725015	1595.224012	-2.57166E-05
Ho 165	30.04283358	143.7800068	293.7497247	2.90374E-05
Er 167	58.21593781	323.4159847	692.1865781	-5.4096E-05
Tm 169	1.415228399	8.318624859	18.09711128	2.17046E-06
Yb 173	47.18790947	273.8354144	611.0557558	0.000177353
Lu 175	7.434800823	38.97485561	84.24221808	2.65869E-05
Hf 178	50.36259301	112.3304788	69.86548943	0.000565895
Ta 181	0.166963921	0.263635529	0.318815012	0.000119176
Pb 208	1652.756819	17886.27658	14389.47711	-0.012262456
Th 232	1080.037451	5539.005688	6962.329598	0.013487487
U 238	212.5995344	292.9799799	693.7347645	3.20103E-05

ICP-MS RSES/ANU	Karolta rock refractory organics	Karolta weathered rock refractory organics	Karolta varnish refractory organics	matrix blank refractory organics
Isotope	**PPB**	**PPB**	**PPB**	**PPB**
Mn 55	9939.951079	28929.55817	44376.04021	0.014474196
Rb 85	6514.728259	16688.75867	6729.345664	0.003770118
Sr 88	446.2650786	32242.77646	3885.80963	-0.001348512
Zr 90	5673.031703	7198.062394	2072.271687	0.031539894
Nb 93	2.615753779	3.408069721	2.050607766	-0.000459621
Ba 135	5753.722877	42304.99851	14267.25702	-0.003492123
Ba 137	5765.920617	42294.27188	14189.32865	-0.004760016
Ba 138	5197.595887	40617.13042	13815.05318	-0.002562455
Ce 140	4577.931701	17176.32423	13320.00375	0.001978131
Pr 141	549.8080441	2162.559753	1519.681077	0.000140975
Nd 143	2232.513335	7532.642483	5997.447167	-0.000140181
Nd 146	2226.826665	7590.544652	6090.89906	4.78506E-05
Sm 147	461.238988	1295.470998	1211.0117	0.000157789
Sm 149	462.1916821	1318.670153	1247.527507	2.78236E-05
Eu 151	78.81701902	233.0114816	238.8751482	-3.01929E-05
Eu 153	79.29021641	236.9845067	243.3366165	-4.74248E-05
Gd 157	344.5699887	957.4335657	970.3961349	0.000177054
Tb 159	39.66806947	114.917626	126.3968407	-7.59668E-06
Dy 163	165.040997	515.310344	607.8412624	-5.85452E-05
Ho 165	28.29407034	81.74732594	104.7252292	-7.52115E-06
Er 167	71.04455137	198.111461	266.0465813	-3.33005E-05
Tm 169	2.069656886	4.390166579	6.148639612	5.87749E-07
Yb 173	77.08842845	143.0233772	201.8556237	9.86657E-05
Lu 175	12.87333919	20.20641389	29.11821559	2.38552E-05
Hf 178	200.4002902	214.5200868	69.22552175	0.000728663
Ta 181	0.046817537	0.110577168	0.291403449	-6.80974E-05
Pb 208	230.8155537	6146.19904	2489.580042	-0.013587199
Th 232	5185.307171	6527.23994	11972.67992	0.01890166
U 238	362.0105562	216.5206578	168.0193747	-2.98527E-05

ICP-MS RSES/ANU	**Karolta rock** residual fraction (silicates)	**Karolta weathered rock** residual fraction (silicates)	**Karolta varnish** residual fraction (silicates)	**Blank** total dissolution
Isotope	**PPB**	**PPB**	**PPB**	**PPB**
Mn 55	46633.03762	65961.72561	155684.5247	-0.12682236
Rb 85	3743.656078	6542.9646	71079.68372	-0.000903515
Sr 88	48715.20739	52090.19833	81306.49804	0.002828959
Zr 90	340700.2856	266257.1824	289547.5421	0.175135892
Nb 93	14723.66096	11193.54267	13533.39271	0.001703401
Ba 135	391791.7816	245995.7864	164190.3603	0.004910159
Ba 137	390944.3764	246204.4612	164368.6379	0.002768855
Ba 138	374917.8896	234558.7943	160246.4666	0.004725681
Ce 140	877.5943366	3536.864765	21150.82452	-0.000607459
Pr 141	114.2157222	486.7572787	2295.299362	-9.6895E-05
Nd 143	533.561435	1835.258644	8081.147788	-0.000314604
Nd 146	539.6182754	1878.790024	8188.564845	-0.000953023
Sm 147	202.7713747	444.3886879	1447.887625	-0.000272008
Sm 149	210.3718414	448.7537256	1499.102277	-0.000480018
Eu 151	54.155381	101.4438764	302.3401802	-9.94517E-06
Eu 153	54.0450454	105.6108727	308.0269235	-0.000105106
Gd 157	338.2113448	558.6432262	1452.626092	-9.71683E-05
Tb 159	76.66728591	111.7512962	250.345954	-3.81382E-05
Dy 163	563.1182097	779.3061148	1599.0417	1.8815E-05
Ho 165	132.5989126	182.6344567	350.1470295	-4.59717E-06
Er 167	417.7074572	570.0403303	1069.241645	1.8734E-05
Tm 169	11.18095796	15.10348253	28.31763	-4.6841E-06
Yb 173	405.3361206	547.9244479	1029.236307	-0.00017659
Lu 175	63.6675127	88.18735977	160.3594208	-2.10906E-05
Hf 178	10189.4862	8532.765846	8600.063629	0.006400187
Ta 181	1131.998126	968.098689	1165.32146	0.013739158
Pb 208	2803.699606	10373.84705	12655.74156	-0.000902446
Th 232	938.3988872	1371.030097	8618.692491	-0.002646703
U 238	3393.977531	2844.75543	2389.585052	0.035411978

ICP-MS RSES/ANU	**Karolta rock** total dissolution	**Karolta weathered rock** total dissolution	**Karolta varnish** total dissolution	**Blank** total dissolution
Isotope	**PPB**	**PPB**	**PPB**	**PPB**
Mn 55	501825.4161	Overrange	Overrange	-0.12682236
Rb 85	75860.88099	12813.66863	53860.57989	-0.000903515
Sr 88	171541.8123	182549.4211	343588.163	0.002828959
Zr 90	219996.3322	328326.4229	271571.6416	0.175135892
Nb 93	9372.068332	13097.09065	12092.13808	0.001703401
Ba 135	356807.2793	1246528.831	3565443.746	0.004910159
Ba 137	371862.4702	1239796.189	3553500.6	0.002768855
Ba 138	356960.9537	1196228.306	3445080.833	0.004725681
Ce 140	50603.17931	154607.8238	1062532.841	-0.000607459
Pr 141	6110.538937	7947.599268	31587.04615	-9.6895E-05
Nd 143	23829.25558	31328.37188	121091.5521	-0.000314604
Nd 146	24112.36193	31849.35876	122523.7568	-0.000953023
Sm 147	5040.653213	6516.460776	22522.0019	-0.000272008
Sm 149	5163.678525	6675.945387	22935.27613	-0.000480018
Eu 151	941.8861901	1284.822714	4370.470114	-9.94517E-06
Eu 153	949.4859448	1295.688434	4425.433909	-0.000105106
Gd 157	5057.269731	6303.08136	20275.89639	-9.71683E-05
Tb 159	801.5493642	926.971331	2641.838576	-3.81382E-05
Dy 163	4760.778175	5204.06389	13596.59003	1.8815E-05
Ho 165	995.8171756	1022.775287	2510.229115	-4.59717E-06
Er 167	2913.617977	2842.113751	6596.099424	1.8734E-05
Tm 169	73.65664336	67.89398069	155.4229951	-4.6841E-06
Yb 173	2663.850094	2257.95671	5080.859261	-0.00017659
Lu 175	411.1378911	331.3416897	725.5372169	-2.10906E-05
Hf 178	6473.088364	9654.364915	7838.483098	0.006400187
Ta 181	804.0919023	1147.660409	948.9905824	0.013739158
Pb 208	23000.45272	221774.1145	372911.2284	-0.000902446
Th 232	10639.10059	7722.621016	34144.00459	-0.002646703
U 238	2936.06656	4905.80523	6574.276019	0.035411978

ICP-AES	Element-oxyde	Fe	Mn
INRS-ETE	Raie analytique	Fe_238.204	Mn_257.610
	Unite	%	%
Numéro client	Limite Instrumentale	0.00004	0.000001
Varnish			
exchangeable/adsorbed/carbonate		1330.32	1809.00
labile organics		2445.36	865.00
amorphous Fe-oxyhydroxides/Mn-oxides		4028.65	69908.00
crystalline Fe-oxides		31558.60	9307.83
sulphides		22343.84	367.00
refractory organics		7184.72	95.10
Wrock			
exchangeable/adsorbed/carbonate		6116.79	11575.69
labile organics		2712.35	868.47
amorphous Fe-oxyhydroxides/Mn-oxides		9401.97	5240.74
crystalline Fe-oxides		28661.26	2287.07
sulphides		24897.69	397.99
refractory organics		4848.26	75.02
Rock			
exchangeable/adsorbed/carbonate		11197.68	701.12
labile organics		2231.42	29.42
amorphous Fe-oxyhydroxides/Mn-oxides		7370.40	201.46
crystalline Fe-oxides		24247.35	448.83
sulphides		9546.96	162.49
refractory organics		2885.94	33.00
Blanc		< 0.0065	< 0.00097

Solution U-series
RSES/ANU

	Delta 234U	± Delta 234U	[230Th/238U]	± [230Th/238U]	[230Th/232Th]	± [230Th/232Th]	uncorected Age ka	± Age ka	Initial delta 234U	± Initial Delta 234U
Timor #3	114.6	1.1	0.2722	0.0017	21.2	0.11979527	30.3	0.2	124.9	1.2
Timor #2	88.3	2.2	0.2289	0.0019	13.8	0.10736993	25.6	0.2	95.0	2.4
Timor #1	92.2	0.9	0.0660	0.0008	10.9	0.14254863	6.8	0.1	94.0	1.0
exchangeable/adsorbed/ carbonate	3057.3	5.7	0.0833	0.0014	0.9	0.02271007 8			3077.0	5.7
labile organics	2873.0	14.6	1.0338	0.0164	0.9	0.01330078 3			148.3	1.3
amorphous Fe-oxyhydroxides/Mn-oxides	2016.7	6.1	0.1154	0.0360	0.8	0.69577300 4			2710.0	2.4
crystalline Fe-oxides	2505.8	5.6	0.0760	0.0016	1.0	0.02380816			2523.0	5.5
sulphides	2081.4	5.5	2.8429	0.0086	0.8	0.00339316 4			148.3	1.3
refractory organics	1153.0	16.1	18.6355	0.2555	0.8	0.00463885 6			148.3	1.3
residual fraction (silicates)	1786.9	4.3	1.3704	0.0058	0.8	0.00253971 2			2166.0	4.8

ANNEXE 3

Demande de subvention au Australian Research Council :
A reliable uranium-series chronology for Australian rock art

AUSTRALIAN RESEARCH COUNCIL
DISCOVERY PROJECTS
APPLICATION FORM FOR FUNDING COMMENCING IN 2009

DP

PROPOSAL TITLE

A reliable uranium-series chronology for Australian rock art

AIMS AND BACKGROUND

Rock art is one of the most intimate and potentially informative archives of the past. In Australia, visible rock art sites far outnumber excavated archaeological sites, and should hold the key to a far greater understanding of Australia's past - from the first phase of human occupation to Asian and European contact. However, it is extremely difficult to relate rock art to below ground archaeology because of the lack of reliable absolute chronology for paintings that span the last c.40,000 years.

This project aims to provide a firm chronological footing for the rock art in Australia, thus allowing its integration with the below-ground archaeological record and its correlation with cultural groupings and environmental and climate changes. In doing so, it will apply, for the first time in Australia, cutting-edge chronometric techniques across a variety of landscape and art bodies.

In this project, uranium series (U-series) dating methods will be used to date mineral coatings (calcite coatings and amorphous silica skins) that have naturally formed in direct association with rock art. This approach has become possible with the development of highly sensitive microsampling and dating techniques that generate ages and compositions of individual microstrata at unprecedented resolution (Aubert *et al.*, 2007).
This program will:

- Provide for the first time a robust chronology for a number of Australian rock art traditions;
- Integrate the chronology of art traditions with existing regional archaeological and palaeoclimatic information, including what is known about the arrival of the first humans, their settlement and subsistence patterns and climatic events such as sea level and faunal changes that have influenced human life-ways; and
- Provide a framework for sustainable management and conservation strategies.

The specific aims of the project are to:

1 Determine the ages of individual laminations in calcite coatings and amorphous silica skins directly associated with rock paintings and carvings;
2 Explore strategies for 'virtually' non-destructive dating; and
3 Develop Protactinium dating and use it in concert with Thorium-Uranium dates in order to verify age accuracy and identify and date possible 'open systems'.

SIGNIFICANCE AND INNOVATION

Rock art is of unique heritage value. The Australian region has one of the greatest bodies in the world (many have been inscribed on the World and National Heritage Lists) spanning many tens of thousands of years of human cognitive and cultural evolution. This treasure is of national importance and of particular concern to Aboriginal people across the continent.

Rock art is one of the few sources of archaeological information about the belief systems and aesthetic abilities of the earliest known artists. Elsewhere in the world, it has been critical in defining chronocultural groupings and successions (e.g. Leroi-Gourhan, 1968; Clottes, 1993), and in recent years has been incorporated into discussions of cultural responses to climate change (e.g. D'Errico *et al.*, 2001). It provides information on various 'steps' in the evolution of modern humans. While its specific meaning will probably always remain debated, it is undoubtedly one of the most intimate windows to the archaeological past.

However, chronological uncertainty seriously hampers our understanding of nearly all aspects of rock art, including its relationship to past climate changes. This project will redress this situation by producing one of the largest corpuses of radiometric dates for one of the richest (and possibly the oldest) rock art regions in the world. The results will considerably improve our understanding of the diachronic patterning and climatic background of the art, of its technical and stylistic development, and of the homogeneity and extent of cultural groupings.

This research has the potential to further our knowledge about the process of the emergence of figurative art, one of the most fundamental cultural developments in the evolution of humankind. In particular, it will contribute to the debate concerning its causes, as primarily related to biological (anatomical and cognitive modernity) or social and demographic factors (population packing and increased levels of interaction as an adaptive response to climate oscillations).

The results of this research will also inform management and conservation land-use strategies.

Dating rock art

Methods of estimating the age of rock art are generally divided into indirect and direct methods. Indirect methods fall broadly into the categories of iconographic determination, style sequences, the use of diagnostic subject matter (e.g. depictions of extinct animals; introduced European or Asian objects and animals), presumed technique of execution, association with archaeological finds by excavation, dating of the sealing off of caves or rock shelters, topographic proximity, weathering and patination study, superimposition of motifs, and a combination of these approaches. Direct dating of rock art requires that the dated sample can be directly related to the rock art: it is either of the same age (e.g. a paint binder), older than the art (e.g. its support surface), or younger than the art (e.g. a subsequent mineral deposit).

Accelerator Mass Spectrometry (AMS) has been used to determine the age of the organic binders or other inclusions (e.g. filaments from paint brushes) collected from pictographs (e.g. Cole et al, 1995). However, this is rarely possible as organic binders were not often used in the composition of pigments.

Beeswax rock art figures are a local but widespread feature in northern Australia and these figures are perhaps the most amenable for radiocarbon (^{14}C) dating, where the age of the wax is

unlikely to differ significantly from the time the art was created. They range from the present time to about 4000 years, but the overwhelming majority of the ages fall within the last 500 years (e.g. Nelson *et al.*, 1995; Taçon 1996; Taçon and Garde, 2000; ***Nelson et al., 2000)***.

Radiocarbon dating has been used to date carbon bearing layers above and below a painting (e.g. Watchman, 2000a, 2000b). Unfortunately, there are various factors complicating the radiocarbon dating of rock art. Some of these concern the age of the organic materials when they were put on the wall. Others involve sources of contamination, both in the form of bacteria, algae and other organic activity, or the intrusion of modern or ancient carbon through the activity of environmental factors such as water or wind (Watchman, 2000). There is also the problem of retouching of motifs in ancient times, potentially contaminating the images with younger pigment.

^{14}C dating used in speleothem (and calcite coating) chronology is also considered problematic, principally because of potential variability in the contribution of dead carbon from the host rock (Russell *et al.*, 2006). Fractionation of carbon isotopes also occurs on precipitation of calcite, depending on environmental conditions (Russell *et al.*, 2006).

In general, the problems are so severe with radiocarbon dating of rock art that, unless the source of carbon can be identified, radiocarbon dates on art should be taken as of unknown accuracy (Pettitt and Pike, 2007).
Furthermore, even when using the most sophisticated modern equipment and sample pre-treatment techniques, reliable use of ^{14}C dating is limited to materials certainly younger than 60,000 years and in most cases younger than 40,000 years (e.g. Bird *et al.* 1999). Therefore, if rock art was made by early humans in Australia, their antiquity cannot be determined either by conventional or AMS ^{14}C dating methods because the small quantities that can be sampled are beyond the present limit of radiocarbon measurement.

Optically stimulated luminescence (OSL) was used on quartz grains from mud-wasp nests physically related to rock paintings (Roberts *et al.*, 1997). However, this technique is only reliable if the mud in the nest was exposed to adequate daylight to bleach all grains. There are also very few suitable sites where mud-wasp nests are found in clear association with rock art.

By contrast, natural calcite laminations and amorphous silica skins covering rock paintings and engravings are much more common in the Australian landscape and can provide estimates of the minimum and maximum ages of pigment layers using uranium-series methods. This is possible because each sub-millimetre-thick lamination can now be precisely and accurately studied, chemically and isotopically analysed, and dated at extraordinary and unprecedented spatial and temporal resolutions using multi-collector inductively coupled plasma mass spectrometry (MC-ICPMS) (Aubert *et al.*, 2007).

Studying prehistoric human responses to environmental changes
As well as being an important source of information about ancient cultures, rock art also provides a valuable record of human responses and adaptation to environmental changes. Such changes are well illustrated in the rock art of Northern and Western Australia. Here, many 'episodes' of Aboriginal rock paintings are layered on top of each other, often in a number of different styles. These 'art on art' sites have been used to determine which styles came first (e.g. Chaloupka, 1993).

For example in Kakadu and western Arnhem Land, the various styles are attributed to different periods. During the pre-estuarine period, from about 50,000 to 8,000 years ago, the sea level was much lower and the climate was much drier. Some extinct mainland species such as the long-beaked echidna, thylacine and Tasmanian devil are represented in rock art. The estuarine period, from about 8,000 to 1,500 years ago, began with the flooding of river valleys and the formation of mangrove swamps. Animals such as barramundi, mullet and estuarine crocodiles migrated into the newly formed estuaries and appear for the first time in rock art. During the freshwater period, less than 1,500 years ago, freshwater billabongs and paperbark swamps replaced saltwater systems. The freshwater wetlands brought new food resources to the area and the paintings reflect these changes, showing waterlilies and magpie geese, humans carrying goose spears, goose-wing fans, complex spear throwers and didgeridoos.

Depictions of fighting scenes (a rare feature in hunter-gatherer art) have also been identified in the Kakadu/western Arnhem Land region. They are thought to reflect changes in society that occurred alongside the extreme environmental changes of the Pleistocene-Holocene transition (Taçon and Chippindale, 1994). Their appear to be an evolution in weapon style and at some sites human figures were arranged in great battle scenes, suggesting the rise of more tightly organised societies and competition over resources. Some paintings are thought to constitute the most ancient depictions of fighting from anywhere in the world (Taçon and Chippindale, 1994).

In the Western Desert, the rock art is characterised by distinct high-density provinces of particular styles. These are thought to demonstrate population migration patterns of early humans over considerable periods of time (McDonald and Veth, 2006; O'Connor *et al.*, 1998). Major aggregation events would have occurred during times of resource stress, when group territories contracted into more concentrated populations (Veth, 1993), or for major ceremonial activities during periods of relative resource abundance. At such times, it has been thought that there would have been a greater diversity of activities, both everyday economic, as well as religious and ceremonial. These types of sites occur where there are more reliable water sources and where there is a range of other resources nearby. Recent work at one such location indicates a long period of art production and a changing graphic structure over the period that this area was occupied (Veth, 2000).

While valuable insight can be gained through such 'art on art' comparisons, the systematic dating of these art bodies will enable the verification of such findings. By comparison of frequency of dates and motifs to climate proxies, uranium series dating methods can be used to test the proposed relationship between the nature and intensity of artistic production and climate change. This innovative approach will provide archaeological insights into the past, as well as insight into some of the complex, long-term consequences of climate change for communities and the environment.

Managing the resource

The immense heritage of prehistoric art is vulnerable to natural processes of erosion, obliteration and destruction, which are further accelerated by human acts. The increasing popularity of rock art as an attraction for cultural tourists is accelerating the deterioration of many sites. Every day rock surfaces are being eroded and urgent research is necessary before these archives of human

behaviour disappear forever. Measures need to be taken to document and record rock art in its current state to ensure that its testimony will remain for future generations.

The information acquired from uranium series dating will help conservators and managers of rock art sites to determine the length of time since paintings and engravings were made in order to calibrate the rate of deterioration of the art and inform decisions about intervention. Rock art sites are endowed with cultural, natural and economic value that makes them exceptionally important in the landscape of Australia. The systematic dating of this art will inform future integrated management plans towards the sustainable use of the land by custodians and other users.

These dating breakthroughs are sorely needed for urgent management planning where art is under impact such as the Burrup Peninsula and the Woodstock-Abydos Reserve in NW Australia and future potential mine sites – such as Karlamilyi (Rudall River) Kintyre uranium mine in the Western Desert. These areas collectively have over 1M art motifs at potential risk (Veth, pers. comm.).

Technical innovations

This proposal will build on a range of existing and remarkable innovations in the areas of dating and environmental analysis and will take full advantage of a unique combination of world leading analytical instruments at the Research School of Earth Sciences at the Australian National University (RSES ANU). For details see section Approach and Methodology.

APPROACH AND METHODOLOGY

High resolution U-series dating

Uranium-series dating is based on the radioactive decay chain which includes ^{238}U, ^{234}U and ^{230}Th (fig. 1). Laser ablation multi-collector inductively coupled plasma mass spectrometry (LA-MC-ICPMS) will be used for U-series analysis where the samples are relatively pure (i.e. free of detrital material indicted by a ^{230}Th/^{232}Th ratio higher than 10) and where the U-concentration is high enough (greater than 1 to 2 ppm) (Eggins *et al.*, 2005). For samples with lower U concentration, the desolvating nebuliser equipped Finnigan Neptune MC-ICPMS will be used. The Neptune ICPMS provides a significant advantage over ^{230}Th/U analysis by Thermal Ionisation Mass Spectromatry (TIMS), as it avoids the need for chemical separation of U from Th prior to analyses and therefore has a much higher ionisation efficiency for Th, which considerably minimises sample size requirements. It also significantly minimises the size of the errors. Mineralogically pure carbonate and silica precipitated from oxygenated soil water are likely to have negligible initial contents of Th, because of the much greater solubility of U relative to Th. However, where samples contain significant amounts of ^{232}Th, reflecting contamination of the authigenic minerals by fine-grained detrital components implying the presence of detrital ^{230}Th, correction for detrital ^{230}Th, ^{234}U, and ^{238}U will be made using isochrons (for detail see Ludwig and Titterington, 1994).

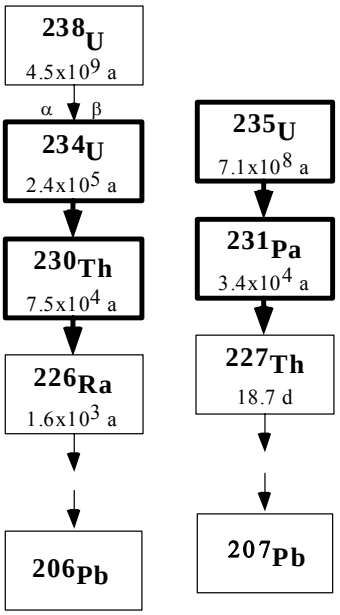

Figure 1: The ^{238}U and ^{235}U decay chains. For simplification, only the first alpha decays are shown. The bold boxes indicate the isotope pairs that are used for U-series dating.

Dating calcite coatings

The feasibility of dating finely layered calcite deposits by MC-ICPMS has recently been demonstrated, where only micrograms of samples are needed (Aubert et al, 2007) (and Fig. 2). This has so far never been applied in Australia. Calcite coatings are formed from the deposition of dissolved calcium bicarbonate from saturated solution. Because ^{238}U and ^{234}U isotopes are soluble in aqueous solutions but ^{230}Th is not, calcium carbonate ($CaCO_3$) crystals precipitated in calcite coatings will initially not contain any ^{230}Th. Subsequently, ^{234}U will decay to ^{230}Th. The measurement of the ^{230}Th, ^{238}U and ^{234}U isotopes allows the age of the formation of the carbonate host to be calculated.

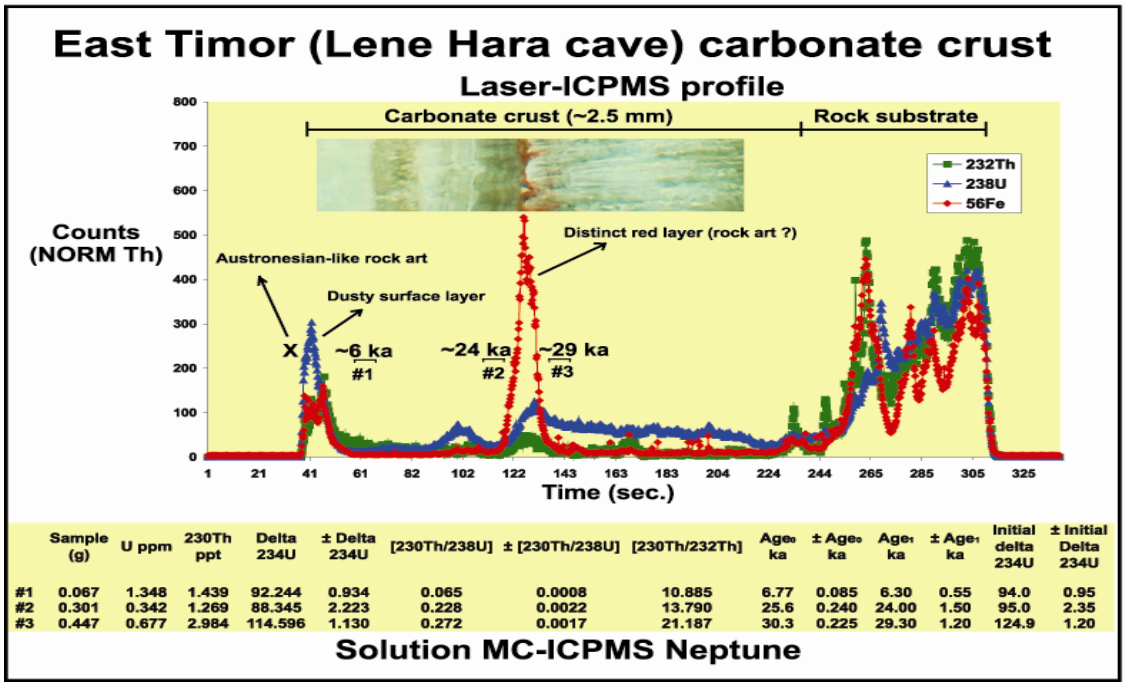

	Sample (g)	U ppm	230Th ppt	Delta 234U	± Delta 234U	[230Th/238U]	± [230Th/238U]	[230Th/232Th]	Age₀ ka	± Age₀ ka	Age₁ ka	± Age₁ ka	Initial delta 234U	± Initial Delta 234U
#1	0.067	1.348	1.439	92.244	0.934	0.065	0.0008	10.885	6.77	0.085	6.30	0.55	94.0	0.95
#2	0.301	0.342	1.269	88.345	2.223	0.228	0.0022	13.790	25.6	0.240	24.00	1.50	95.0	2.35
#3	0.447	0.677	2.984	114.596	1.130	0.272	0.0017	21.187	30.3	0.225	29.30	1.20	124.9	1.20

Figure 2. Chemical spectrum obtained from the laser ablation ICPMS analysis of a sectional profile across a small chip of calcite from Lene Hara Cave, East Timor. The surface layer of paint is younger than 6 ka, and the older red pigment layer, which could also be paint, is bracketed between 24 and 29 ka. The table summarises the analytical data measured by solution MC-ICPMS. Values for Age_1 are corrected ages assuming an initial $^{230}Th/^{232}Th$ ratio for Bulk Earth at secular Equilibrium = 0.8 ± 0.8 (Aubert *et al.*, 2007).

Dating amorphous silica skins

Hydrated amorphous silicon dioxide ($SiO_2.nH_2O$), or opal-A, is deposited naturally from seepage and runoff water as white or brown rock surface coatings, called 'skins', that often partly obscure rock paintings and engravings. Occasionally, a thin translucent silica skin can form a protective film over rock art. White lustrous silica skins occur where seepage water regularly flows from bedding and joint planes, whereas thinner brown skins form on the sides of boulders and cliffs where runoff water periodically flows. Silica skins initially begin to form on stable rock surfaces by a process involving a combination of evaporation and ionic-induced polymerisation of silicic acid in seepage and runoff water. Condensation reactions, random clustering of small silica spheres and deposition of the resulting aggregates eventually produce a thin surficial silica film.

Deposition of silica often traps micro-organisms that live in the damp seepage and runoff water zones, and these fossils in finely laminated skins enable attempts at dating rock art using radiocarbon measurements (e.g. Watchman *et al.*, 2000a). Unfortunately, this method is subject to problems such as the antiquity and contamination of the organic matter. Uranium-series analysis of pedogenic silica coating pebbles show that these silica skins are very well suited to U-series dating (Ludwig and Paces, 2001), but as yet this has never been applied to rock art dating. Several silica skin coatings not related to rock art have recently been profiled (with laser ablation ICPMS) and all of them have sufficient uranium for solution U-series dating. They are also relatively pure with negligible amount of contamination from ^{232}Th.

Protactinium dating

A fundamental assumption for dating a depositional event is that the system has remained 'closed'. This means that there has been no exchange of parent or daughter isotopes with the environment. Many processes, such as diagenesis or weathering can result in 'open-system behaviour' rendering any dates suspect. Open system behaviour can be identified and modelled in particular circumstances.

The build-up of Protactinium-231 (^{231}Pa) from the decay of ^{235}U in carbonates and silicates can be used as a dating tool analogous to the ^{230}Th method. The greatest strength of ^{231}Pa/^{235}U is its use in combination with ^{230}Th/^{234}U/^{238}U data in verifying age accuracy and identifying 'open-systems' where there has been a gain or loss of uranium which will affect the apparent U-series age. Moreover, because the ^{231}Pa and ^{230}Th dating methods share a common parent element (U), they form a single U–Th–Pa system. The significance of this technique is that a combination of U–Th and U–Pa analyses can be used to date systems that have been partially opened during their history (e.g. Cheng *et al.*, 1998).

The number of studies involving ^{231}Pa data measured by mass spectrometry is limited. This method is not currently used in any Australian laboratory. Unlike U and Th, there is no long-lived isotope to serve as a spike for measurement of Pa. The short-lived ^{233}Pa isotope ($t_{1/2}$ = 26.967 days) is the only spike option. A standard isotope dilution approach must be modified because no certified reference standard for Pa exists and the ^{233}Pa spike concentration cannot be accurately determined before spiking and analysis. This is due to the rapid decay of ^{233}Pa to ^{233}U; the ^{233}Pa concentration must be calculated by reverse isotope dilution methods.

Two methods of preparing ^{233}Pa are in use. The first, described by Pickett *et al.* (1994), involves periodically 'milking' of ^{233}Pa from a solution of Neptunium-237 (^{237}Np). This is done by ion exchange chemical separation, but it must be done under a stringent radiological protection regime because the parent isotope is very highly active. In this proposal, an alternative much less hazardous technique for tracer production is suggested. This involves periodic neutron activation of ^{232}Th in a nuclear reactor, to produce ^{233}Th. This short-lived species ($t_{1/2}$ = 22 minutes) then decays into ^{233}Pa. Because the parent (^{232}Th) has low activity, the ion-exchange purification can be done under normal laboratory conditions, after allowing short-lived by-products of the activation process to die away. Should neutron activation not be feasible (the new Australian Nuclear Science and Technology Organisation (ANSTO) reactor does not have the same facilities for neutron activation as its predecessor), Pa/U dating will be carried out with the more

conventional 'milking' of the Np spike. This can be carried out safely in the existing RSES laboratory.

Dating range
The dating range of the U-series approach depends on the ability to measure isotopic ratios that are different from but close to equilibrium. This is based on the size of the errors, which is a function of the U-concentrations in the sample and the detection system. MC-ICPMS measurements can be used to estimate closed system $^{230}Th/^{234}U/^{238}U$ ages ranging from just a couple of years up to about 500 ka, while the limit for $^{231}Pa/^{235}U$ dating is approximately 200 ka.

Virtually non-destructive dating analysis
It is inappropriate for a geochronologist to take large pieces of a painting or stone slabs bearing motifs back to a laboratory to find out how old they are. The aesthetic impact from removal of large samples to Traditional Owners can be palpable. Consequently, only micro-samples will be removed with prior permission and collaboration from Indigenous Owners and their legal counsel.

The laser ablation system will be used to drill a hole through the mineral coatings on micro-chips removed from rock art to determine the U-content. Samples that have U-concentrations of greater than 1 to 2 ppm will be directly analysed (with the laser ablation system) for U-series disequilibrium. For samples that have less then 1 ppm of uranium, solution analyses will be carried out by micro-drilling the samples and isotopic ratio measurements will be determined on a Finnigan Neptune multi-collector ICPMS equipped with desolvating nebuliser. Due to its significantly higher ionisation efficiency than thermal ionisation mass spectrometry (TIMS), multicollector inductively coupled plasma mass spectrometry (MC-ICPMS) permits the analysis of samples with much lower U concentrations in smaller samples. For example, TIMS usually requires about 100 nanograms of Th while MC-ICPMS needs less than 10 (0.000 000 010 grams) (Nakai *et al.*, 2001). The method has therefore a much wider applicability on rock art coatings, where often only minute sample masses are available. Furthermore, it allows for greater spatial resolution and minimises the visual impact of sampling so as to be negible.

Sampling locations
Australia is a typical region showing significant ongoing ecological processes, particularly associated with the effects of climate change, biological evolution and peoples' interaction with their natural environment. Australian rock art is an exceptional example of this interaction and bears remarkable and valuable witness to past environments and to the interaction of people with these environments. These rock art sites (one of the greatest concentrations of rock art in the world) are ancient and represent a continuous temporal span from the Pleistocene period to the present.

Carbonate deposits associated with art have been identified in caves (Susan O'Connor, pers. comm.) and along ephemeral streams (Wright, 2000) in the Kimberley region of North-Western Australia (Peter Veth, pers. comm.). Amorphous silica skins are also present at many rock art sites in the Kimberley (Watchman *et al.*, 2000a), Keep River (Watchman *et al.*, 2000b), Arnhem Land (Paul Taçon, pers. comm.), Kakadu (Watchman, 2000a), the Western Desert (Peter Veth, pers. comm.) and Central Australia (Mike Smith, pers.com.). These carbonate deposits have

never been dated although some silica skins have already been studied and dated with AMS ^{14}C (Watchman *et al.*, 2000a; Watchman *et al.*, 2000b).

This project will be carried out in close collaboration with local Aboriginal communities and archaeologists who are currently working in Western Australia (Peter Veth and Jo McDonald), Arnhem Land and Kakadu (Paul Taçon and Sally May) and Central Australia (Mike Smith and June Ross). These partners will collaborate in interpreting the rock art and integrating the chronology with their archaeological, temporal and environmental contexts: It is important that direct dating of rock art surfaces relate to wider archaeological studies where the relative chronology of the rock art has been worked out by archaeologists and where regional patterns of prehistoric occupation are known in some detail. These considerations structure the choice of case studies. The research projects they are already involved with will provide archaeological and logistical framework for this project. Permission to collect samples has already been granted for many sites.

When possible, the uranium-series results will be compared to existing chronology (including radiocarbon) in order to check the accuracy of the technique. I am planning to analyse between 100 and 200 samples per year (20 days of MC-ICPMS per year @ 5-10 samples per day).

The regional case studies provide a continental transect from the arid core of the continent to tropical monsoon-dominated northern Australia, allowing cross-comparison of the age and chemistry of silica and calcite skins in a range of environmental and archaeological settings.

Canning Stock Route (Western Desert)

An associated project will be carried out in the context of an ongoing ARC Linkage grant entitled: The recognition, interpretation and management of significant rock art and related dreaming (*Jukurrpa*) sites on the Canning Stock Route, Western Australia (LP0776332). This is the largest rock art dating project ever attempted in the arid zone of Australia. The dating aspect of this grant is supervised by Professor Marvin Rowe and Dr Karen Steelman and features AMS radiocarbon dating of charcoal pigment from black paintings and organic binders from inorganic pigment paintings. So far, this technique has been successfully applied to four localities and has focused on the most recent phase of art production (McDonald et al, 2008). Major galleries of engraved and pigment art (up to 100,000 motifs) have been recorded by Veth and McDonald from the Calvert Ranges (east of Well 15), Durba Hills (Well 17), the Carnarvon Ranges (west of Well 5) and near Wells 48, 50 and near Billiluna on the Tanami Road. Silica veneers and carbonate crusts have been recorded on art from all provinces.

Arnhem Land and Kakadu

The rock art of this region is the subject of an ARC Discovery grant entitled: Picturing change: 21st Century perspectives on recent Australian rock art (DP0877463). This project focuses on the rock art produced by Aboriginal people since the recent arrival of Asians and Europeans in different parts of Australia. It is also concerned with contemporary Aboriginal views about contact period rock art, related oral histories and contact period stories manifested visually. A key project goal is to raise national and international awareness of this little studied body of rock art and Australian indigenous rock art more generally. Access to sites in western Arnhem Land is already available but by dating a range of motifs from this area not only will we gain a better

understanding of exactly what rock art was made after the arrival of non-indigenous people but also what was made before and when. This will help chart stylistic change and stability over time periods associated with great environmental and/or cultural change. Many paintings and engravings are found in close association with amorphous silica skins.

Central Australia

Central Australia has long been recognised as containing a regionally distinct suite of rock art. In this region, the rock art records fundamental changes in graphic vocabulary, style, and composition. These coincide with other evidence for changes in the geographic linkages. The production of pigment art and engravings appears to have begun a long time ago and indicates a growing concern by people with using graphic art to record their relationship with the environment (Rosenfeld and Smith, 2002). Mike Smith (National Museum of Australia) and June Ross (University of New England) are currently working in the region and have identified sites with amorphous silica skins. During 2008-2010 they will extend their current field survey north of the MacDonnell Ranges further into the summer rainfall region of the arid zone to explore the effects of variability in the Australian monsoon on patterns of prehistoric occupation. There are many identified archaeological and rock art sites between the central ranges and the Tanami Desert. This research provides the opportunity to prospect for rock art sites with optimal characteristics for U-series dating and to embed the dating of rock art panels within a wider program of archaeological research.

NATIONAL BENEFIT

The proposed project will directly address Research Priority One "An Environmentally Sustainable Australia" with Priority Goals "Sustainable use of Australia's biodiversity" and "Responding to climate change and variability" (Social Sciences & Humanities enhanced goals).

Australia's rock art is part of an extremely important cultural, ritual and economic landscape and its sustainable management and conservation should be a high priority. Without engaging directly with land management, this project will provide an enhanced understanding of the status, importance and spread of rock art traditions. In addition to informing users of the landscape, this study will contribute to the prioritisation of conservation and land management issues currently undertaken by national bodies such as the Department of the Environment, Water, Heritage and the Arts and the National Parks and Wildlife Services. This will feed directly into the priority goal of sustainable use of Australia's biodiversity.

There is clear evidence that use of land by both commercial operators and tourists is increasing at an accelerating rate and that this will put greater pressure on its cultural and natural resources. Opportunities exist to produce quality materials that may be used for management, interpretation, training, educational and cultural tourism initiatives. Land users such as mining companies would also benefit from the synthesis of this information (another research priority) minimising negative ecological and social impacts.

The changing distributions of particular graphic traditions and the themes depicted in the art provide an indication of human responses to climate change that is otherwise invisible in the archaeological records. By comparing the frequency of dates and motifs to climate proxies, this research will enable archaeologists to test hypotheses regarding the relationship between the

intensity and nature of artistic production and climate. While the impact of climate change on industrial societies is subject to many studies worldwide, archaeology may hold the key to the impacts on indigenous societies.

This newly revealed 'library' of world heritage would be an enormous gift to future generations. Only a fraction of the world's rock art has been adequately studied. It is imperative that this essential source of information is preserved and understood. This research will demonstrate Australia's leadership and innovative capabilities in the fields of chronometric studies, archaeology, palaeoclimatology and palaeoenvironmental studies. Furthermore, the establishment of protactinium dating expertise in Australia has far-reaching implications for a broad range of research disciplines in the geological, environmental and archaeological sciences. It will add to an existing sophisticated base of analytical research facilities funded by national resources.

This will put Australia at the forefront of world rock art dating and the uniqueness of the technique will undoubtedly have international and commercial applications (e.g. for the management of conservation estates and Indigenous Protected areas).

COMMUNICATION OF RESULTS

Communication and participation with the traditional owners is an integral part of this research methodology. Traditional knowledge of the local culture, history and environment will inform the trajectory of the research and the research findings will then feed back into Aboriginal communities via plain English reports, copies of scientific reports and presentations. All field results and data will also feed into management programs being run by several partners.

This project aims to produce results of the highest scientific standards in the fields of archaeology, geochemistry, palaeoclimatology and palaeoenvironmental studies for publication in international journals of the highest quality such as Nature, Science, Earth and Planetary Science Letters, and Antiquity. Information about the work will be conveyed nationally and internationally through public lectures and conferences. Rock art has always fired the imagination and curiosity of people throughout the world and many of the findings of this research will be of wide public interest and will be shared with the wider community through media releases by the ANU Media Team.

REFERENCES

Aubert, M. *et al.* (2007) *Journal of Archaeological Sciences*, 34: 991-996. **Bird, M.I. *et al.*** (1999) **Radiocarbon,** 41 (2): 127-140. **Chippindale, C. and Taçon, P.** (1993) Occasional AURA Publication No. 8. **Chaloupka, G.** (1993) Reed Books. **Cheng, H. *et al.*** (1998) *Geochimica et Cosmochimica Acta*, 62: 3437–3452. **Clottes, J.** (1993) J*ournal of Archaeological Science*, *20: 223-235*. **Cole, N. *et al.*** (1995) In M.J. Morwood and D.R. Hobbs (eds), Quinkan prehistory: the archaeology of Aboriginal art in S.E. Cape York Peninsula, Australia, pp. 146-60. Tempus 3, Queensland University Anthropology Museum, Brisbane. D'Errico, F. *et al.* (2001) *Antiquity,* 75: 309-318. **Eggins *et al.*** (2005) *Quaternary Science Reviews***,** 24: 2523-2538 **Leroi-Gourhan, A.** (1968) Treasures of prehistoric art. **Ludwig, K.R. and Titterington, D.M.** (1994) *Geochimica et Cosmochimica Acta*, 58, 5031–5042. **Ludwig, K.R. and Paces, J.B.** (2001) *Geochimica et Cosmochimica Acta*, 66: 487-506. **McDonald, J. and Veth, P.** (2006) In I. Lilley (ed.) Archaeology of Oceania: Australia and the Pacific Islands. Blackwell Studies in Global Archaeology. Oxford: Blackwell. **McDonald, J. *et al.*** (2008) Report produced the Department of Aboriginal Affairs, WA and the Australian Institute of Aboriginal and Torres Strait Islander Studies. AIATSIS, Canberra. **Nakai, S. *et al.*** (2001) *Analyst*, 126; 1707e1710. **Nelson D. E. *et al.*** (1995) *Archaeometry,* 37(1): 151156. **Nelson D.**

E. *et al. (2000)* In E. Nelson ed., **The beeswax art of northern Australia**, Simon Fraser University, Burnaby. **O'Connor, S. *et al.*** (1998) *Australian Archaeology,* 46: 12-22. **Pettitt, P. and Pike, A.W.G.** (2007) **Journal of Archaeological Method and Theory,** 14(1): 27-47. Pickett, D.A. *et al.* (1994) *Anal. Chem*. 66, 1044–1049. **Roberts, R. *et al.*** (1997) *Nature*, 387: 696-9. **Rosenfeld, A. and Smith, M.** (2002) *Proceedings of the Prehistoric Society,* 68: 103-124**. Russell, S. *et al.*** (2006) The Geological Society of America, Special Paper 404. **Taçon, P.S.C.** (1996) **Archaeology in Oceania,** 31(3):103-24. **Taçon, P.S.C and Chippindale,C.** (1994) *Cambridge Archaeological Journal*, 4:211-48. **Taçon, P.S.C. and Garde, M.** (2000) In G. Ward and C. Tuniz eds. **Advances in dating Australian rock-markings: papers from the First Australian Rock-Picture Dating Workshop**, pp. 71-75. Occasional AURA Publication 10. Archaeological Publications, Melbourne. **Veth, P.** (1993) *Australian Archaeology*, 37: 73-74. **Veth, P.** (2000) *Archaeology in Oceania*, 35(1): 11-19. **Watchman, A.** (2000) *Earth-Science Reviews,* 49: 261–277. **Watchman, A. *et al.*** (2000a) *Journal of Archaeological Science*, 27, 315-325. **Watchman, A. *et al.*** (2000b) *Archaeology in Oceania*, 35: 1-10. **Wright, J.S.** (2000) *Australian Geographer,* 31, 333-347.